Spring 1-1-2013

Evaluation of Thermal and Thermo-Mechanical Behavior of Full-Scale Energy Foundations

Kyle Daniel Murphy
University of Colorado at Boulder, kyle.murphy@colorado.edu

Evaluation of Thermal and Thermo-mechanical Behavior of Full-scale Energy Foundations

by

Kyle D. Murphy

B.S.C.E., University of Missouri, 2011

A thesis submitted to the

Faculty of the Graduate School of the

University of Colorado in partial fulfillment

of the requirement for the degree of

Master of Science

Department of Civil, Environmental and Architectural Engineering

2013

This thesis entitled:

Evaluation of Thermal and Thermo-Mechanical Behavior of Full-Scale Energy Foundations

written by Kyle D. Murphy

has been approved by the Department of Civil, Environmental, and Architectural Engineering

_____

Professor John S. McCartney (committee chair)

_____

Professor Dobroslav Znidarčić

_____

Professor Karen Henry

Date_____

The final copy of this thesis has been examined by the signatories, and we find that both the content and the form meet the acceptable presentation standards of scholarly work in the above mentioned discipline.

ABSTRACT

Murphy, Kyle Daniel (M.S. Civil, Environmental, and Architectural Engineering)

Evaluation of Thermal and Thermo-mechanical Behavior of Full-scale Energy Foundations

Thesis directed by Associate Professor John S. McCartney

This study focuses on the thermo-mechanical and thermal behavior of full-scale energy foundations installed as part of two buildings recently constructed in Colorado. The soil stratigraphy at each of the sites differed, but both foundations were expected to function as primarily end-bearing elements with a tip socketed into rock. The heat exchanger configurations were also different amongst the foundations at both sites, permitting evaluation of the role of heat exchange. A common thread for both energy foundation case histories was the monitoring of the temperature and axial strain within the foundations during heat exchange operations.

The first case study involves an evaluation of the long-term thermo-mechanical response of two full-scale energy foundations installed at the new Denver Housing Authority (DHA) Senior Living Facility at 1099 Osage St. in Denver, Colorado. Due to the construction schedule for this project, the thermal properties of the foundations and surrounding subsurface could not be assessed using thermal response tests. However, instrumentation was incorporated into the foundations to assess their long-term heat exchange response as well as the thermo-mechanical strains, stresses, and displacements that occurred during construction and operation of the ground-source heat pump system. The temperature changes within the foundations during heating and cooling operations over a period of approximately 600 days ranged from 9 to 32 °C, respectively. The thermal axial stresses in the foundations were calculated from the measured strains, and ranged from 3.1 MPa during heating to –1.0 MPa during cooling. These values are

within reasonable limits for reinforced concrete structures. The maximum thermal axial stress was observed near the toe of both foundations, which is consistent with trends expected for end-bearing toe boundary conditions. The greatest thermal axial strains were observed near the top of the foundations (upward expansion during heating). The mobilized thermal expansion coefficients inferred from the instrumentation confirm that side shear stresses provide resistance to thermally induced movements, as the measured strains are less than the theoretical thermal expansion and contraction of the reinforced concrete. The thermal axial displacements indicate that the head of the foundation moves up by -0.8 mm relative to the toe during heating to 32 °C (cooling of the building) and downward by 0.3 mm relative to the toe during cooling to 9 °C (heating of the building).

The second case study evaluated the thermal and thermo-mechanical properties of eight full-scale energy foundations constructed as part of a new building at the U.S. Air Force Academy (USAFA). The foundations were constructed as part of this project, using lessons learned from the other case history in Denver. The foundations were designed so that the impact of 5 different heat exchanger configurations on the thermal response of the foundations could be assessed through evaluation of the temperatures of the heat exchanger fluids entering and exiting the foundations. The thermal response tests were analyzed using the infinite line source analysis to determine the apparent system thermal conductivity of four foundations. The heat exchange per unit meter was also assessed as a secondary measure of the thermal response of the foundations as the assumptions of the line source method are not fully satisfied. The thermal response tests were also compared to evaluate the impact of the run-out length from the heat pump to the location of the foundations, and to assess the role of different geometrical configurations of the heat exchangers within the foundations. The values of system thermal

conductivity ranged from 1.7 to 2.3 W/mK, which are consistent with previously published values for energy foundations and sandstone. These correspond to heat exchange per unit meter of 64.5 to 108.5 W/m, which is within the range of values reported for energy foundations in the literature. Greater runout lengths were observed to decrease system thermal conductivity and heat exchange rate. In addition, the temperature distributions in the foundations and the surrounding subsurface were also measured during these tests, which can provide a secondary measure of the thermal conductivity of the subsurface surrounding the foundations. The thermal conductivity of the subsurface measured using the temperature distribution in boreholes installed around the foundations ranged from 2.0 to 2.3 W/mK, which is consistent with the results from the line source analysis.

Three of the foundations are instrumented with strain gages and thermistors, and their thermo-mechanical response during a heating and cooling test were evaluated. For a temperature increase of 18°C during heating of the foundation, the maximum thermal axial stress ranged from 4.0 to 5.1 MPa, which is approximately 25% of the compressive strength of concrete (estimated at 21 MPa) and the maximum upward displacement ranged from 1.4 to 1.7 mm, which should not cause angular distortions sufficient enough to cause structural or aesthetic damage of the building.

A common conclusion from both studies is that the sum of the mechanical axial stresses and the thermal axial stresses are less than both the tensile and unconfined compressive strength of the concrete. Even if the foundations were fully restrained from moving by side friction and end restraints at the head and toe, the thermal axial stresses would be less than those set in most design regulations ($0.33\ f'_c$). The mobilized side shear stresses in both projects tended to increase with depth, and the magnitudes were consistent with the undrained shear strength of stiff soils.

The thermal axial displacements estimated by integrating the thermal axial strain values were not sufficient to lead to angular distortions that would cause structural or aesthetic damage to the overlying structure or connecting utilities.

ACKNOWLEDGEMENTS

I would like to express my sincere gratitude to Dr. John McCartney for providing guidance and encouragement throughout my studies and always being open to support my ideas and research. I am also very appreciative of the opportunity to work on a project that I have a strong interest in. His continuous high expectations have pushed me to become a better person, and for that I am very grateful.

I also extend my gratitude to my committee members who have been very helpful throughout my time as a student at The University of Colorado. Professor Znidarčić was perhaps the most entertaining instructor I have ever had as a student. He taught not only the technical engineering skills, but also how to think like an engineer and look at the bigger scope of a project. I cherish his insightful and thoughtful comments and suggestions during my time at CU.

I would like to thank Professor Karen Henry for being so supportive through the evolution of our project from just an idea to reality. I enjoy her presence as she is full of energy and is always willing to stick to it and get the job done. Her assistance throughout my research is deeply appreciated.

There have been many people who have made my life more enjoyable as a student at The University of Colorado. My office mates have become some of my best friends and I will always cherish the time we spent together. I would like to thank Joseph Goode, C.J. Coccia, Melissa Stewart, Erik Jensen, Kenny Gillis, and Jenna Svoboda for giving me the entertainment I needed to get through the day. Their assistance with my project is very meaningful and I could not have made it this far without the extra hand they have provided me from time to time.

I owe the most gratitude to my parents, Bruce and Tina Murphy, for supporting me in life. Their continued encouragement and words of wisdom throughout my childhood and

adulthood has pushed me to study hard and try my best at everything I do. For this, I dedicate my work to them as they have instilled in me the qualities and principles of what it means to be a good person.

Support from DoD ESTCP project EW-201153 is gratefully acknowledged, as are the contributions of the 819th Air Force RED HORSE Squadron, who constructed the building and provided support for the U.S. Air Force Academy test site.

TABLE OF CONTENTS

LIST OF TABLES

LIST OF FIGURES

1. INTRODUCTION

1.1. Overview of Energy Foundations

Heating and cooling of commercial and residential buildings comprises a large portion of the total energy usage in the United States and throughout the world (Energy Information Administration 2008). Energy foundations are a form of ground-source heat exchanger (GSHE) that can be used to reduce the electrical energy demand of building heating and cooling systems. Specifically, energy foundations include any geostructure that incorporates a closed loop heat exchanger system with the purpose of transferring heat between the ground and a structure, such as drilled shaft foundations, diaphragm walls, or shallow footings. Energy foundations differ from conventional GSHE systems, which involve installation of heat exchangers into small-diameter boreholes or coiled heat exchangers in shallow trenches. Although conventional GSHE systems have been used successfully for many years, the additional cost of drilling deep boreholes for the sole purpose of exchanging heat with the ground may lead to long-payoff periods and requires space outside of the building footprint (Hughes 2008).

GSHE systems take advantage of the relatively constant natural ground temperature below the depth of seasonal variation (Brandl 2006). The subsurface below a depth of 4 m generally has a relatively steady temperature approximately equal to the mean annual air temperature at a given location, which has been observed in recent studies (Moel et al. 2010; McCartney and Murphy 2012). The constant temperature of the ground as a heat source or sink permits the efficiency of a ground-source heat exchange system to be higher than that of an air-source heat exchange system as the temperature of the outside air changes frequently (Kavanaugh et al. 1997).

In this study, energy foundations refer to drilled shaft foundations constructed with a set of closed-loop heat exchanger attached to the inside of the reinforcement cage so that they can serve the dual purposes of providing structural support and a providing access to ground-source thermal energy, as shown in Figure 1.1 and Figure 1.2.

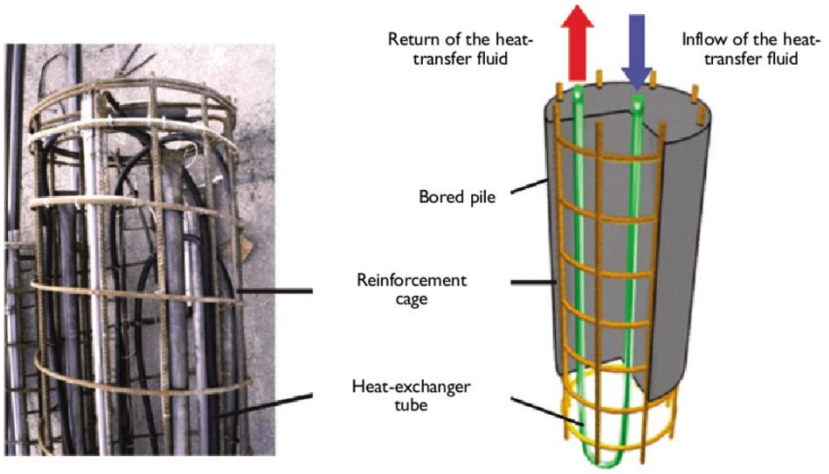

Figure 1.1: Schematic representation of an energy foundation (after Laloui 2011)

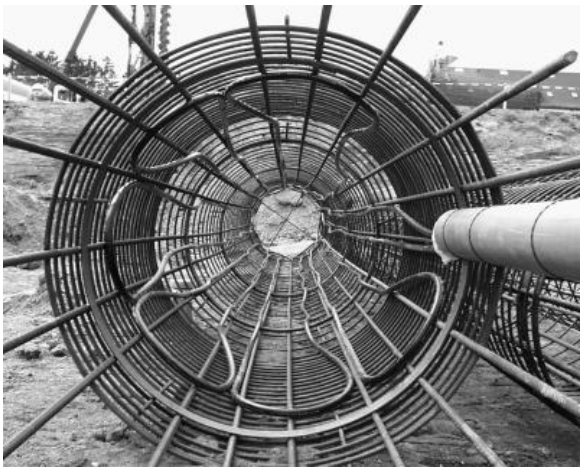

Figure 1.2: Energy foundation reinforcement cage with attached heat exchanger tubing (Brandl 2006)

While energy foundations are gaining popularity throughout the world (Brandl 2006), further research is required to fully understand their performance regarding their thermal

properties, their thermal response during actual heating and cooling of buildings, as well as the thermal strains, stresses, and displacements induced in the foundations in-situ as a result of heat pump heating and cooling operations. Several studies have been published regarding the behavior of energy foundations from characterization-type tests immediately after construction. For example, previous thermal response and thermo-mechanical tests have been performed directly at the head of the pile using a load frame, which may not consider the geometry of the complete heat exchange systems and the impact of the overlying structure on the thermal and thermo-mechanical response (Bourne-Webb et al. 2009). However, no study has thoroughly investigated the behavior of energy foundations installed under and actual building with typical heat pump operation. In addition to providing an insulating upper boundary condition to the soil surface, the restraint boundary conditions for an energy foundation beneath a real building may differ from that in a load frame apparatus and boundary conditions at the head of a pile, which can influence the stress and strain distribution as the foundation is heated and cooled.

1.2. Objective

The objective of this study is to understand the behavior of full-scale energy foundations under actual building loads (and corresponding end restraint boundary conditions), as well as actual building heat pump demands. Another objective is to understand the role of heat exchange configuration on the thermal response of energy foundations in the same soil profile. An associated issue regarding the heat exchange configuration in actual buildings is the role of the connections between different energy foundations within a building and the heat pump in a central location. All geothermal heat exchangers must be connected to a manifold system in the mechanical room for a building, and the run-out length from the building to the energy foundation is typically not insulated. This may have important effects on the system performance

as heat exchange through the horizontal portion of the loop may decrease the efficiency of the system as the surface temperature is typically cooler or hotter than the temperature of the ground during heating or cooling operations of the heat pump, respectively.

1.3. Approach

The results from two case histories are presented in this study to investigate thermo-mechanical and thermal behavior of energy foundations in real working conditions. The first case study involves two energy foundations beneath an eight-story building in Denver, Colorado that has been fully operational since December 2011. The energy foundations contain three and four loop heat exchanger configurations and are coupled with a conventional deep borehole loop field that is located outside of the building footprint. Instrumentation has been installed to capture the variation of supply and return fluid temperatures as a function of time, based on the heating and cooling demands of the ground-source heat pump system. The axial strain and temperature of the reinforced concrete were monitored continuously at six depths within each foundation.

The second case study involves eight energy foundations beneath a building at the U.S. Air Force Academy in Colorado Springs, Colorado, constructed in 2012-2013. Five different heat exchanger loop configurations are incorporated into the energy foundations to investigate the how each loop configuration influences the heat exchange characteristics during heating and cooling. A comprehensive instrumentation system has been installed at the site to measure the temperatures of the heat exchange fluid entering and exiting each foundation loop, axial strain and temperature at various depths within three of the eight energy foundations, soil temperature surrounding two of the energy foundations, volumetric water content of the unsaturated subsurface around one of the foundations, and energy consumption of each component of the HVAC system.

1.4. Scope of Study

This thesis is organized into seven chapters. A review of previously published literature pertinent to this study is presented in Chapter 2. This chapter includes a theoretical overview of the thermo-mechanical behavior in energy foundations, along with the results obtained from two heavily instrumented case histories reported in the literature. Thermal behavior of energy foundations is discussed in terms of the heat exchange characteristics of energy foundations, thermal response testing procedures and analysis of results, thermal performance assessment of databases of foundations, along with details of relevant case studies that have been performed on energy foundation systems. A comprehensive description of the two case are presented in Chapter 3, including soil stratigraphy, energy foundation geometry, instrumentation, and specifics of the testing procedures at each site. The results from the two energy foundations installed at the Denver Housing Authority in Denver, Colorado are presented in Chapter 4. The results from the system located at the U.S. Air Force Academy in Colorado Springs, Colorado are presented in Chapter 5. An analysis of the results describing the thermo-mechanical and thermal behavior of the two energy foundation systems is presented in Chapter 6. This chapter also includes a comparison of the results from the two case studies with the results obtained from case histories published in the technical literature. The conclusions drawn from this study are presented in Chapter 7.

2. LITERATURE REVIEW

2.1. Energy Foundations

The use of geotechnical systems as heat exchangers, including energy foundations, was proposed and investigated in several early studies, including those of Brandl (1998), Ennigkeit and Katzenbach (2001), Laloui et al. (2001), and Brandl (2006). These studies described different approaches to configure heat exchangers within drilled shaft foundations and other thermally-active geotechnical systems, established the theoretical equations used to describe conductive heat flow away from energy foundations, and provided laboratory-scale validation of the different equations. Since then, full-scale energy foundations have been constructed in many locations throughout the world, primarily as part of pilot studies to evaluate their performance in different in-situ conditions. Tests have been performed on these full-scale energy foundations to evaluate their thermal response (Ooka et al. 2007; Adam and Markiewicz 2009; Wood et al. 2009; Loveridge and Powrie 2012; Bourne-Webb 2013, Murphy et al. 2014) as well as their thermo-mechanical response (Laloui et al. 2006; Bourne-Webb et al. 2009; Amatya et al. 2012; McCartney and Murphy 2012). Although the results from these cases are often variable, these studies have established the important issues that should be considered in evaluating thermal properties (Loveridge and Powrie 2012); and the general mechanisms of thermo-mechanical soil-structure interaction (Bourne-Webb et al. 2009; Amatya et al. 2012).

Several types of deep foundations have been used as heat exchangers to access ground-source thermal energy. The most common configuration of energy foundations consists of drilled shafts that feature embedded ground-source heat exchange elements used to transfer heat to or from the subsurface to the building (Brandl 2006; Laloui et al. 2006; McCartney 2011; Bourne-Webb 2013). Other configurations of deep foundations that may be adapted as ground source energy systems are shown in Figure 2.1. Closed-loop standing column well systems can be

installed in hollow pipe piles that may be driven or screwed into the ground and work by injecting fluid at one location in the pile and extracting fluid that has been heated or cooled at another location in the pile (Suver 2012). Pipe piles may also be filled with concrete or grout while having embedded heat exchanger tubing within the inside of the piles and function in a similar manner as drilled shaft-type energy foundations.

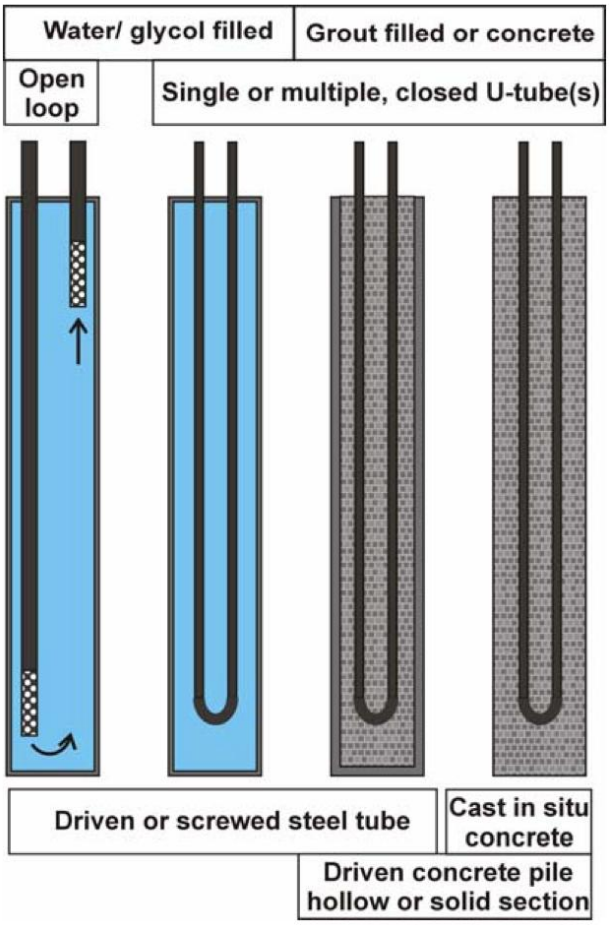

Figure 2.1: Schematic of differing pile adaptations for ground source energy systems (Bourne-Webb 2013)

2.2. Thermo-Mechanical Behavior

2.2.1. Thermo-Mechanical Response of Energy Foundations

As an energy foundation is heated or cooled, it may expand or contract, respectively, depending on the restraint boundary conditions. For unconstrained conditions, the axial thermal strain in an energy foundation can be calculated as follows:

$$\varepsilon_{T,free} = \alpha_c \Delta T \quad (2.1)$$

where α_c is the coefficient of linear thermal expansion of reinforced concrete, and ΔT is the change in temperature. The value of $\varepsilon_{T,free}$ is an upper limit on the thermal strains that may be encountered due to heating or cooling. To be consistent with geotechnical engineering conventions, the axial strain is defined as positive for compression (or contraction). Accordingly, α_c is defined as negative in this study as structural elements expand during heating (positive ΔT). If the foundation were fully constrained by the end restraint boundaries or side shear resistance, the axial strain would be zero. A change in temperature would induce the maximum thermal axial stress $\sigma_{T,constrained}$, in the reinforced concrete and can be calculated as follows:

$$\sigma_{T,constrained} = -E\alpha_c \Delta T \quad (2.2)$$

where E is the Young's modulus of reinforced concrete. For an increase in temperature (i.e., heating), the maximum thermal axial stress would be positive (compression) based on the sign convention for strain. The boundary conditions for energy foundations are likely between the unconstrained and constrained conditions as a result of the soil-structure interaction and finite stiffness at the building and tip of the foundation which will permit some strain to occur. In this case the energy foundation is partially constrained, and the actual thermal strains will be less than those predicted by Eq. 2.1. The thermal axial stresses induced in a partially constrained energy foundation during a change in temperature can be calculated as follows:

$$\sigma_T = E(\varepsilon_T - \alpha_c \Delta T) \quad (2.3)$$

where ε_T is the measured thermal strain in the reinforced concrete.

For real energy foundations embedded in soil or rock, soil-structure interaction mechanisms will restrict the movement of the foundation during heating. Specifically, the side shear resistance, end bearing, and the characteristics of the overlying building will lead to different distributions in thermal axial stresses and strains in an energy foundation. The mobilized side shear stress due to changes in foundation temperature was calculated from the difference in thermal axial stress values at different heights in the soil layer, as follows:

$$f_{s,mob,j} = \frac{(\sigma_{T,j} - \sigma_{T,j-1})D}{4\Delta l} \quad (2.4)$$

where D is the shaft diameter and Δl is the distance between gages. The sign convention for the mobilized side shear stress implies that positive side shear stresses are upward (in the same direction as those mobilized during mechanical loading), while negative side shear stresses are downward (in the opposite direction as those mobilized during mechanical loading).

Another important variable to consider in the thermo-mechanical soil-structure interaction of energy foundations is the thermal axial displacement. Specifically, the thermal axial displacement of the foundation head may indicate if the heat exchange operations are leading to excessive heave or settlement during heating or cooling of the foundation. If the thermal axial strain is measured in the foundation, the relative thermal axial displacements to the bottom of the foundations can be calculated by integrating the thermal axial strain profiles, as follows:

$$\delta_{T,i} = \delta_{T,i-1} + \frac{1}{2}(\varepsilon_{T,i-1} + \varepsilon_{T,i})\Delta l \quad (2.5)$$

where $\delta_{T,i}$ is the thermal axial displacement at the midpoint between a pair of strain gages, $\varepsilon_{T,i}$ is the thermal axial strain at the location of strain gage *i*. In this study a positive thermal axial displacement denotes downward movement.

Soil-structure interaction mechanisms have been studied in centrifuge-scale tests for simplified soil profiles (McCartney and Rosenberg 2011; Stewart et al. 2012; McCartney et al. 2013). However, evaluation of full-scale foundations in the field permits consideration of realistic boundary conditions and soil strata. Several full-scale energy foundations have been evaluated to study the thermo-mechanical stresses and strains during mechanical loading, heating, and cooling (Laloui et al. 2006; Boume-Webb et al. 2009; Amatya et al. 2012; McCartney and Murphy 2012). The information from these studies has been implemented into thermo-mechanical load-transfer analyses (Knellwolf et al. 2011).

2.2.2. Idealized Axial Stress and Strain Behavior during Heating and Cooling

Thermo-mechanical behavior of a full-scale energy foundation can be understood by considering the idealized behavior for a floating foundation with no end bearing resistance. A schematic is presented in Figure 2.2 showing axial stress in the foundation vs. depth for different loading and thermal conditions. As the foundation is loaded mechanically, axial stress is highest at the head then sheds with depth as the side shear resistance of the foundation-soil interface carries the load. The axial stress will decrease to zero if the side shear resistance is sufficient to support the building load, but it may also decrease to a non-zero value if the foundation had non-zero end bearing at its tip.

If the same semi-floating foundation is heated in the absence of a mechanical load, it will expand about the center, and compressive stresses will be encountered due to the restraint provided by the side shear resistance. The maximum axial stress should ideally occur at the

midpoint of the foundation, as this is the location where the soil provides the most shear resistance to axial movement at this point. The axial stress will reduce to zero toward the top and bottom of the foundation (Bourne-Webb et al. 2009). In addition, as the foundation is heated, radial expansion of the foundation will occur. If the expansion of the foundation is greater than that of the surrounding soil, an increase in ultimate side shear resistance may occur due to the increase of lateral confining stress (Rosenberg 2010). If the mechanical and thermally induced axial stresses are superimposed on one another, there will be an increase of axial stress everywhere in the foundation, with the highest stress occurring at the foundation head.

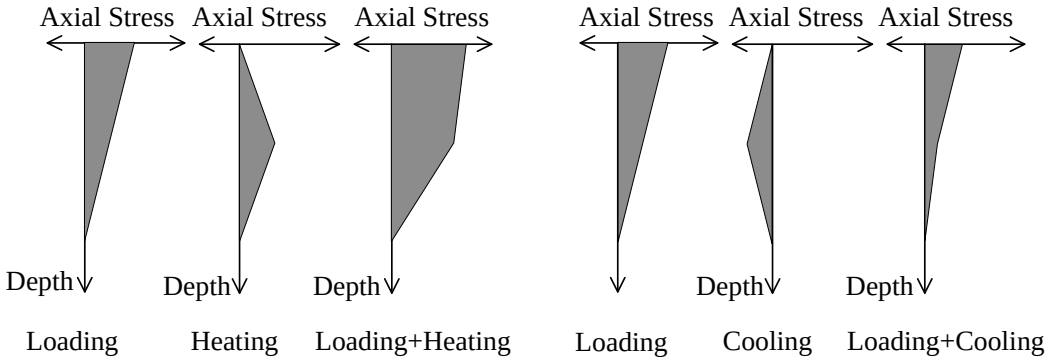

Figure 2.2: Schematic of simplified representation of thermo-mechanical response of energy foundation with floating boundary conditions (after Bourne-Webb et al. 2009)

As an energy foundation is cooled, the reinforced concrete will tend to contract about a point referred to as the "null point". The null point is defined as the point of zero axial displacement during heating or cooling, and may change as the end restraints or side shear interaction of the soil changes. As the contraction occurs, the axial stress in the foundation will be of the opposite sign as the mechanically induced axial stress, indicating the foundation is in tension. If cooling and mechanical loading occur simultaneously, a net reduction in axial stress will take place. In theory, tension in the foundation may occur if the cooling of the foundation causes greater negative axial stress than the positive axial stress induced by mechanical loading. The thermal contraction of the foundation during cooling may result in a reduction in radial

confining stresses and a reduction in the ultimate side shear resistance. However, heating and cooling cycles to ambient temperature indicate that heating may lead to positive effects in the side-shear resistance due to permanent consolidation of the soil surrounding the foundation during the first heating stage (McCartney and Rosenberg 2011).

The side shear stress at the foundation-soil interface needs to be considered during heating and cooling of an energy foundation. A schematic of the mobilized side shear stress with depth in an energy foundation is shown in Figure 2.3 for heating and cooling of a floating foundation. For mechanical loading only, side shear stress is assumed to be constant with depth. During heating in the absence of a mechanical load, upward (negative) side shear stress will be mobilized above the null point, while downward (positive) side shear stress will be mobilized below. If heating and loading are simultaneously induced on an energy foundation, a reduction in side shear stress will occur in the upper half of the foundation and an increase in side shear stress will be present below the null point. During cooling, the opposite trend is expected, as shown in the right schematic of Figure 2.3.

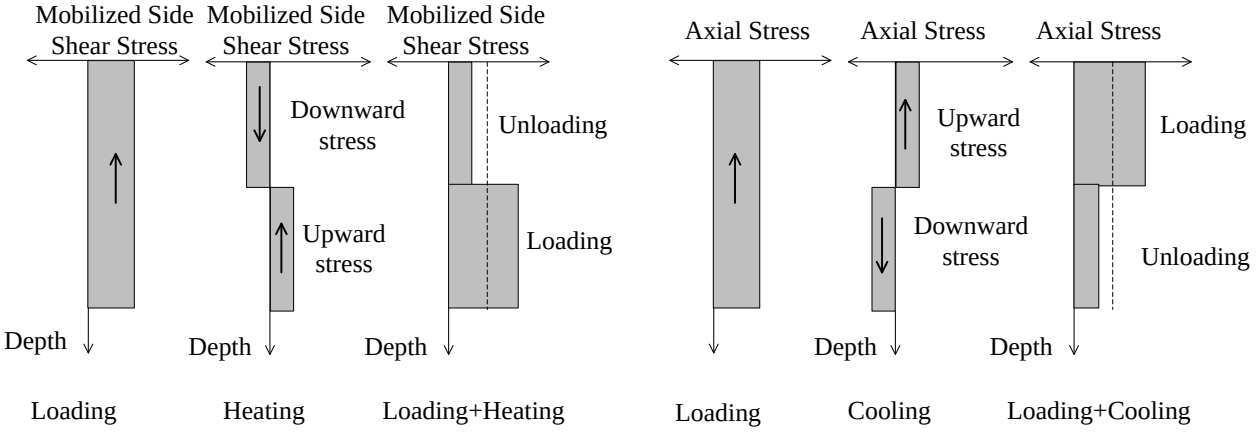

Figure 2.3: Schematic of shear resistance response for a floating energy foundation during heating and cooling operations (free at top and bottom) (after Bourne-Webb et al. 2009)

Most energy foundations in the field are installed in soil profiles that lead to different boundary conditions than those of a floating foundation. Specifically, restraints are typically

present at the top (head) of the foundation as a result of the stiffness of the overlying structure, and at the bottom as a result of end bearing capacity of the underlying material. The end restraints play an important role in the distribution of axial stress and side shear resistance during heating and cooling of an energy foundation. Amatya et al. (2012) presented a simplified representation for the behavior of energy foundations during heating for different end restraints shown in Figure 2.4. If partial restraint for the foundation is provided by the soil or overlying superstructure at the toe and base, respectively, heating will lead to non-zero thermal stresses near each end of the foundation as the stiffness of the structure and end bearing soil material resist thermal expansion. The restraints at the top and bottom of the foundation may cause the null point to be located at a different depth than the midpoint. If a stiff material is at the base, the null point will be closer to the bottom of the foundation. Conversely, if the restraint at the foundation head is greater than at the toe, the null point will be above the midpoint.

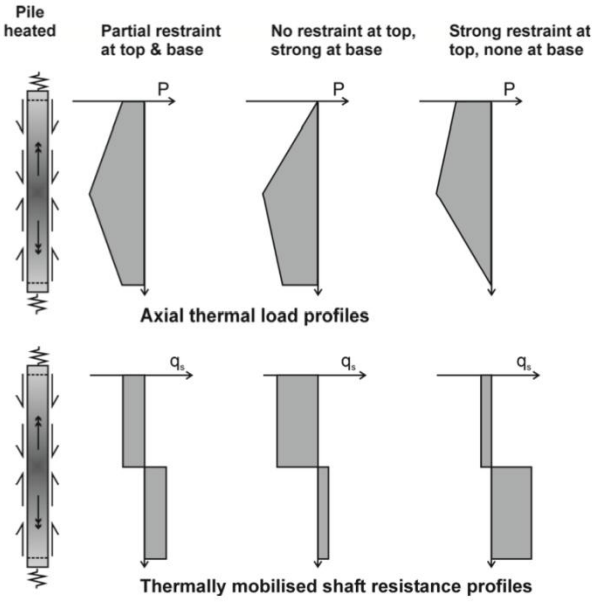

Figure 2.4: Effects of foundation end restraints on axial load and shaft resistance profile (NOTE: Sign convention for load in the upper set of figures is opposite that used in this study, where negative loads are compressive)

For the condition of no restraint at the top and strong restraint at the base, the null point would be located at the toe and the foundation would be referred to as an end-bearing foundation, as shown in Figure 2.5. Since the foundation is restricted from moving downward by the rigid end restraint, all of the thermal axial displacements would be upward, and the greatest movement would occur at the head of the foundation. The thermal axial stress would increase with depth. The mobilized side shear resistance would be upward above the null point, with only negligible mobilized side shear resistance near the toe of the foundation. This behavior was observed for an end-bearing foundation in a centrifuge test by Stewart and McCartney (2014).

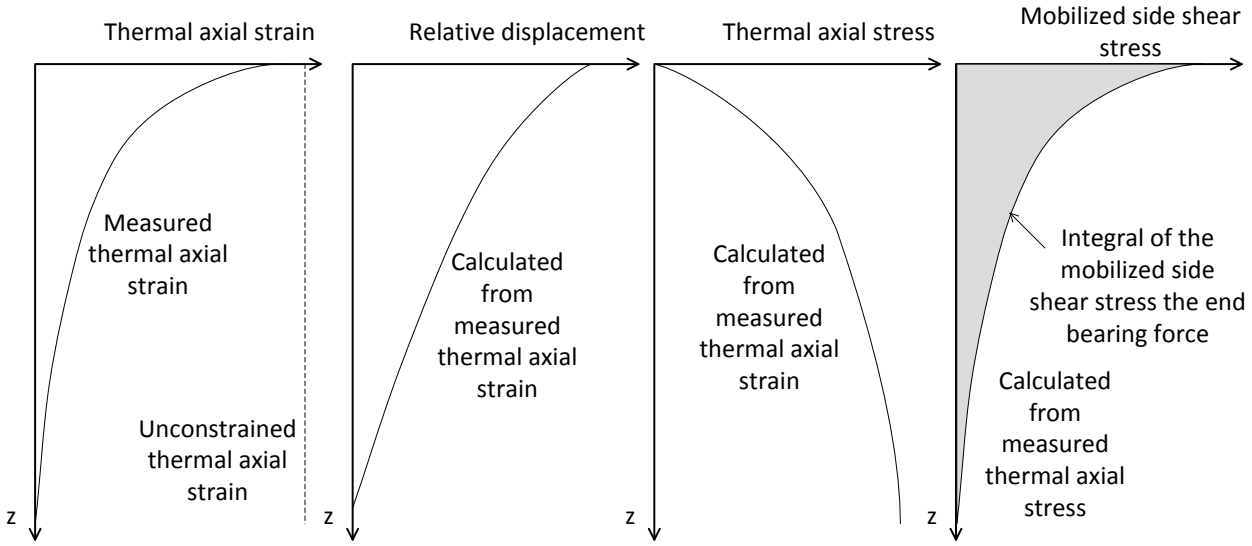

Figure 2.5: Thermo-mechanical behavior of a purely end-bearing foundation

2.2.3. In-situ Energy Foundation at EPFL, Switzerland

Laloui and Nuth (2006), Laloui et al. (2006), and Laloui (2011) presented results from a series of thermo-mechanical loading tests performed on an energy foundation in Switzerland that was beneath a 7 story building. A heating test was performed after construction of each story. The drilled shaft foundation was 25.8 m long with a diameter of 0.88 m. The upper 12 m of soil was comprised of alluvial deposits of sand and gravel, with the bottom portion of the foundation embedded in sandy, gravelly moraine, and founded in the Molasse Formation, which is a soft,

impervious sandstone material. Optical fiber strain gauge (SMARTEC) sensors, radial strain gauges, and extensometers were embedded in the foundation to capture the strain and temperature distribution during thermo-mechanical loading with depth.

The test conducted by Laloui and Nuth (2006) consisted of heating the energy foundation prior to any building dead load, allowing the foundation to move freely upward. The foundation was heated to 20.9 °C above ambient ground temperature over the course of 12 days then cooled to 3 °C above ambient ground temperature, as shown in Figure 2.6. The axial strain distributions in the foundations during heating and cooling are shown in Figure 2.7. The axial strain with depth is not uniform during the heating stage and is influenced by the frictional side shear resistance to foundation movement and may be a result of the non-uniform stratigraphy throughout the depth of the foundation.

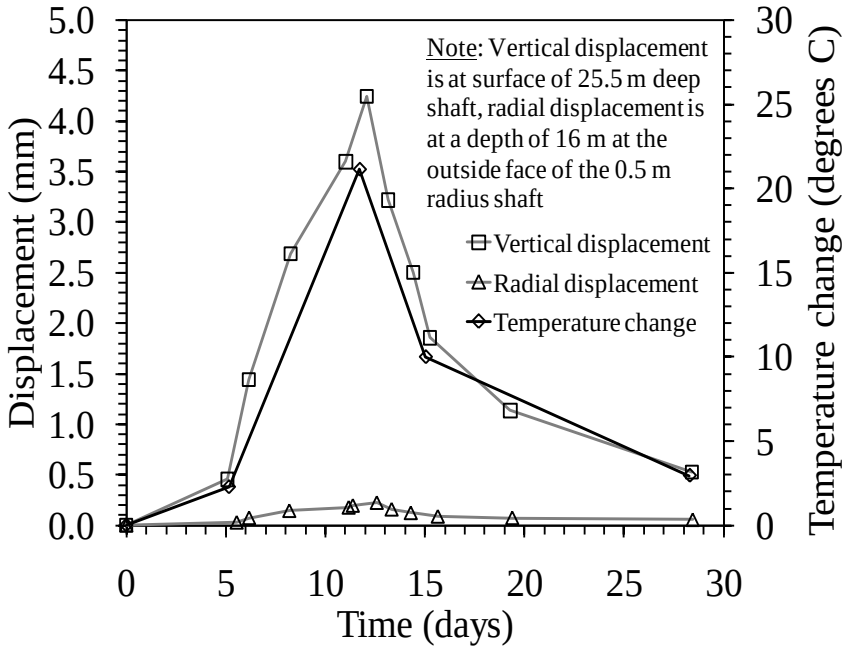

Figure 2.6: Temperature induced axial and radial displacements in an active energy foundation (Laloui et al. 2006) (NOTE: Sign convention of displacement data in figure is opposite the sign convention from this paper, where positive displacements indicate upward movement)

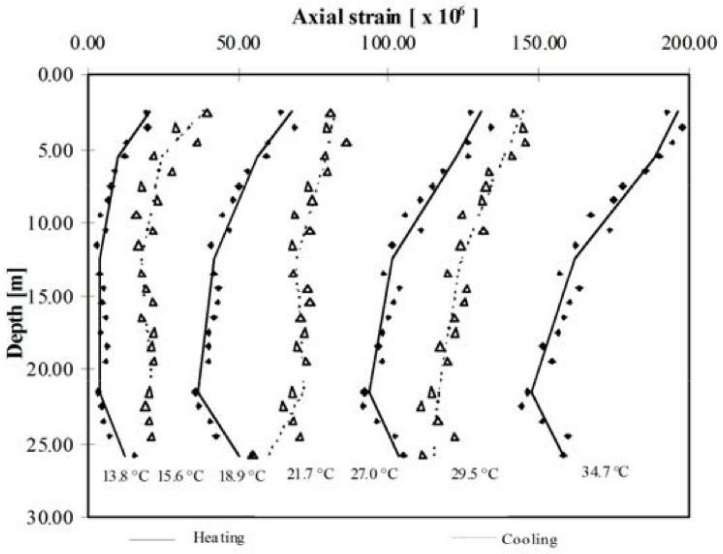

Figure 2.7: Measurements of strains in the test energy foundation at EPFL during heating by 21 °C and cooling by 3 °C (Laloui 2011) (NOTE: Sign convention of data in figure is opposite the sign convention in this thesis, with positive thermal strains denoting expansion)

The axial strain distribution pattern observed in the energy foundation during heating and cooling indicates that the strain induced during heating is significant and leads to increased compressive stress in the foundation. Residual strain in the foundation is also present after cooling and is indicated by the cooling strain being non-zero. The displacement at the head of the energy foundation is shown on Figure 2.7. A maximum upward displacement of nearly -4.5 mm was observed for a temperature increase of 20.9 °C with no restraint at the head of the foundation.

After the building was completed, a mechanical load of 1300 kN was applied to the foundation head and foundation was heated 13.4 °C. Mechanical, thermal, and combined thermo-mechanical stresses are shown in Figure 2.8. The addition of the thermal load causes the axial stress near the top of the foundation to increase from 1.2 to 2.6 MPa. The greatest increase in axial stress occurs at the base of the foundation. The overall trend in the thermally induced stress

is consistent with an energy foundation that is partially restrained at the head and toe as described using the hypothetical model of Amatya et al. (2012) in Section 2.2.2.

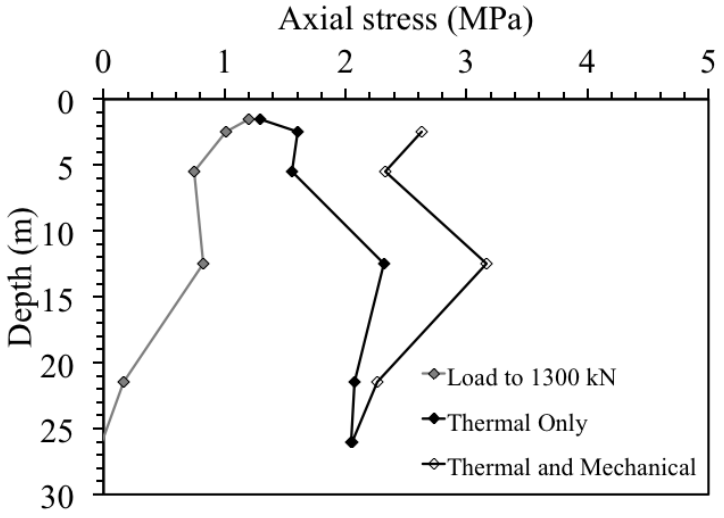

Figure 2.8: Stress profiles for a full-scale energy foundation during loading and after heating by +13.4 °C (after Laloui 2011)

2.2.4. In-situ Energy Foundation at Lambeth College, UK

Bourne-Webb et al. (2009) reported the results from a series of thermo-mechanical loading tests on an energy foundation at Lambeth College, UK. These test results were further investigated by Amatya et al. (2012). The energy foundation under investigation had a diameter of 0.56 m and a length of 23 m, and contained three heat exchanger loops. The upper 4 m of the foundation was embedded in sandy granular fill and the lower 19 meters was socketed in stiff, fissured silty clay. The groundwater table at the site was approximately 3 meters below grade. The energy foundation contained a series of optical fiber sensors (OFS) to measure strain and temperature at various depths. A load frame was used to load the energy foundation axially to 1200 kN before investigating various heating and cooling scenarios. The top boundary condition of the test foundation is load controlled, allowing the foundation to move as the load cell adjusts to maintain the constant load.

The time series of loading and thermal cycles is presented in Figure 2.9. The axial load profile for mechanical loading under ambient ground temperatures is shown in Figure 2.10 and also shows thermo-mechanical loads during heating to $\Delta T = +10$ °C and to cooling to $\Delta T = -19$ °C. An initial mechanical loading test was performed to measure the strain in the foundation with the absence of any thermal effects. The behavior observed in Figure 2.10 indicates that the load sheds with depth, but the toe is relatively soft, and free to move downward. During cooling coupled with the 1200 kN mechanical load, the overall stress in the energy foundation tended to decrease, with the foundation encountering tension. As the foundation was heated to +10 °C, the overall stress in the foundation increased, with a maximum measurement of axial load of 1800 kN occurring at a depth of 6.5 meters. The heating and cooling tests demonstrate that heating of the foundation leads to increased compressive axial stress, while cooling relaxes the axial stress in the foundation, causing a decrease in compressive axial stress.

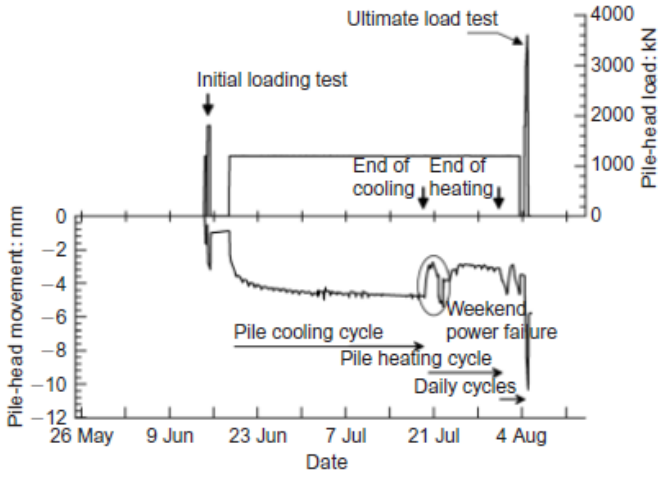

Figure 2.9: Thermally induced foundation displacement and head load time series during heating test (Bourne-Webb et al. 2009) (NOTE: Sign convention of displacement data in figure is opposite the sign convention from this paper, where positive displacements indicate upward movement)

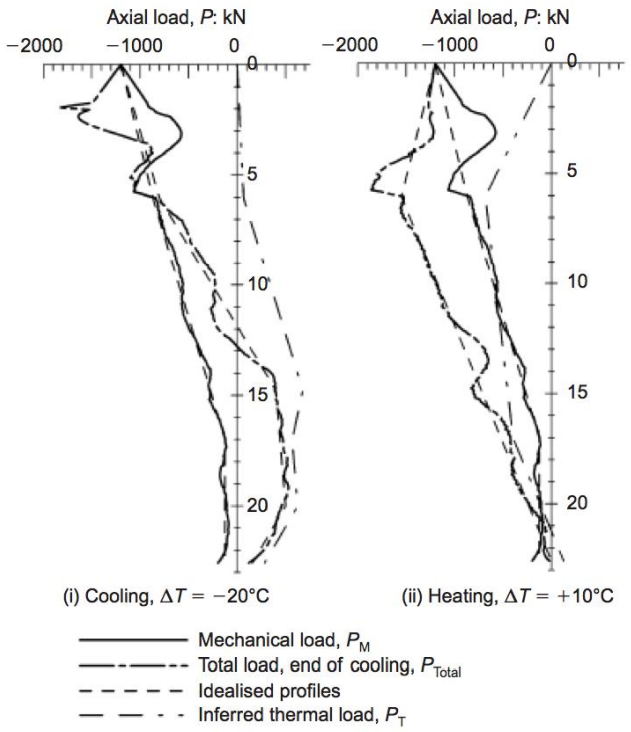

Figure 2.10: Load and temperature induced load profile for a full-scale energy foundation (Amatya et al. 2012) (NOTE: Sign convention of load data in figure is opposite the sign convention from this paper, where negative loads denote compression)

2.2.5. Comparison of Thermo-Mechanical Tests from the Literature

A summary of the details from the two case histories is presented in Table 2.1. The sign conventions for the data presented in this table is consistent with those used in this study, where positive displacements are downward, positive strains denote contraction, and positive stresses denote compression. While both studies involved inducing a thermo-mechanical load, the response of the stress and strain distribution for each study varies. The strain distributions during heating in the absence of a mechanical load for both studies are shown in Figure 2.11. The test foundation at Lambeth College exhibits a very weak end bearing material, while the toe of the foundation at EPFL carries a portion of the thermo-mechanical load (Amatya et al. 2012).

Table 2.1: Details of case histories from Laloui et al. (2006) and Bourne-Webb et al. (2009)

Case	EPFL, Switzerland (Laloui et al. 2006)	Lambeth College, UK (Boume-Webb et al. 2009)
Site stratigraphy	Alluvial soil, sand and gravel, founded in soft sandstone, groundwater table near surface	Granular fill and sand and gravel, founded in stiff fissured silty clay, groundwater table at 3 m.b.g.l.
Foundation type	Piled raft	Single foundation
Foundation length (m)	25.8	23
Foundation diameter (m)	0.88	0.56
Load mechanism at foundation head	Building dead load	Load frame
Max. mech. load during heating test (kN)	0 (T-1), 1300 (T-7)	1200
Range of ΔT (°C)	+20.9 (T-1), +13.4 (T-7)	-19, +29.4
Location of min. thermally induced Strain after heating (m)	21	17
Max. rate of increase of axial stress (kPa/°C)	104	192

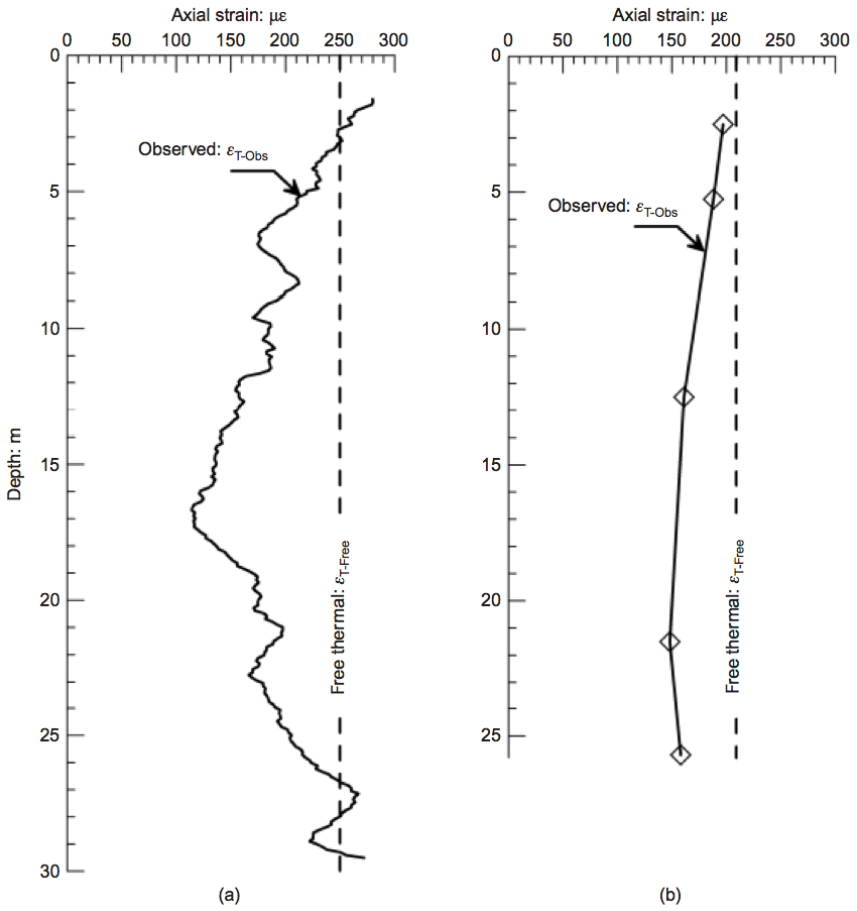

Figure 2.11. Observed free thermal strain profiles due to heating: (a) London heat sink pile ΔT = +29.4 °C; (b) EPFL energy foundation test T-1, ΔT = +20.9 °C (Amatya et al. 2012)

The thermal axial stress of each test foundation is plotted versus an average change in temperature, shown in Figure 2.12. In both cases, a nearly linear increase in axial stress is shown for increasing temperature. If each of the test foundations were completely restrained from deformation at the top and bottom, the theoretical stress increase due to heating would have been 340 kPa/°C and 292 kPa/°C for the Lambeth College and EPFL cases, respectively. Since the stress increase is less than the theoretical values, foundation movement in each case did occur and indicates partial restraint.

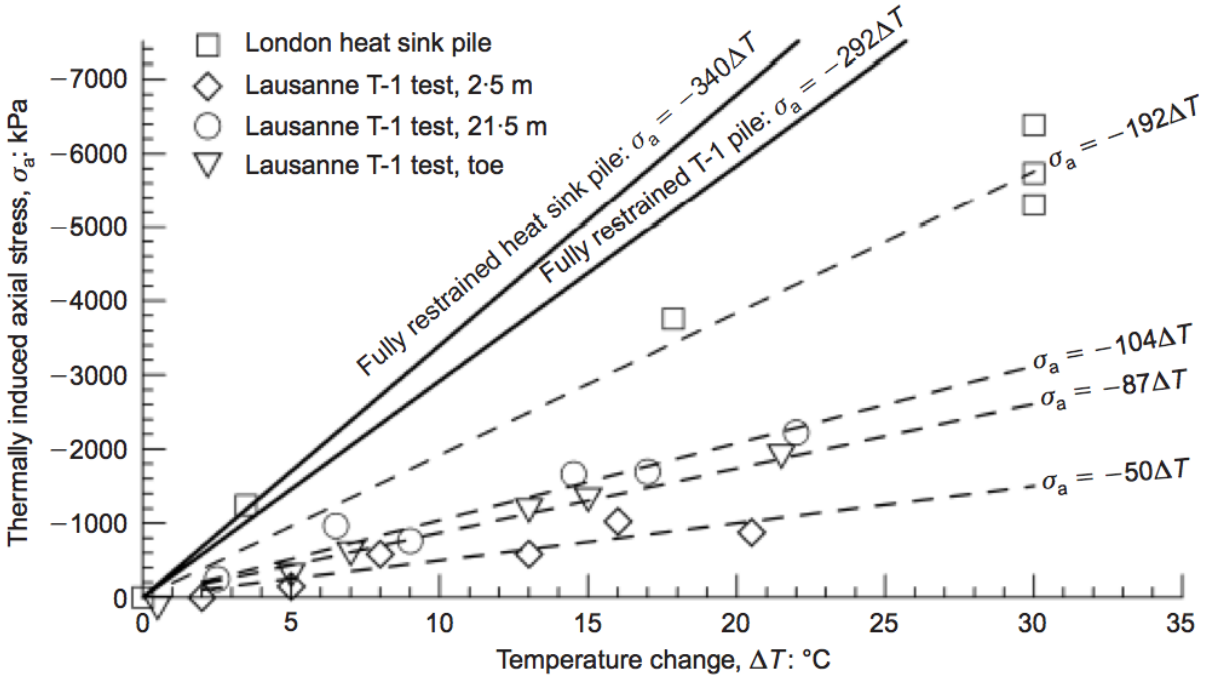

Figure 2.12: Thermally induced axial stress during heating for different energy foundations reported in the literature (Amatya et al. 2012) (NOTE: Sign convention of load data in figure is opposite the sign convention from this paper, where negative stresses denote compression)

2.3. Thermo-Mechanical Design Practices

Design of energy foundations in previous years has mainly relied on empirical and conservative approaches to account for additional axial stresses induced during heating and cooling. Recently, researchers have developed numerical models to account for thermal loads in the foundation in addition to mechanical loads from the overlying structure (Burlon et al. 2013; Mimouni and Laloui 2013). Numerical models have the capability of incorporating boundary conditions and temperature variations to gain a thorough understanding of the anticipated foundation displacements and stresses that will be generated during mechanical and thermal loading.

Typically numerical models utilize a load transfer method used to compute stress, strain, and displacement. This involves separating deformations into an elastic portion from mechanical

loading and a thermal portion from heating or cooling operations. Several iterations are conducted to obtain force balance in the energy foundation then the vertical displacement and stress at any depth can then be determined. Numerical modeling of specific site conditions can be used to construct design charts to anticipate the head load and displacement for a given foundation head stiffness and temperature change. An example of an energy foundation design chart is shown in Figure 2.13. The chart shows that for increasing head stiffness at a given change in temperature, head settlement will decrease but the load generated will increase. An issue with this design approach is that definition of the head stiffness may be complex. At the moment, the only approach to obtain the head stiffness is to measure the thermal axial strain distributions using embedded instrumentation. A load-transfer analysis such as that of Knellwolf et al. (2011) can be used to estimate the head stiffness to match the observed strain profile.

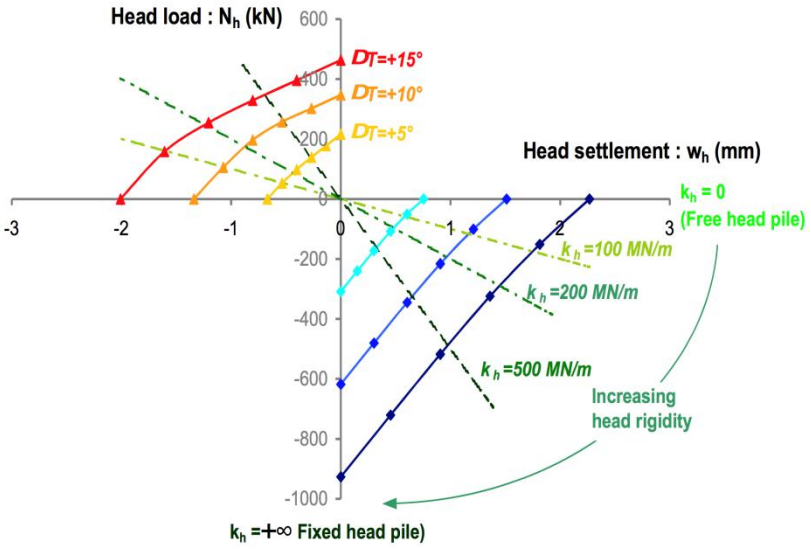

Figure 2.13: Thermo-mechanical design chart for energy foundation (Burlon et al. 2013)

2.4. Thermal Behavior of Energy Foundations

2.4.1. Overview

The thermal behavior and efficiency of energy foundations depends on many factors including material characteristics, site stratigraphy, heat exchanger configuration in each energy foundation, and demands of the building system (Brandl 2006). To optimize design of ground-source heating systems, system thermal conductivity, specific heat capacity, borehole resistance, and heat exchange rate must be evaluated accurately (Sanner 2005). The primary mode of heat transport in the soil surrounding energy foundations is by conduction. The heat transfer from a cylindrical source (i.e., an energy foundation) is given by:

$$\dot{Q} = -2\pi R l \lambda \frac{dT}{dr} \tag{2.4}$$

where $\dot{Q}$ is the heat transfer in Watts being supplied to the energy foundation, R is the radius of the energy foundation, l is the length of the energy foundation, λ is the thermal conductivity of the subsurface surrounding the energy foundation, and dT/dr is the temperature gradient in the radial direction around the energy foundation. As it is often difficult to assess the thermal properties of the individual soil layers and materials in energy foundations such as those in Table 2.2, they are typically characterized using a system value.

Table 2.2: Typical thermal properties for materials used in energy foundations (after Gao et al. 2008)

Material	Thermal Conductivity (W/mK)	Density (kg/m^3)	Heat Capacity (J/kgK)
Concrete	1.6	2500	850
Steel Reinforcement	43	7850	490
HDPE Pipe	0.4	1100	1465
Water	0.58	1000	4180
Ethylene Glycol	0.25	1097	2470

Soil thermal conductivity is strongly influenced by water content, soil density, mineralogy, and chemical properties of the pore water (Brandl 2006). Thermal conductivity ranges for different soils are shown in Table 2.3.

Table 2.3: Typical ranges of thermal conductivity for soils and weak rock (after GSPA Thermal Pile Standard 2012)

Material	Thermal Conductivity (W/mK)
Dry Sand	0.3-0.8
Dry Gravel	0.3-0.4
Peat	0.2-0.7
Dry Clay/Silt	0.4-1.0
Saturated Clay/Silt	0.9-2.3
Saturated Gravel	1.6-2.0
Claystone/Siltstone	1.1-3.5
Saturated Sand	1.5-4.0
Sandstone	1.3-5.1

As fluid is circulated through a heat exchanger system embedded in an energy foundation, heat must flow from the fluid then through several materials before finally being extracted or injected in the surrounding soil. An illustration by Loveridge and Powrie (2012) is shown in Figure 2.14 that shows the geometry and thermal resistances of the different materials surrounding a heat exchanger in an energy foundation. Convection is the main heat flow process in the fluid itself as the fluid flow rate is sufficient to lead to a turbulent flow pattern, while conduction is dominant through the heat exchanger pipe, concrete, and into the ground. As it is difficult to measure the thermal properties of the individual soil layers and materials in energy foundations, they are typically characterized using a system value.

Each component of the energy foundation system possesses a different value of thermal conductivity. Accordingly, the highest temperature gradient will occur across the material with the lowest thermal conductivity. In this case, the HDPE heat exchanger tubing has a low thermal conductivity and contributes most to the borehole thermal resistance, R. As each material is

selected in design, materials with high thermal conductivity may be preferred to reduce temperature loss in the energy foundation, thus increasing heat transfer abilities.

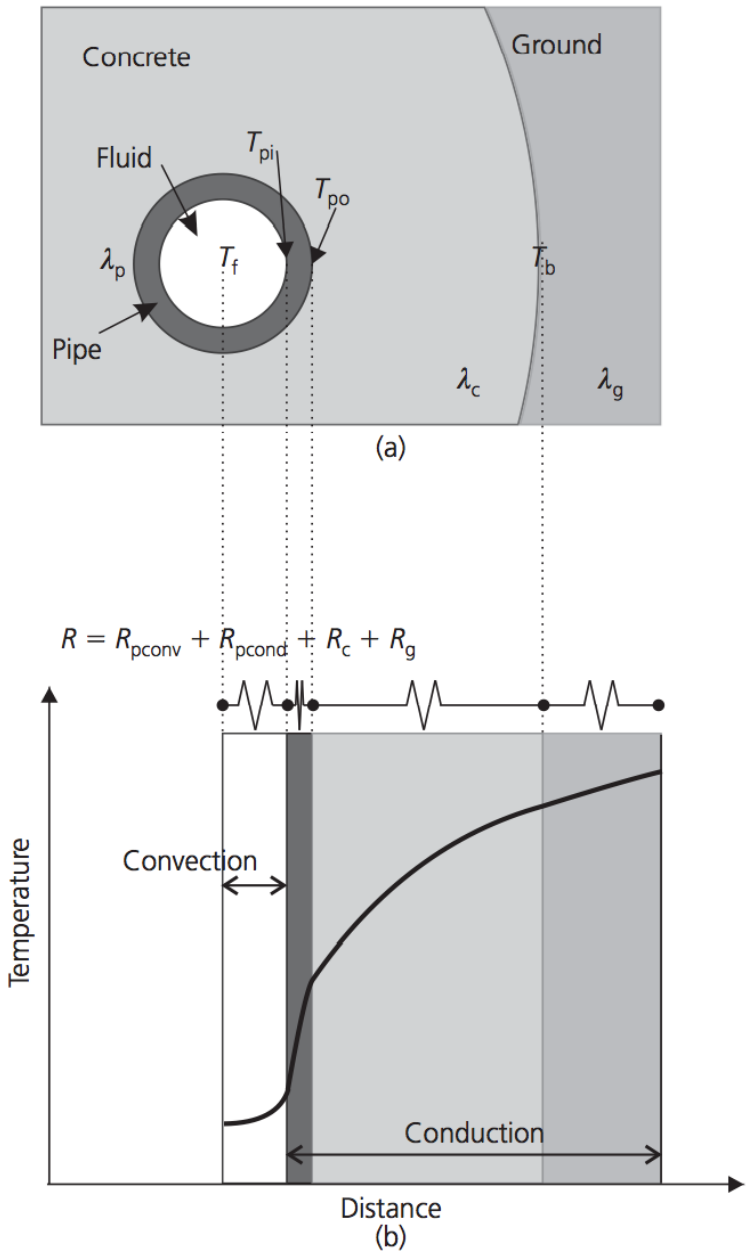

Figure 2.14: Energy foundation heat transfer concepts: (a) plan view of energy foundation components, (b) temperature differences and competent resistances (Loveridge and Powrie 2012)

2.4.2. Heat Pump Response

Several full-scale studies involved the evaluation of heat exchange efficiency in energy foundations during operation of a heat pump (Ooka et al. 2007, Adam and Markiewicz 2009, Wood et al. 2009). Performance of ground source heat pumps can be characterized as the ratio of thermal energy delivered to the system by the heat pump process to the electrical energy input required to operate the heat pump. This is referred to as the coefficient of performance (COP), and can be calculated as follows:

$$COP = \frac{Energy\ output\ after\ heat\ pump\ [kW]}{Energy\ input\ for\ operation\ [kW]} \tag{2.5}$$

A typical COP value for a GSHP is 3 or greater, whereas the COP for an air source heat pump system is in the range of 1-3 (Brandl 2006). A study was conducted by Wood et al. (2009) where twenty one 10 meter deep energy foundations, each with one U-loop, were subjected to the heating demands of a two story structure with a ground floor area of 72 m^2 over the course of the 2007-2008 heating season. The heating load and coefficient of performance from this study are shown in Figure 2.15(a). A relatively steady COP of 3.62 was maintained throughout the duration of the test despite the changes in the heating load applied to the system. Ooka et al. (2007) constructed two 1500 mm diameter by 20 m deep energy foundations near Tokyo, Japan. Each foundation contained eight polyethylene U-tube pairs installed around the perimeter of the foundation. The energy foundations were subjected to heating and cooling to correspond with the summer and winter seasons, respectively. Results from the study showed the COP of the energy foundation system to be 1.7 times higher than that of the air-source heat pump system in operation at the site. A maximum COP of 6.7 was achieved during building cooling (heating of the foundation) and 5.0 during building heating (cooling of the foundation). The COP as a function of time for the GSHP and ASHP at the site are shown in Figure 2.15(b). These cases

demonstrate that energy foundations have good potential to be more energy efficient than air-source heat pump systems.

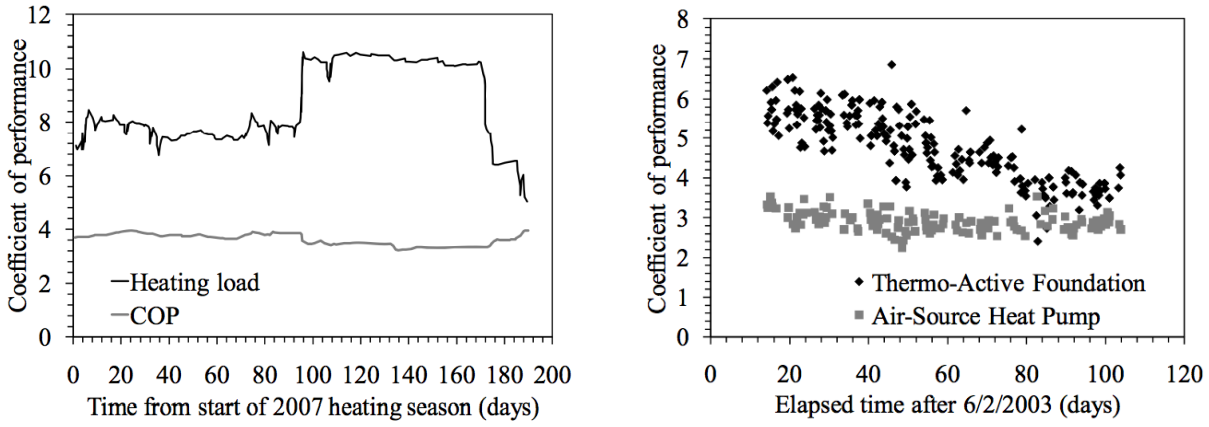

(a) **(b)**

Figure 2.15: Examples of measured variations in coefficient of performance for different ground source heat systems incorporated into test building foundations: (a) Wood et al. (2009); (b) Ooka et al. (2007)

2.4.3. Thermal Response Test

Thermal response tests are the preferred method of determining thermal properties of the subsurface and energy foundation system (Brandl 2006). Thermal response testing of geothermal borehole heat exchangers has been in use for several years (Sanner et al. 2005), and involves circulating fluid through a heat exchanger while supplying a constant amount of power to the fluid. The temperatures of the fluid entering and exiting the foundation are monitored over a period of several days. The history behind the development of testing standards and analysis approaches is described by Sanner et al. (2005) and Loveridge and Powrie (2012). Energy foundations differ from borehole heat exchangers in that the concrete can store heat during a thermal response test, and the geometry of the foundations and embedded heat exchangers do not satisfy the assumptions of most simple thermal response test analyses. The heat exchange characteristics of energy foundations depend on the thermal properties of the different materials and geologic strata, groundwater flow, foundation dimensions, heat exchanger configuration,

thermal response test procedures, and the analysis method.

2.4.4. Thermal Response Test Analysis

Several possible approaches can be used to estimate the thermal properties of the energy foundation-soil system. The most rigorous approach would be to solve Fourier's law considering the boundary conditions and estimating the thermal properties of the different layers using inverse analysis (e.g., Shonder and Beck 1997). However, it may be impossible to find a unique solution for such a complex system. Alternatively, there are several analytical solutions to this equation for different heat exchanger geometries including the infinite or finite line or cylinder sources. The analytical solutions have the shortcoming that the thermal heat capacity of the different materials cannot be considered, which is a relevant issue in the transient heating and cooling of energy foundations (Bourne-Webb 2013).

The measured values of the fluid supply and return temperatures and the mass flow rate through each foundation can be used to calculate the heat flux, as follows:

$$Q = \Delta T \dot{V} \rho_{fluid} C_{fluid} \tag{2.6}$$

where ΔT is the difference between the supply and return fluid temperatures in K (T_{supply} and T_{return}, respectively), $\dot{V}$ is the fluid flow rate in m^3/s, ρ_{fluid} is the mass density of the fluid kg/m^3, and C_{fluid} is the specific heat capacity of the fluid in J/(kgK).

The infinite line source equation is simplest analytical solution to the Fourier's law, acknowledging the fact that the heat exchanger is not a linear element in an infinite media. The line source method involves prediction of the change in temperature of a medium surrounding a line heat source with constant heat input energy. The change in temperature of medium at a radial distance of r away from the line source will depend on the thermal conductivity of the surrounding material, as follows:

$$T(t,r) = -\frac{Q/L}{4\pi\lambda} Ei\left(-\frac{r^2}{4\alpha t}\right) \quad (2.7)$$

where r is the distance from the source in meters, Q/L is the heat input energy per unit length (W/m), λ is the effective thermal conductivity in W/mK, α is the effective thermal diffusivity, and t is the time from the initiation of heating. The function Ei is the solution to the following integral, which can also be presented in a linearized form for small values of r, as follows:

$$-\mathrm{Ei}(-\mathrm{x}) = \int_{\mathrm{x}}^{\infty} \frac{\mathrm{e}^{-\mathrm{t}}}{\mathrm{t}} \mathrm{dt} \cong -0.58 - \ln(x) \quad (2.8)$$

After inserting Eq. (2.8) into Eq. (2.7), the following linearized version is obtained:

$$T(t,r) = -\frac{Q/L}{4\pi\lambda}\left[0.58 + ln\left(\frac{r^2}{4\alpha t}\right)\right] \quad (2.9)$$

the differential form of Eq. (2.9) can be rearranged to define the system thermal conductivity, as follows:

$$\lambda_{app} = \frac{Q}{4\pi L}\left[\frac{dT}{d(\ln t)}\right]^{-1} \quad (2.10)$$

where λ_{app} is the apparent thermal conductivity of each foundation, L is the effective length of each foundation system which represents the distance from the heat source to the tip of the foundation, and the term in brackets represents the slope of the change in mean fluid temperature versus logarithmic time. It is important to calculate this slope after the slope has stabilized, as the differential form of the line source equation does not consider the impact of heat capacity of the line source (i.e., the energy foundation) on the transient heating response.

2.4.5. Energy Foundation Thermal Performance

The heat exchange response of an energy foundation in a building depends on the heating or cooling load applied by the heat pump (Sanner 2001). Loveridge and Powrie (2012) and

Bourne-Webb (2013) collected data from a number of studies and observed that foundations with a low length to diameter ratio have a greater heat flux per unit meter, shown in Figure 2.16. Further, transient heating tests lead to a greater heat flux per unit meter than steady-state heating tests due to the thermal mass of the concrete, which has a higher specific heat capacity than the surrounding soil. A comparison of transient and steady state heat transfer potential observed by Bourne-Webb (2013) is shown in Table 2.4, where heating and cooling modes refer to building heating and cooling, respectively.

Table 2.4: Heating and cooling potential comparing transient and steady-state thermal loading (Bourne-Webb 2013)

Thermal loading	Heat transfer, W/m	
	Cooling mode	Heating mode
Transient	70 – 120	50 – 85
Steady-state	25 – 60	15 – 25

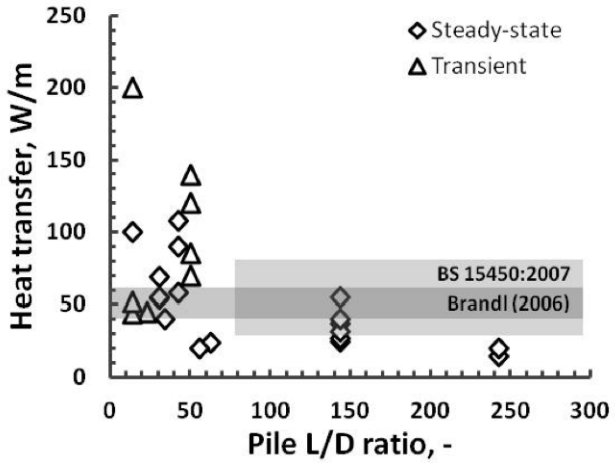

Figure 2.16: Observations of heat transfer for energy foundations compared with recommended values for borehole heat exchangers and foundations < 0.5 m diameter (Bourne-Webb 2013)

Several studies have been performed to investigate the thermal behavior of full-scale energy foundations in different soil types with various heat exchanger loop configurations and foundation geometries. The observations from these studies are as follows:

- Hamada et al. (2007) performed thermal response tests on a series of 26 driven piles with 1 and 2 U-loop configurations. The foundations were cooled over the course of 131 days and produced a heat exchange rate varying from 54 W/m for a single U-loop to 69 W/m for the indirect double pipe configuration.
- Ooka et al. (2007) performed thermal response tests in heating and cooling modes on two energy foundations with lengths of 20 m and diameters of 1500 mm. both with 8 U-loops. Results from the study indicated that heat rejection into the foundations produced significantly higher heat exchange rates than heat extraction. As heat was injected into each foundation, the heat exchange rate of 100-120 W/m was achieved, compared to 44-52 W/m in heat extraction mode.
- A study by Gao et al. (2008) investigated the efficiency of energy foundations with different heat exchanger configurations using field testing and numerical analysis. Experimental results indicated that greater numbers of heat exchanger loops lead to higher heat exchange rates. A numerical simulation was also conducted to determine soil thermal conductivity and temperature distribution surrounding the foundation system based on results from field testing.
- Lennon et al. (2009) conducted thermal response tests to compare the thermal performance of steel and concrete pipe piles during heating. Results indicated that steel pipe piles have a lower borehole resistance than concrete piles. Soil thermal conductivity from both piles was determined using the line source equation and produced values of 2.56 W/mK and 2.37 W/mK for concrete and steel piles, respectively.
- Brettmann and Amis (2011) conducted a series of thermal response tests on three auger cast in place foundations, each 18.3 m deep with 2 U-loops. A heating test of the three

foundations was conducted over the course of 8 days. Thermal conductivity calculations based on each of the foundation temperatures during the duration of the test yielded values of 2.5-2.6 W/mK using the line source TRT analysis method.

Details of each study are presented in Table 2.5. It is clear that the values of thermal conductivity are greater than those of most geological materials (Farouki 1981), which indicates that the thermal conductivity values from the TRT may be overestimated due to the heat storage capacity of the concrete.

Table 2.5: Summary of TRT results from the literature

Case	Hamada (2007)	Ooka (2007)	Gao (2008)	Lennon (2009)	Brettmann (2011)
Foundation type	26×D.P.	2×D.S.	1×D.S.	4×D.P.	3×A.C.I.P.
Foundation length (m)	9	20	25	12-17	18.3
Foundation diameter (mm)	300 (square)	1500	600	244 (round), 270 (square)	300-450
# Heat Exchanger Loops	1,2, Indirect/ Direct Pipe	8	1-3	1	2
TRT Analysis Method	N/A	N/A	Num. Method	Line Source	Line Source
Thermal Conductivity (W/mK)	N/A	N/A	5.8-6.0	2.4-2.6	2.5-2.6
Heat Exchange Rate (W/m)	54-69 (ext.)	100-120 (rej.) 44-52 (ext.)	57-108 (rej.)	N/A	73-80 (rej.)

***Note: Cases are listed by first author only.**
****D.S.: Drilled shaft, A.C.I.P.: Auger cast in place pile, D.P.: Driven Pile**
***** Rej.: Heat rejection into foundation, Ext.: Heat extraction from pile**

2.4.6. Thermal Design

The thermal design of energy foundations largely depends on building type, usage, climate, properties of the soil, and the presence of groundwater (GSHPA 2012). Since deep foundations are expensive to construct, it is typical that a designer will estimate the thermal

capacity of the energy foundation system then compensate for the remainder of the thermal demands of the building with an auxiliary heating and cooling system. In some cases, the energy foundations may be able to support the heating and cooling demands for the entire structure. Estimation of the thermal output of energy foundations requires an estimation of initial ground temperature, thermal conductivity and diffusivity of the soil, thermal storage capacity of the reinforced concrete, and demands of a given heat pump. In some cases, it may prove cost effective to perform a thermal response test on a small diameter borehole over the depth of the energy foundation prior to construction to obtain soil thermal properties. Additionally, a designer may account for losses that occur in the horizontal portion of tubing required to connect the energy foundation system to the manifold. A flow chart for a general energy foundation design is presented in Figure 2.17.

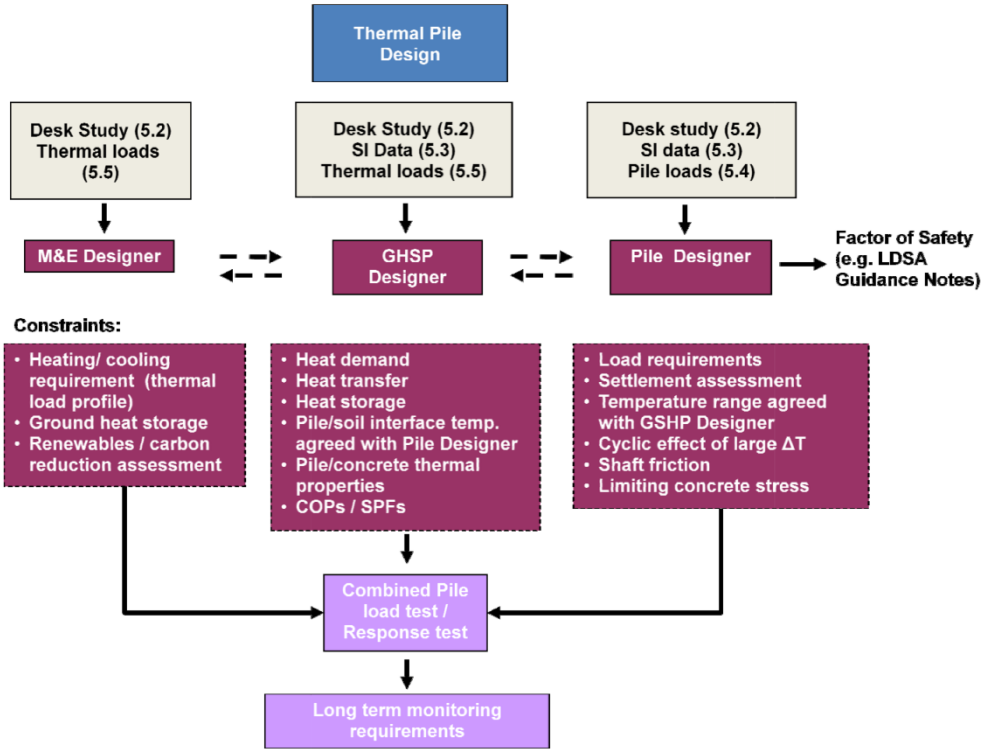

Figure 2.17: Energy foundation design approach (GSPA Thermal Pile Standard 2012)

3. PROJECT DESCRIPTION

3.1. Denver Housing Authority

3.1.1. Building Description

Two of the sixty drilled shaft foundations installed as part of the construction of the new Denver Housing Authority senior residential facility, in Denver, Colorado, were converted into energy foundations as part of this study. The two energy foundations were coupled into a conventional ground-source heat pump (GSHP) system which was already being incorporated into the building. The conventional GSHP system consists of forty 102 mm diameter boreholes, each extending to depths of 143 m below grade, drilled in a parking lot outside of the building footprint. A heat exchanger loop, composed of 44 mm-diameter polyethylene tubing formed in a U-shape, was installed into each borehole. The boreholes were backfilled with sand-bentonite grout after placement of the heat exchanger tubing. A heat pump is used to absorb or reject heat into fluid circulating through the heat exchanger tubing.

The network of borehole heat exchangers in the conventional GSHP system is capable of providing approximately 263.5 kW-hr (75 thermal tons) to the heat pump, which is sufficient to provide the peak heating and cooling load for the building. To absorb this thermal load, the heat pump was designed to circulate a supply line fluid temperature through the borehole network of 32.2 °C during cooling operations or 1.7 °C during heating operations. The fluid within the heat exchange system consists of a 10% methanol-water mixture to prevent freezing during building heating operations. The supply and return lines from the borehole field are connected through a set of two manifolds that run to the inlet and outlet lines of the heat pump. In order to avoid preferential flow through the heat exchangers in the energy foundations (which are much shorter than the deep boreholes), the flow of heat exchanger fluid to the energy foundations was restricted to approximately 50% using ball valves.

3.1.2. Subsurface Conditions

A series of 10 exploratory borings extending to depths ranging from 8.8 m to 11 m below finished grade was performed throughout the site. The conditions encountered in each of the borings were similar, with a typical profile shown in Figure 3.1. Urban fill extends from grade to a depth of approximately 3 m and consists of slightly moist, medium dense, clayey sand with gravel. Beneath the fill, a layer of non-expansive, medium dense, sand and gravel with silt seams extended to a depth of approximately 7.6 m below grade. Below this layer, to the maximum depth explored of 11 m, the subsurface conditions consisted of hard sandy claystone bedrock from the Denver formation. The characteristics of the soil layers measured during the site investigation are listed in Table 3.1. These results indicate that the urban fill layer is relatively soft, while the sand and gravel layer is stiffer. Swell potential tests on the fines fraction indicates that they are non-expansive. Perched groundwater was encountered in three of the ten boreholes at depths ranging from 6.4 m to 8.2 m below grade level. Because of the potential for caving during drilling through the overburden and possible perched ground water conditions, a cased-hole method was chosen for installation of the drilled shaft foundations at the site.

Table 3.1: Soil Properties at the Denver Housing Authority Site

Soil Layer	Depth m.b.g.l.	SPT N-Value (blows/300 mm)	Gravimetric water Content (%)
Urban Fill	0 m – 3 m	8	12
Sand and Gravel	3 m – 4.6 m	22	5
Claystone	7.6 m +	50/10”	N/A

3.1.3. Energy Foundation Descriptions

Profiles of the two energy foundations evaluated in this study along with the different soil and rock strata are shown in Figure 3.1 while a plan view of the foundation layout showing the location of the two energy foundations is shown in Figure 3.2. Foundation A is located below an

interior column while Foundation B is located directly under an exterior wall. Foundations A and B both have a diameter of 910 mm and extend to depths of 14.8 m, and 13.4 m, respectively, and are bearing in the Denver formation (claystone). The foundations at the site function as rock-socketed, end-bearing elements in the bedrock. Foundation A is expected to carry a load of 3.84 MN and Foundation B is expected to carry a load of 3.65MN. Although the rock socket for Foundation B is shorter than that of Foundation A because of difficulty in drilling in the wet claystone, both are within their design depth tolerance set by the structural engineer. Each shaft contains a full-length reinforcing cage 760 mm in diameter with nine #7 (22 mm) vertical reinforcing bars tied to #3 (9.5 mm) lateral reinforcing hoops spaced 0.36 m on center. A reinforced slab on grade with a thickness of 150 mm was cast at grade level.

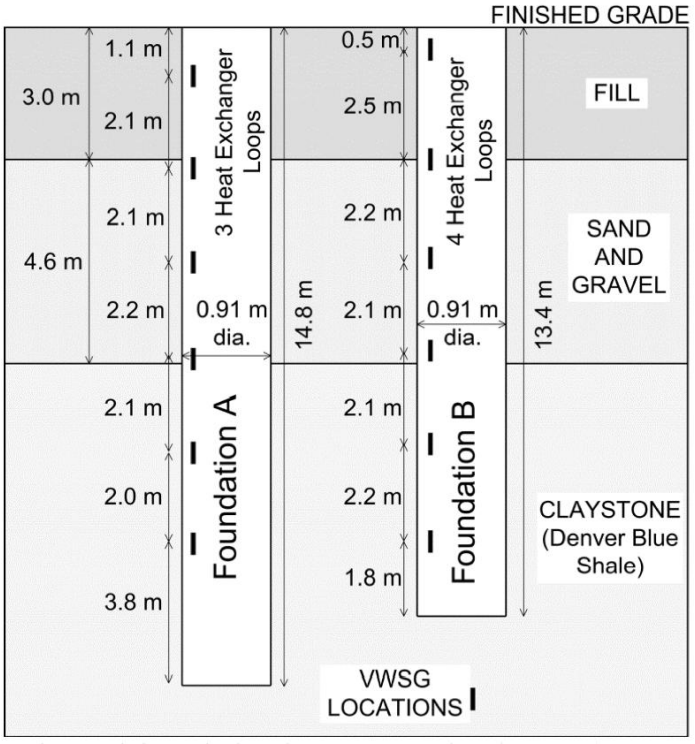

Figure 3.1: Soil stratigraphy and instrumentation layout at DHA

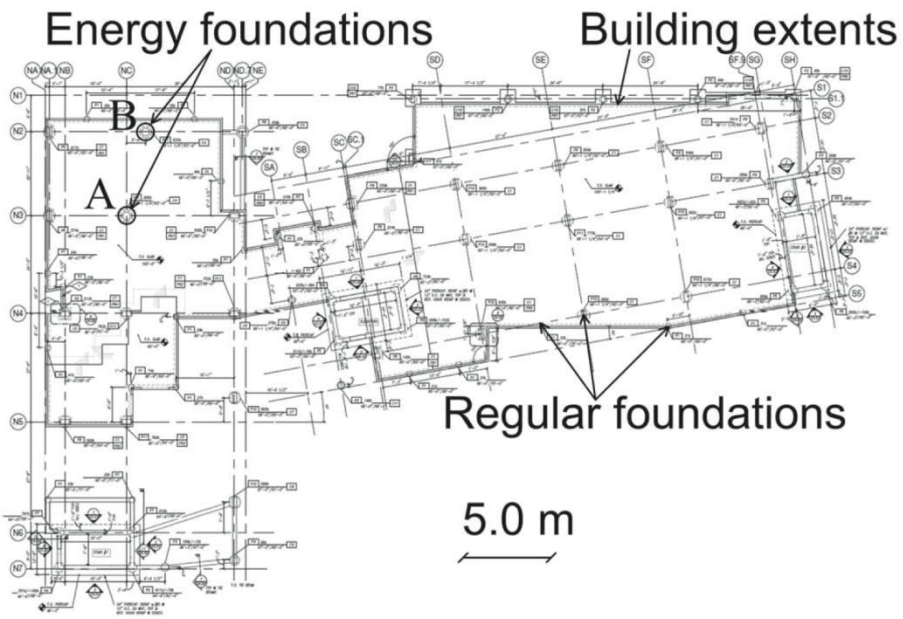

Figure 3.2: Plan view of building extents and locations of energy foundations

The energy foundations were coupled with a traditional deep borehole geothermal system that was already being installed to provide heating and cooling for the building, in order to demonstrate the feasibility of energy foundations. The heat exchanger system in each energy foundation consists of 44 mm diameter polyethylene tubing attached to the inside of the reinforcing cages. Foundation A contains a total of 82.3 linear meters of tubing configured into three loops running the length of the reinforcing cage, as shown in Figure 3.3(a). Similarly, Foundation B contains of a total of 109.7 linear meters of polyethylene tubing arranged in four loops running the length of the reinforcing cage, shown in Figure 3.3(b).

The heat exchanger tubing was attached to the interior of the reinforcing cage using wire ties connected at every other hoop along the length of the reinforcing cage. The heat exchanger tubing was routed along the inside perimeter of the reinforcing cage to avoid crossing the diameter of the cage, which could block concrete flow or cause segregation of concrete. Equal angular spacing of the tubing was maintained to provide relatively uniform temperature along the

circumference of the shafts. The tubing was installed away from the vertical reinforcement to guarantee an adequate bond between the concrete and reinforcement and to ensure good contact between the concrete and the tubing itself. The supply and return lines for each loop were arranged on opposite sides of the reinforcing cage to reduce thermal short-circuiting, which occurs when heat flows directly from the inlet of the loop to the outlet of the loop before the fluid has circulated through the entire energy foundation.

(a) **(b)**

Figure 3.3: Heat exchanger tubing attached to reinforcement cages: (a) Foundation A, (b) Foundation B

3.1.4. Instrumentation

An instrumentation system was incorporated into the two foundations to monitor the distributions of temperature and axial strain with depth, as well as the supply and return temperatures of the heat exchanger fluid. Six vibrating wire concrete-embedment strain gauges were installed in each energy foundation at the locations shown in Figure 3.1. The concrete embedment vibrating wire strain gauges (VWSG) (Model 52640299 from Slope Indicator of Mukilteo, WA) were oriented longitudinally and attached to the lateral reinforcing hoops then cast in concrete during construction. The VWSGs were positioned at depths within the shaft so that the cumulative strain distribution throughout the entire shaft length could be characterized.

Each VWSG contained a thermistor to monitor temperature in the concrete at each sensor location. Cables from each sensor were routed from the energy foundations to the mechanical room prior to casting of the floor slab. A Geokon, Inc. datalogger (Model 8002-16 LC-2×16) was used to record data hourly from December 29, 2011 to April 18, 2012. During installation, a VWSG located at 3.2 m below grade in Foundation A was damaged. Although the VWSG at this depth did not function, the corresponding thermistor remained operational. In addition to the instrumentation in the foundations, four pipe-plug thermocouples were installed in the plumbing manifold to record inlet and outlet fluid temperatures for each of the two energy foundations. Fluid temperature measurements were recorded every five minutes using Lascar EL-USB-TC data loggers to capture the intermittent and long-term operations of the heat pump and the energy foundations.

3.2. U.S. Air Force Academy

3.2.1. Building Description

A one-story, shower-shave building was constructed at the Field Engineering and Readiness Laboratory (FERL) of the US Air Force Academy (USAFA) beginning March, 2012. At the time of this publication, the building is not yet in service (the interior plumbing and drywall is being installed). The building will provide men's and women's restrooms, showers, and laundry facilities for USAFA cadets and other military personnel training at the FERL site. One purpose of the building is to evaluate the performance of energy efficient technologies to aid in the development of "net zero" energy consuming structures for the U.S. Department of Defense (DoD). These technologies include energy foundations, a radiant in-floor heating system, solar photovoltaic panels, and a solar water heating system. Each component will be continuously monitored to evaluate the energy usage or output of each technology. In addition to

the ground-source heat pump coupled with the energy foundations, the building contains a conventional gas-powered heating system. Having both conventional and ground-source HVAC systems permits comparison of their energy efficiencies under similar environmental conditions.

3.2.2. Subsurface Conditions

A site investigation was performed in September 2011 (Hernandez 2011), which consisted of two 102 mm-diameter borings located within the building footprint, extending 12 and 7 m below the ground surface. At selected intervals, disturbed samples were obtained by driving split-spoon with a 622.75 N hammer falling 762 mm. Penetration resistance measurements were made during driving. Exploration results from both boreholes were similar and showed three prominent strata, and relevant data is shown in Table 3.2. The top layer is approximately 1 m thick and consists of sandy fill. Beneath the fill is a very dense 1 m-thick sandy gravelly layer. The bedrock is comprised of Dawson-Arkose sandstone that extends to the maximum depth explored. No groundwater was encountered during the site investigation or foundation installation, so it is assumed to be at a depth greater than 16 m. The engineering properties measured include water content, grain size distribution, dry unit weight, consolidation/expansion, and plasticity index. Lab tests indicate that all materials are non-plastic and non-expansive.

The geology at the site was also reported by Hernandez (2011). The project site is located within the Colorado Piedmont section of the Great Plains physiographic province, characterized by relatively flat uplands and broad valleys. Surficial geologic conditions indicate that the site is overlain by colluvium of recent age, Lehman Ridge Gravel of Pleistocene age, and the Dawson-Arkose Formation of the upper Cretaceous age. The colluvium consists of coarse-grained sand, pebbles, and some boulders. The Lehman Ridge gravel is composed of pebble-size fragments of

Pikes Peak Granite ranging in size from silt to very large boulders. The Dawson-Arkose Formation is a coarse sandstone that contains hard, sandy ironstone layers that cap erosion remnants. Cross-bedding and cut-and-fill channel deposits are characteristic of sandstone in the area.

Table 3.2: Summary of stratigraphy encountered during subsurface exploration at USAFA

Layer	Depth to bottom of stratum (m)	Material encountered	SPT N-value (blows/300 mm)	Gravimetric water content (%)	Dry unit weight (kN/m^3)
1	1	Sandy fill with silt and gravel	70	5	18.4
2	2	Dense sands, silt, and gravel	85	7	19.2
3	12+	Silty sandstone	50/25.4 mm	N/A	N/A

3.2.3. Energy Foundation Descriptions

Eight drilled shafts, each 15.2 m deep by 0.61 m diameter, provide the foundation support for the structure. The one-story building could have been constructed with a slab-on-grade foundation, so the main purpose of incorporating the drilled shafts into the building was to evaluate the thermo-mechanical response of the energy foundations for this research project. Each foundation contains a 0.46-m-diameter steel reinforcing cage that extends the full length of the shaft. The reinforcing cages are composed of six #7 longitudinal bars with #5 radial hoops spaced at 0.3 m on center throughout the length of the cage. The top of the shafts are spliced into a 0.91 m-deep by 0.61 m-wide grade beam that extends around the perimiter of the building. The drilled shafts were constructed using the dry hole method as the subsurface material was competent enough to avoid sloughing and no groundwater was present. Each foundation contains a heat exchanger loop system to exchange heat with the adjacent soil for the purpose of improving heating and cooling efficiency of the building. The loops consist of 19 mm-diameter

HDPE tubing that are plumbed into a manifold located in the mechanical room. At the top of each foundation, which is 1 meter below grade, the heat exchanger loop is connected with tubing which is routed through the grade beam into a manifold within the mechanical room of the building. Photos of construction are shown in Figure 3.4.

Figure 3.4: Construction photos: (a) Reinforcing cages with heat exchangers; (b) Inside view of cage; (c) Vibrating wire strain gauge; (d) Lifting with 3-point pick; (e) Lowering into uncased hole; (f) Concrete tremie; (g) Finished foundation; (h) Tubing in grade beam; (i) Completed grade beam and heat exchanger manifold

Figure 3.4(a) and 3.4(b) show pictures of the reinforcing cages and heat exchangers for the energy foundations evaluated in the heat response study. The heat exchange tubing was attached to the inside of the reinforcing cages with zip-ties at a distance of at least 70 mm from each vertical reinforcing member. The inlet and outlet tubes were seperated diametrically by at least 90°, which minimizes thermal short circuiting where heat is lost by direct transmission from the inlet to outlet tubes. U-shaped couplings were used to connect the inlet and outlet tubes so that the tubing does not cross the bottom of the cage. Cables for the instrumentation embedded in the foundation [Figure 3.4(c)] were bundled at the top of the cage until placement in the uncased hole. The reinforcing cages were lifted with a 3-point pick to minimize bending [Figure 3.4(d)], and the cages were lowered into the hole with a crane [Figure 3.4(e)] and were suspended on wooden beams to ensure that the top of the cage was at the base of the grade beam. Although efforts were made to clean the shafts, it is possible that some loose sandstone debris remained at the bottom of the holes. A concrete pump truck was used to place high-slump 21 MPa concrete in the holes following placement of the reinforcing cages. A tremie pipe was used to avoid excessive segragation of the concrete during free-fall [Figure 3.4(f)]. The use of the tremie also minimized the risk of damage to the heat exchanger loops and embedded instrumentation. The grade beam was constructed around the foundations [Figure 3.4(g)], and the heat exchangers were routed through the grade beam [Figure 3.4(h)] into a manifold in the utility room [Figure 3.4(i)].

Each shaft has either one, two, or three heat exhanger loops configured in different ways, (Figure 3.5). Foundations 1 through 4 have identical heat exchanger configurations, with two continuous heat exchanger loops attached to the inside of the steel reinforcement cage. Foundation 5 has three individual loops; each having a supply and return line running to the

mechanical room; this permits any combination of the loops to be operational in order to evaluate the efficiency of multiple loops in a single foundation. Foundation 6 has three continuous heat exchanger loops with only one supply and return line extending to the manifolds. Foundation 7 contains one loop connected to the interrior of the reinforcing cage. Foundation 8 has a single loop in the center of the foundation to simulate a retrofit where a heat exchanger would be inserted into a corehole bored into an existing foundation. This was constructed with a 100 mm-diameter plastic sleeve in the center of the foundation. After curing, a single heat exchanger loop was inserted into the plastic sleeve and the hole was grouted with sand bentonite grout.

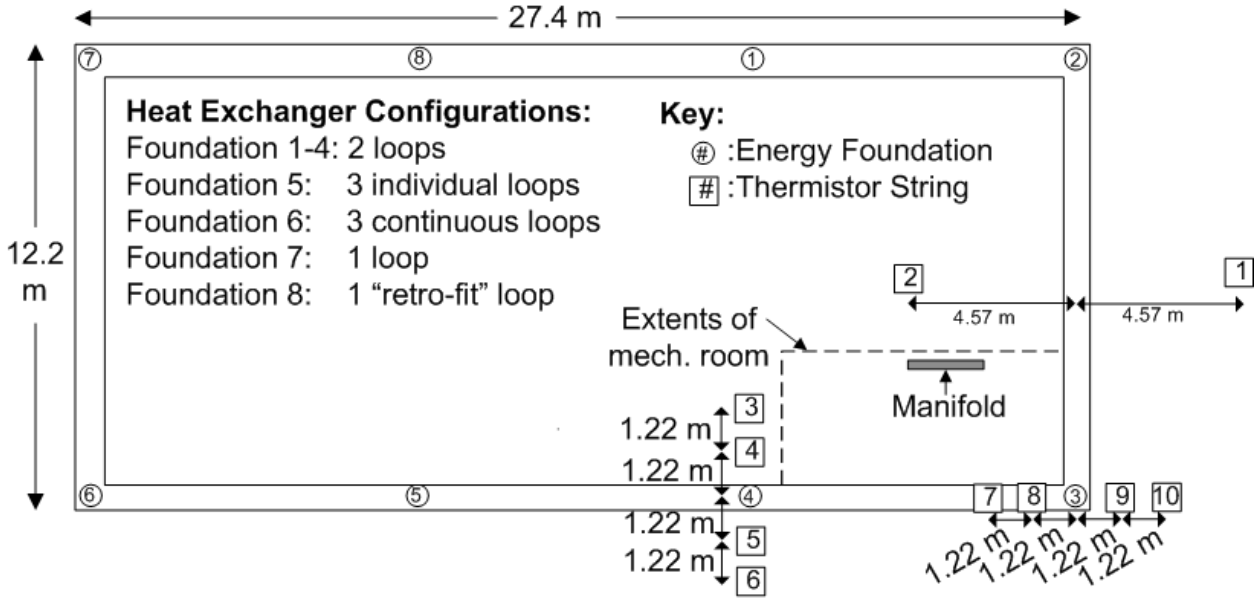

Figure 3.5: Heat exchanger loop configurations in the different energy foundations at USAFA

3.2.4. Instrumentation

Instrumentation was incorporated into three of the eight energy foundations to capture the distribution of axial strain and temperature with depth (Figure 3.6). Foundations 1 and 3 contain six Geokon Model 4200 vibrating wire strain gauges (VWSGs), while Foundation 4 contains

twelve. Foundation 4 has twice the number of gauges with the intent of capturing a more robust strain and temperature distribution along the length of the shaft. At three locations within Foundation 4, gauges were located at the same depth on opposite sides of the reinforcing gage to gain redundancy in temperature and strain readings and to capture any differential strain measurements across the width of the shaft. All of the gauges were oriented vertically and attached to brackets welded to longitudinal steel reinforcing bars, as shown in Figure 3.4(c). The sensor cables were routed to the mechanical room where they are connected to the data acquisition system.

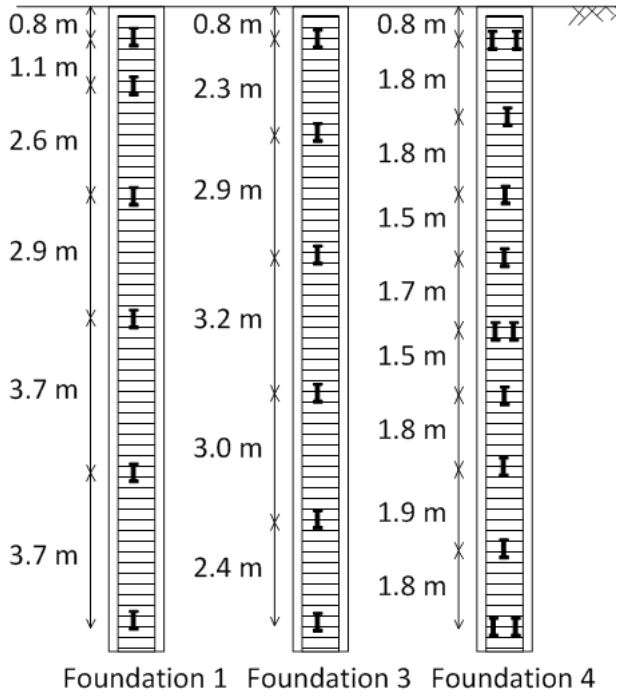

Figure 3.6: Locations of instrumentation in drilled shafts at USAFA

Temperature variations in the soil surrounding the energy foundations are monitored using a series of ten Geokon model 3810 thermistor strings that each have six sensors, installed in boreholes that were then backfilled with CETCO high thermal conductivity grout at the locations shown in Figure 3.5. The temperature around Foundations 3 and 4 are monitored using four thermistor strings each, another thermistor string lies beneath the floor slab to observe any

long-term changes in the ground temperature beneath the slab, and one thermistor string is located outside the building footprint to observe seasonal variations in ground temperature.

3.2.5. Heating Test at USAFA to Investigate Thermo-Mechanical Behavior: Phase 1

A heating test was conducted to evaluate the thermo-mechanical response of Foundation 4. A schematic of the heating system is shown in Figure 3.7. A 125-liter reservoir was first filled with a 20% propylene glycol-water mixture. This heat exchange fluid was circulated through a 12 kW tankless hot water heater using a submersible pump. The heated fluid passed into the inlet port of the heat exchanger tubing, circulated through the foundation, then passed back out of the outlet port. A flow rate of 6.25 L/min was measured from the outlet line at a fluid temperature of 30 °C. During this process, the inlet and outlet temperatures of the heat exchanger fluid were continuously monitored using pipe plug thermocouples installed in the manifold connected to the foundations.

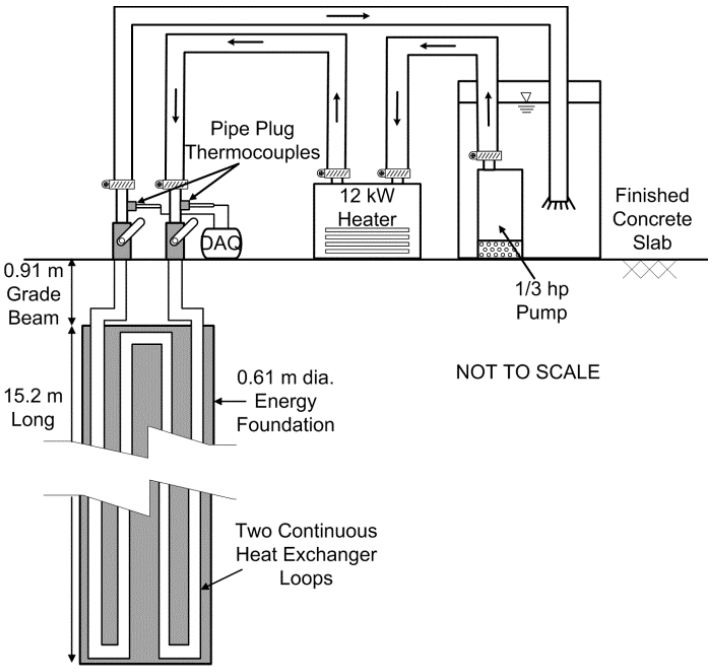

Figure 3.7: Schematic of heating setup for in-situ thermo-mechanical test at USAFA

3.2.6. Heating Test at USAFA to Investigate Thermo-Mechanical Behavior: Phase 2

A second phase of testing was conducted to investigate the thermo-mechanical behavior of Foundations 1, 3, and 4 simultaneously. An 11 kW Precision Geothermal Geocube™ TRT unit was used in this portion of testing. The heated fluid passed into the supply header, circulated through the foundations, and then passed out of return header back to the test unit. The flow rate of each foundation was measured at one instance during the test on each foundation from the pressure/temperature ports (P/T ports) using a differential pressure meter at a fluid temperature of 30 °C. The differential pressure was then used to compute the flow. During the test, the inlet and outlet temperatures of the heat exchanger fluid for each foundation were continuously monitored using pipe plug thermistors installed within ports on the manifold.

3.2.7. Heating Test at USAFA to Investigate Impact of Horizontal Runout Length on Thermal Response of Energy Foundation System

This portion of the study focuses on the thermal behavior of Foundations 1 through 4, which have identical heat exchanger configurations. Each has two continuous heat exchanger loops arranged in a W-shape. Each of the four shafts contain a total of 61 meters of heat exchanger tubing, but each has a different horizontal run-out length. The grade beam was constructed around the foundations and the heat exchangers were routed through the grade beam into a manifold in the mechanical room. A photo illustrating the run-out tubing in the grade beam prior to concrete placement is shown in Figure 3.8. The routing of the run-out pipes and lengths are shown in plan view in Figure 3.9.

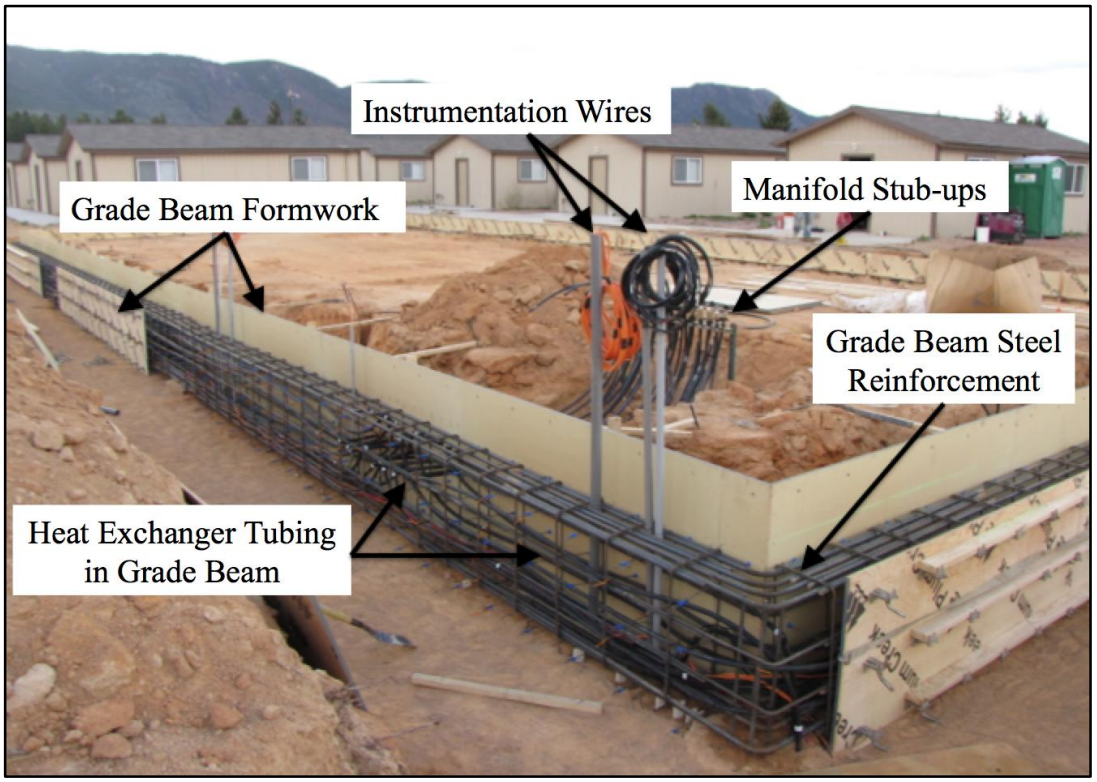

Figure 3.8: Runout tubing in grade beam prior to concrete placement

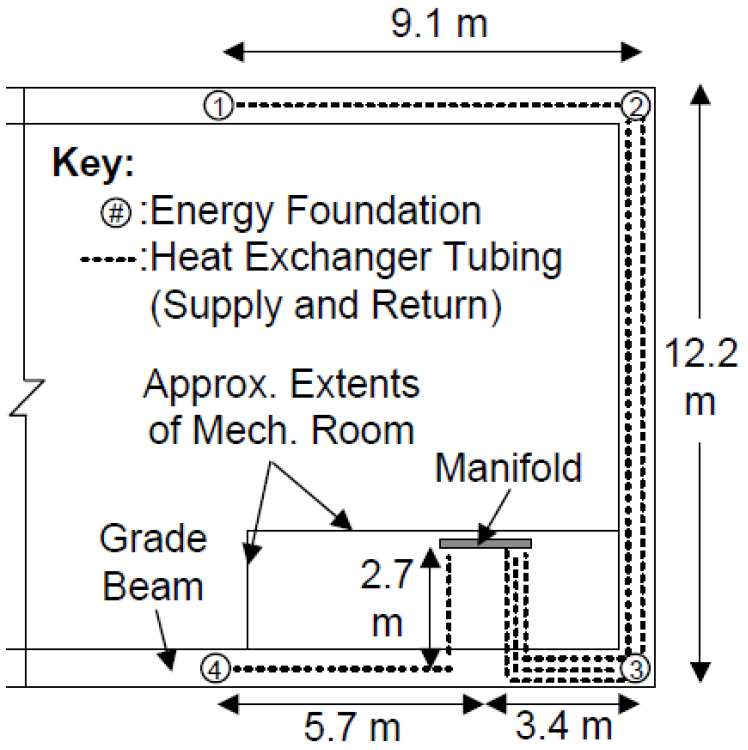

Figure 3.9: Plan view of run-out tubing connecting Foundations 1-4 to the manifold

Since Foundations 1-4 have identical heat exchanger configurations, a comparison of the effect of run-out pipe length on the apparent thermal conductivity of each foundation system could be conducted. A photo of the manifold system is shown in Figure 3.10. The manifold and ball valves were insulated during the test to reduce the influence of ambient outside air temperatures on thermistor readings. The thermal response test unit was used to circulate and heat a 20% propylene glycol-water mixture for a total of 498 hours. Fluid properties of the glycol mixture are shown in Table 3.3. Flow rate of each foundation was measured at one instance during the test from the pressure and temperature ports (P/T ports) using a differential pressure meter at a fluid temperature of 30 °C. The differential pressure was then used to compute the flow rate based on the cross-sectional dimensions of the Venturi balancing valve. During the test, the inlet and outlet temperatures of the heat exchanger fluid for each foundation were continuously monitored using pipe plug thermistors installed within special ball valves on the manifold (shown in Figure 3.10).

Table 3.3: Heat exchange fluid properties

Water to Propylene Glycol Ratio	Molar Heat Capacity (J/molK)	Molecular Weight (g/mol)	Specific Heat Capacity (J/kgK)	Density (g/ml)
5:1	98	30	3267	1.008

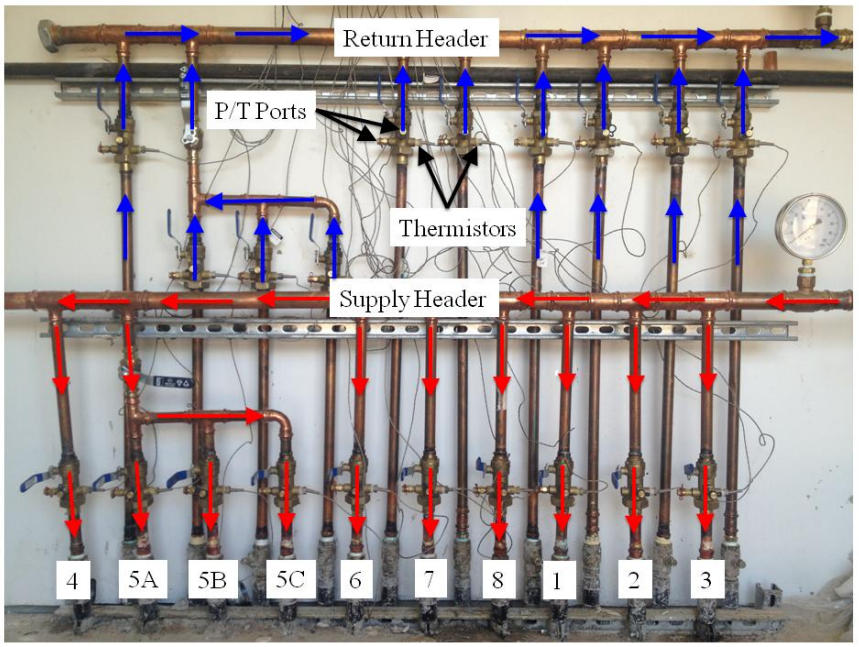

Figure 3.10: Energy foundation manifold configuration prior to insulation

3.2.8. Heating Test to Determine Influence of Heat Exchanger Configuration on Thermal Output of Energy Foundations

A series of seven test stages were performed to investigate the thermal response of various components of the energy foundation system at USAFA, as summarized in Table 3.4. An 11 kW thermal response test unit was used to circulate and heat a 20% propylene glycol-water mixture through the foundations. The TRT unit is comprised of four heaters, two rated at 2.5 kW and two at 3 kW. A combination of heaters may be activated to achieve a nominal heat input to the heat exchange fluid ranging from 2.5 kW to 11 kW. In each stage, a nominal heat input was selected to avoid heating any foundation component too rapidly. Stage 1 involved heating Foundations 1-4 simultaneously. Stage 1 operated for 498 hours with the intent of allowing sufficient time to increase the temperature of the soil surrounding the foundations and to observe the temperature rise in the boreholes 3-10. Stages 2-4 were conducted on Foundations 6-8 individually with a nominal heat input to the fluid of 5 kW and duration of approximately one week for each stage.

Stages 5-7 were conducted on Foundation 5, which has 3 individual loops that can be turned on and off at the manifold. Stage 5 operated on only Loop 5A. During stage 6, Loop 5B of was activated while continuing to pass fluid through Loop 5A. In stage 7, all 3 loops in Foundation 5 were switched open so that flow was permitted to pass through all three loops. Stages 5-7 utilized a 2.5 kW heater in the thermal response test unit. The input heat flux was calculated using Eq. 2.6 for each heat exchanger loop during each stage.

Table 3.4: Summary of thermal response testing stages and heat input details

Testing stage	Foundation	Testing dates	Approximate duration (hours)	Nominal heat flux applied (kW)	Measured heat flux Q (kW)
1	1 2 3 4	6/18/13 – 7/9/13	498	11.0	3.133 2.696 2.180 2.081
2	6	7/11/13- 7/18/13	175	5.0	4.534
3	7	7/18/13- 7/25/13	167	5.0	4.431
4	8	7/25/13- 8/1/13	165	5.0	4.075
5	5A	8/1/13- 8/5/13	119	2.5	2.285
6	5A 5B	8/5/13- 8/28/13	530	2.5	1.164 1.150
7	5A 5B 5C	8/28/13- 9/4/13	163	2.5	0.797 0.803 1.201

3.3. Processing of Strain Values from Vibrating Wire Strain Gages

An important aspect of this study was to evaluate thermally induced axial strains and stresses in the energy foundations caused by temperature changes during normal operation of the

building heat pump. The resonant frequency values f from the VWSGs during the heating test were first converted into axial strain ε, as follows:

$$\varepsilon = -Gf^2 \tag{3.1}$$

where G is the gauge factor of 3.304×10^{-3} and the units of ε are micro-strain. The negative sign follows the geotechnical sign convention for positive strains being compressive. The strain values calculated with Eq. 3 were then converted to thermal strains, as follows:

$$\varepsilon_T = [(\varepsilon_i - \varepsilon_0)B + (T_i - T_0)\alpha_s] \tag{3.2}$$

where B is the batch calibration factor of 0.975, ε_i and T_i are the axial strain and temperature at any time i, ε_0 and T_0 are the initial axial strain and temperature, and α_s is the coefficient of thermal expansion of the steel wire of –12.2 με/°C. This equation accounts for the elongation of the steel wire in the gage during heating.

The next step to define the thermal axial strain is to isolate the impact of the mechanical loading due to the self-weight of the building. The value of mechanical strain after this point is constant, assuming that there is negligible drift in the mechanical strain over time. Accordingly, the measured strain values ε_m were zeroed by subtracting the mechanical axial strain $\varepsilon_{mechanical}$. Next, the zeroed strain values were corrected to account for thermal effects on the gauge. During heating of the gauge, the vibrating wire within the VWSG will expand, causing the VWSG to appear to go into compression instead of correctly showing expansion. The thermal axial strains were defined from the measured strains as follows:

$$\varepsilon_t = (\varepsilon_m - \varepsilon_{mechanical}) + \alpha_s \Delta T \tag{3.3}$$

where α_s is the coefficient of linear thermal expansion of the steel wire in the gauges (-12.2 με/°C) and ΔT is the change in temperature of the foundation.

4. DENVER HOUSING AUTHORITY PROJECT RESULTS

4.1. Seasonal Ground Temperature Profiles

Seasonal variations in ground temperature beneath the building were characterized using measurements from the thermistors prior to operation of the GSHP system, as the foundations were installed in October 2010 but the heat pump was not operational until March 2012. Typical temperature profiles at different times throughout the year shown in Figure 4.1 indicate a decrease in seasonal variability of temperature with increasing depth and a relatively constant ground temperature below a depth of 6 m, which is consistent with observations of Moel et al. (2010). Foundation A exhibited less seasonal variability due to the location within the building footprint and was relatively insulated by the concrete floor slab. Foundation B was located at the outer edge of the building, so the temperature in the upper portion of the foundation was more susceptible to fluctuations in outside ambient air temperature. These observations demonstrate that ground temperatures in the winter months will be warmer than surface air temperatures and can be used as a source of heat. Conversely, the subsurface ground can be used as a heat sink in warm months when ground temperatures are lower than surface air temperatures.

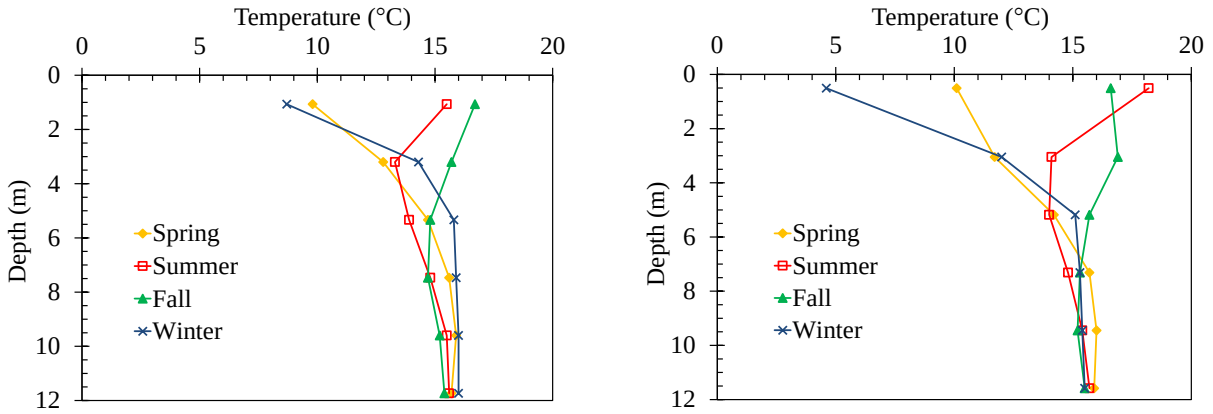

Figure 4.1: Seasonal Ground Temperature fluctuations measured after installation of the foundations but before operation: (a) Foundation A, (b) Foundation B

4.2. Heat Exchange Fluid Temperatures

The temperatures of the heat exchange fluid entering and exiting the foundations during heat pump operation were monitored using pipe-plug thermocouples installed in the inlet and outlet ports of the manifold for each of the two energy foundations. The temperature of the heat exchange fluid entering the foundations is controlled by the heat pump. Because the temperature of the ground is beneath about 6 m is at a constant temperature, the fluid will cool off if the temperature of the heat exchange fluid is above the average ground temperature, while the fluid will heat up if the temperature of the heat exchange fluid is below the average ground temperature. In this manner, the fluid flowing through the tubing in the energy foundations is able to extract or inject heat into the ground. The heat exchanger fluid temperatures as a function of time are shown in Figure 4.2(a) and Figure 4.2(b) for Foundations A and B, respectively. The difference in the inlet and outlet temperatures, $\Delta T_{out\text{-}in}$, also shown in Figure 4.2, reflects the magnitude of heat exchange. Further, the sign of $\Delta T_{out\text{-}in}$ reflects whether the GSHP system is in heating or cooling mode. Although Foundation A appears to be in cooling mode during the winter months, the building was not occupied until March 2012. Further, the pipe-plug thermocouples in the manifold were not properly insulated until February 23, 2012, before which the temperatures of the heat exchange fluid measured were affected by the ambient temperature of the mechanical room. After March 2012, the two foundations show similar behavior consistent with normal operation of conventional heat pump systems. The reason that the inlet and outlet temperature show spikes is that the heat pump only pumps heat exchange fluid through the GSHP system when it is trying to change the temperature of the building. Typical of spring weather conditions in Denver, the system transitioned frequently from heating to cooling.

The heat exchange capacity of the energy foundations can be assessed by evaluating the values of $\Delta T_{out\text{-}in}$ observed in Figure 4.2 and the temperatures within the foundation. Thermal energy is withdrawn from the ground to heat the building by introducing a cold fluid to the heat exchange loops within the energy foundation, which absorbs heat from the ground and returns to the heat pump at a warmer temperature. Larger values of $\Delta T_{out\text{-}in}$ reflect a greater amount of heat gained or lost from the ground. Brandl (2006) indicates that a temperature difference of $\Delta T_{out\text{-}in} > 2°C$ between supply and return lines of the heat exchanger fluid is sufficient for normal operation of a heat pump, as long as the temperature of the ground does not start to change significantly. The data in Figure 4.2 indicates that the maximum difference in inlet and outlet temperatures observed in this project was approximately 10 °C, indicating potential for good heat exchange. As this energy foundation system was plumbed in parallel with the conventional borehole heat exchange system fluid flow rate measurements could not be recorded. Furthermore, the heat pump in the building uses a variable flow pump, so no assumption could be made based on the make and model of the heat pump itself. Since no flow rate was obtained, thermal energy from the energy foundations could not be calculated.

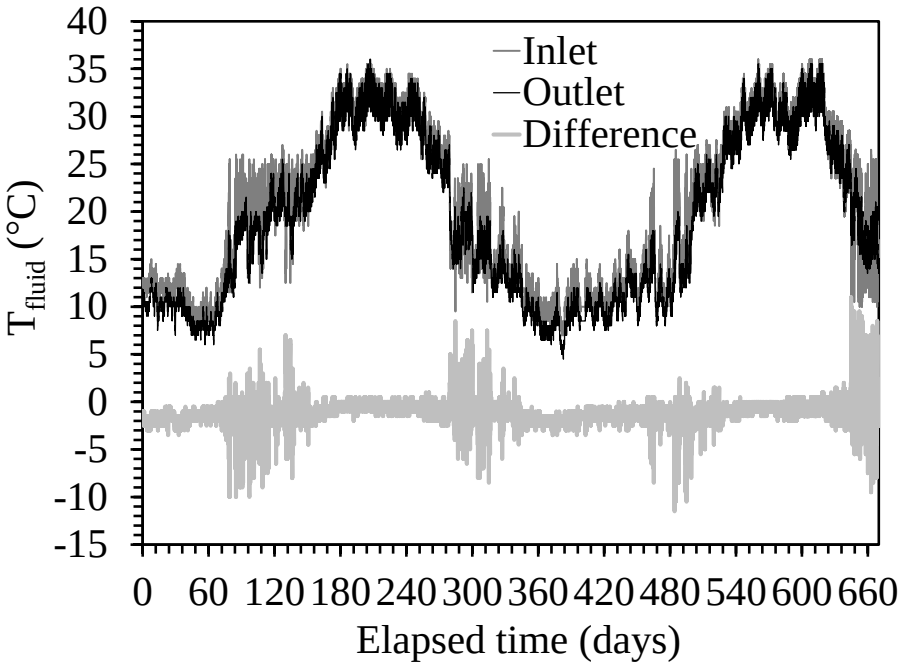

(a)

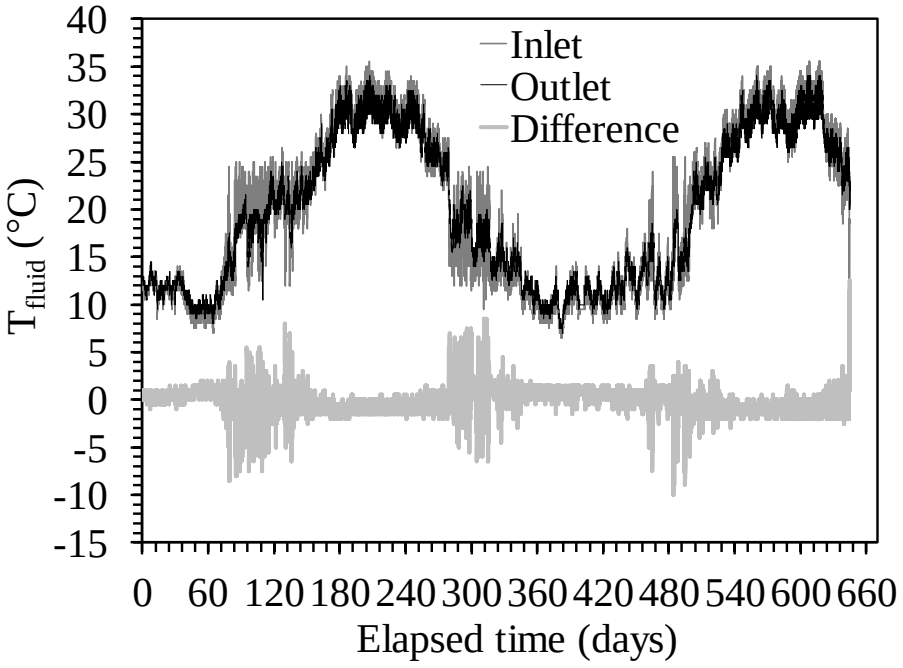

(b)

Figure 4.2: Inlet and outlet temperatures of the fluid circulating within the heat exchange loops in the energy foundations: (a) Foundation A, (b) Foundation B

4.3. Embedded Thermistor Data

The thermistors at different depths within each of the foundations were used to monitor temperatures within the foundation on an hourly basis, as shown in Figure 4.3(a) and Figure 4.3(b) for Foundations A and B, respectively. Once the heat pump operation started in March 2012, the temperature distributions throughout the length of both energy foundations were relatively uniform. The only exception is the top of Foundation B, which showed slightly greater changes in temperature than the rest of the foundation. This is because Foundation B is located under the corner of the building and the top of the foundation is sensitive to variations in ambient air temperature. However, the effect of the ambient outside air temperature on the temperature of the foundation is much less significant after heat pump operations started than before (see changes in temperature observed in Figure 4.1). For one portion of the test, the datalogger malfunctioned, causing a loss of temperature and strain data from day 120 to day 180. On Figure 4.3, this is represented by the gap in the trend lines. The change in foundation temperature at each thermistor throughout the course of heat pump operation is shown in Figure 4.4(a) and Figure 4.4(b) for Foundation A and Foundation B, respectively.

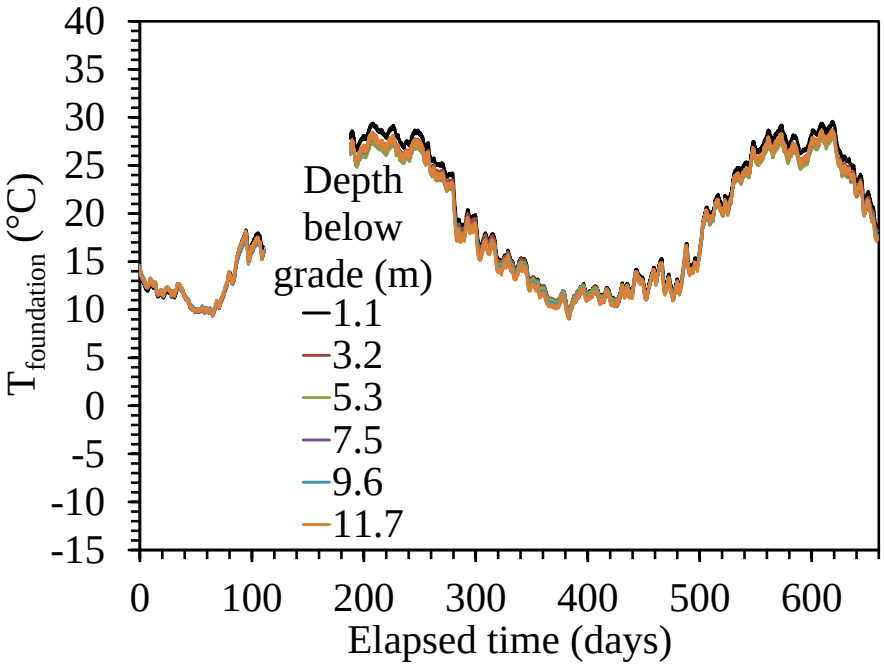

(a)

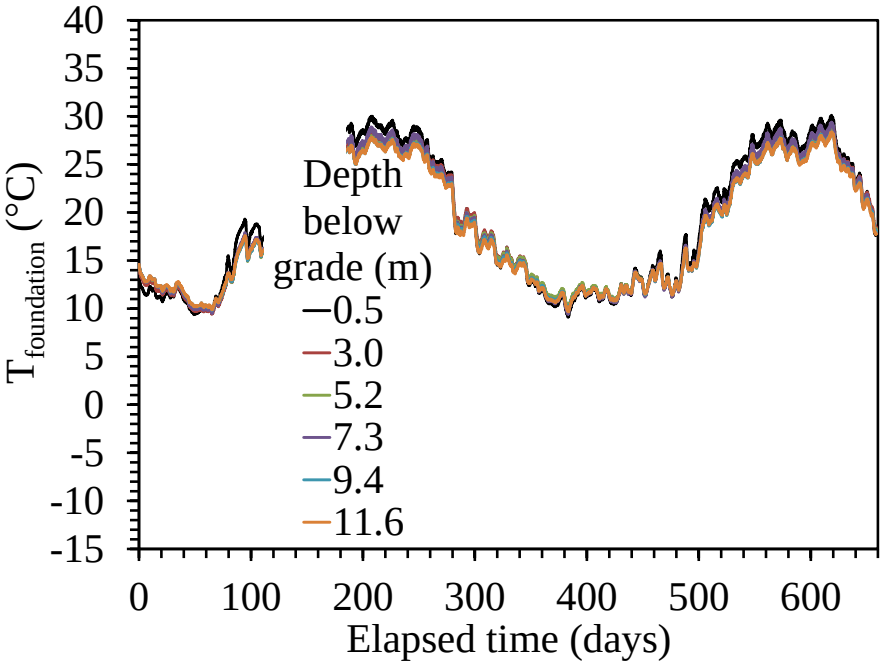

(b)

Figure 4.3: Temperature time series of energy foundations during heat pump operation: (a) Foundation A, (b) Foundation B

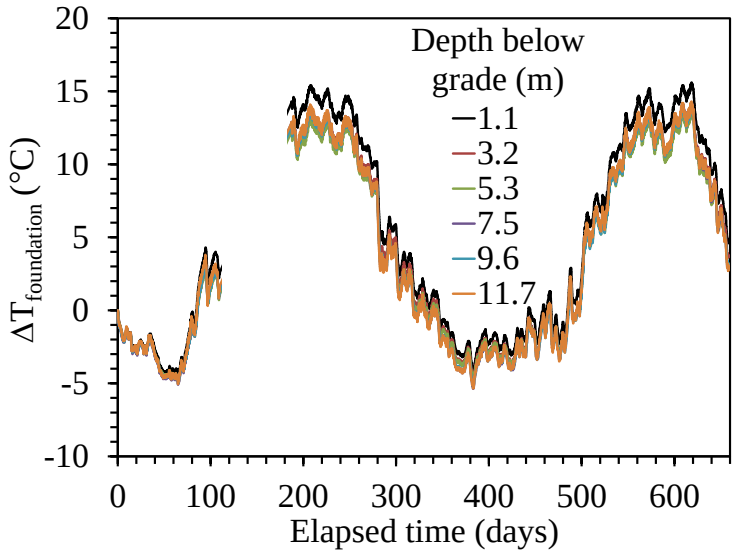

Figure 4.4: Changes in foundation temperature during heat pump operation: (a) Foundation A; (b) Foundation B

4.4. Thermal Axial Strain Data

The thermal axial strains were defined in a same manner as the preliminary analysis performed by McCartney and Murphy (2012), using a global strain correction factor B = 0.5, as follows:

$$\varepsilon_t = [(\varepsilon_m - \varepsilon_{mechanical}) + \alpha_s \Delta T] B \quad (4.1)$$

where α_s is the coefficient of linear thermal expansion of the steel wire in the gauges (-12.2 με/°C), ε_m is the measured strain values from the strain gages defined using the approach described in Section 3.3, $\varepsilon_{mechanical}$ is the portion of the axial strain corresponding to mechanical loading, and ΔT is the change in temperature of the foundation. Positive thermal axial strain indicates contraction and negative thermal axial strain indicates expansion. The time series of thermal axial strain is presented in Figure 4.5 for Foundations A and B.

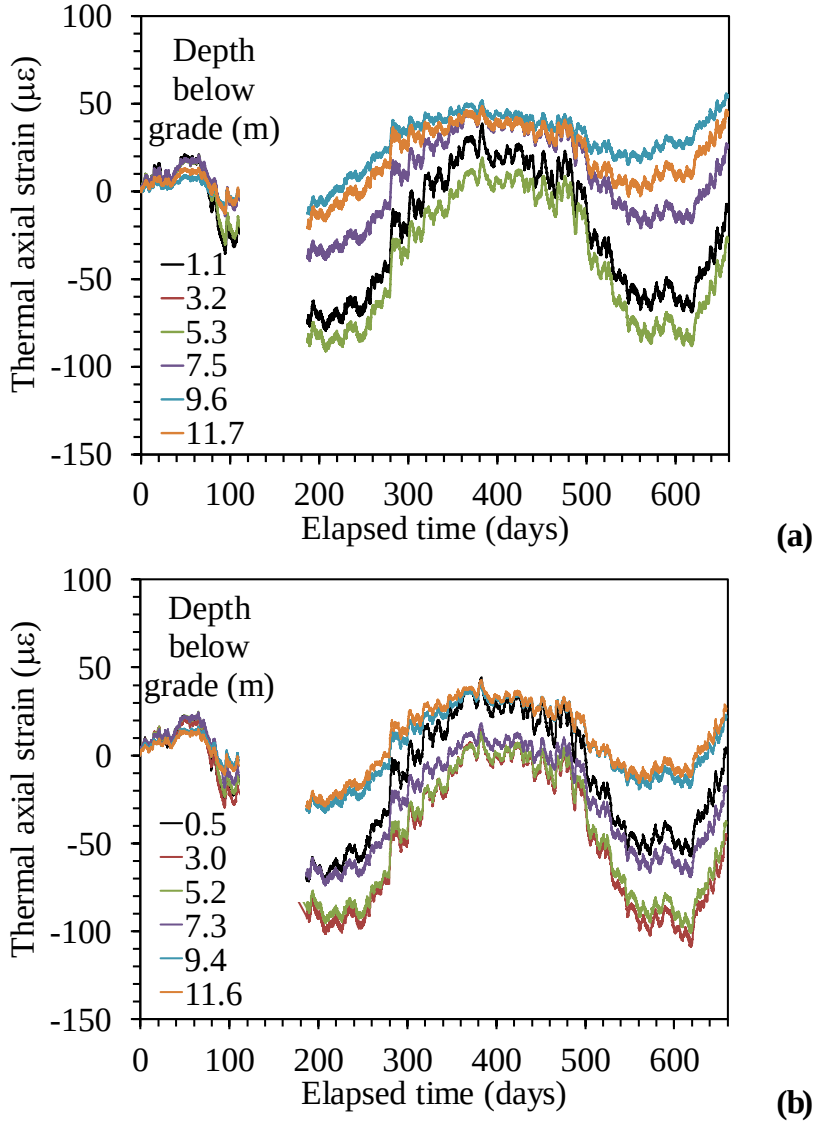

Figure 4.5: Thermal axial strain: (a) Foundation A; (b) Foundation B

In each foundation, the strain gauges near the top display a more dramatic change in thermal axial strain than gauges near the toe of the foundation. A maximum strain during heating at strain gauges near the surface was observed to be -90 με, while cooling led to thermal axial strain of 50 με. The fluctuations in strain closely follow changes in temperature shown in Figure 4.3 and Figure 4.4. As the temperature in the foundation increases, elongation occurs, thus causing the thermal axial strain to decrease. The behavior of Foundations A and B are similar throughout the duration of monitoring.

5. U.S. AIR FORCE ACADEMY PROJECT RESULTS

5.1. Seasonal Ground Temperature Profiles

Seasonal temperature vs. depth was recorded at various times over the course of a year, as shown in Figure 5.1. Ground temperature fluctuates between 5 °C and 16 °C near the surface then becomes relatively stable at a temperature of 9 °C at depths below 6 m. The depths in this figure (and other figures) are measured from the bottom of the grade beam, which is 0.91 m below the ground surface.

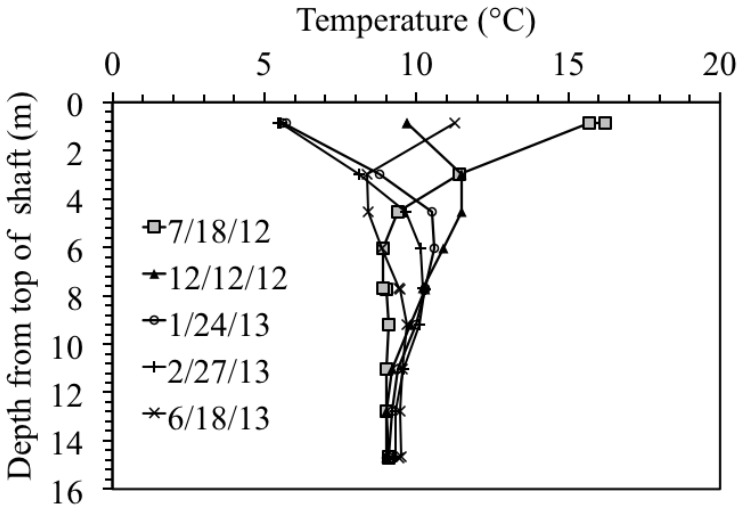

Figure 5.1: Seasonal temperature profile of Foundation 4

5.2. Mechanical Strain Profiles

Mechanical strains were measured immediately following concrete placement in the drilled shaft foundations, as shown in Figure 5.2. The axial strains measured in July 2012 reflect the impact of concrete curing, with some tensile strains observed near the head of the foundation. Construction of the floor slab, walls, and roof occurred in Fall 2012, reflected in the increase in axial strain at the head of the foundation. The difference in the strain profiles between February 2013 and July 2012 was assumed to be equal to the mechanical strain in the foundation due the majority of the building load. The strain decreases with depth as expected, with a maximum

strain corresponding to an axial load of 833 kN. Similar behavior was noted from the temperatures and strains measured in Foundations 1 and 3.

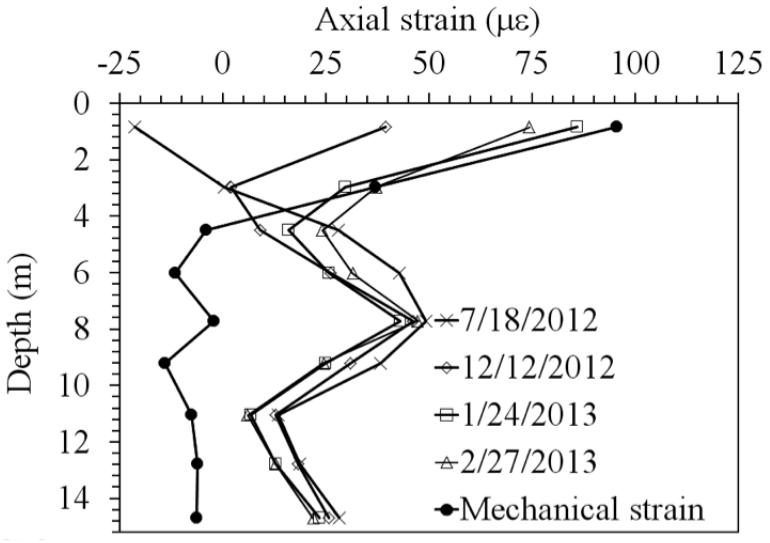

Figure 5.2: Profiles of axial strain during foundation curing and building loading, with strains due to mechanical loading.

5.3. Thermo-Mechanical Study: Phase 1

An in-situ heating test was conducted on the most densely instrumented energy foundation (Foundation 4) in order to evaluate its thermo-mechanical behavior prior to operation of the heat pump system at the building. During the heating test, the system operated continuously for 39 hours. Since the ambient temperature at the site ranged from 0 to 10 °C during test, the heat exchange fluid partially cooled in the reservoir before being recirculated. Over the progression of the test, the temperature of the fluid reservoir gradually rose, causing the fluid entering the system to increase in temperature, as shown in Figure 5.3. The drop in temperature after 10 hours was due to the very cold ambient air temperature overnight. The pump was shut off for a moment after 15 hours.

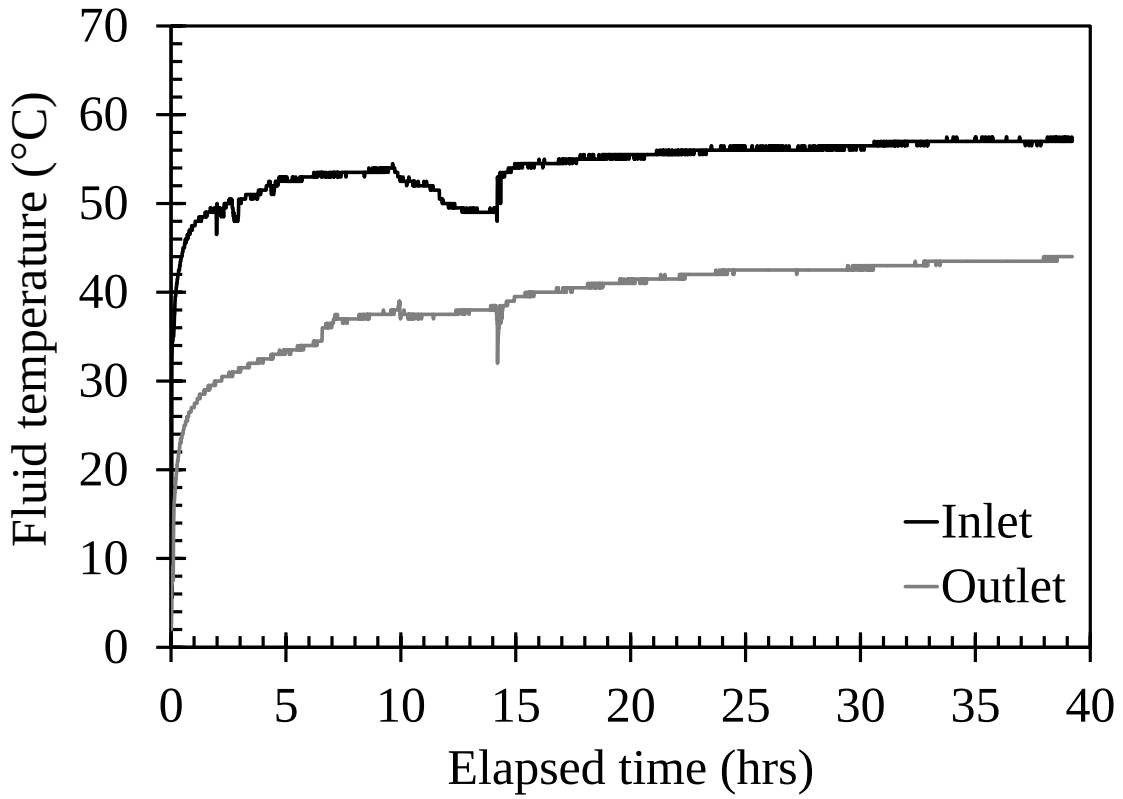

Figure 5.3: Inlet and outlet fluid temperatures during heating test on Foundation 4

5.3.1. Foundation Temperature

The foundation temperature steadily rose during circulation of the heat exchange fluid, as shown in Figure 5.4(a) and reached a maximum temperature of 31 °C at a depth of 7.6 m below grade. For a maximum inlet fluid temperature of 57 °C, the foundation changed in temperature by about 20 °C. The change in temperature at each gauge location in Foundation 4 is presented in Figure 5.4(b). The temperature in the foundation is relatively constant with depth during the heating process.

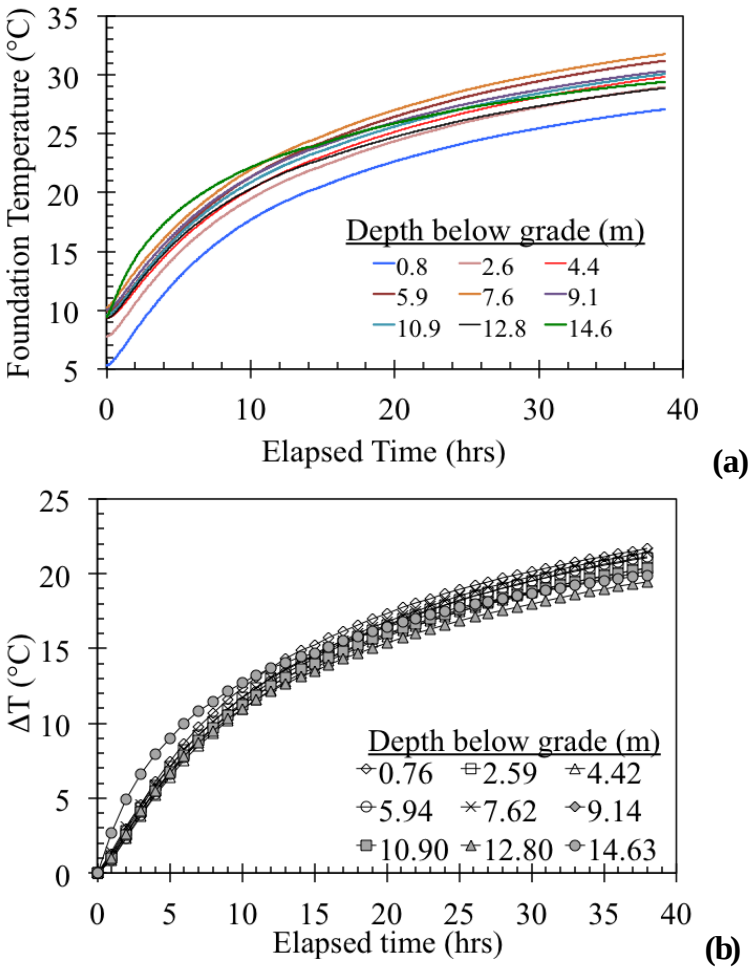

Figure 5.4: Foundation 4 temperature rise curves: (a) Actual temperature; (b) Change in temperature

5.3.2. Thermally Induced Axial Strains

The increase in thermally induced strain in Foundation 4 during the in-situ thermo-mechanical heating test is presented in Figure 5.5. As the foundation undergoes heating, the strain at each location within the foundation rises in roughly the same shape as the change in temperature, shown in Figure 5.4(b). The variation of change in strain between each gauge location is a result of the resistance provided by the concrete-soil interface as well as top and bottom boundary conditions of the foundation. Strain measurements near the top and bottom of the foundation show the greatest change in thermal strain during heating and approach -150 με.

Strains at the mid-depth of the foundation are the lowest throughout the test and reach approximately -60 με.

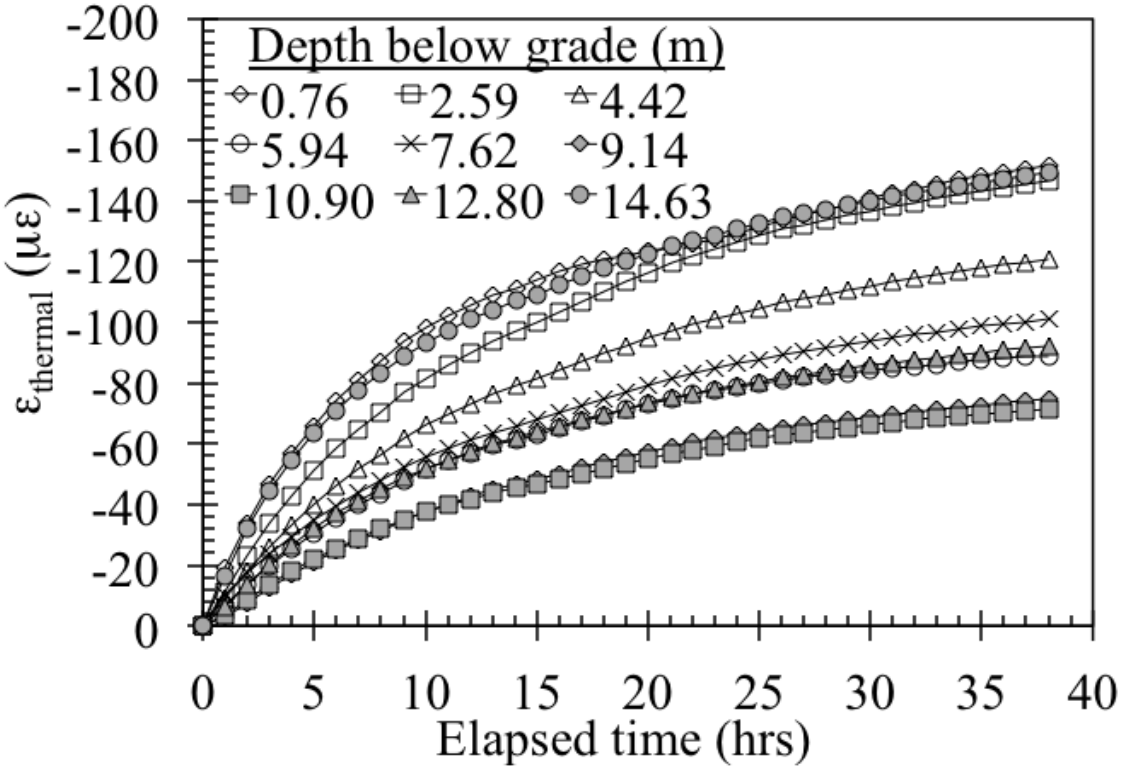

Figure 5.5: Thermally induced strain in Foundation 4 during in-situ thermo-mechanical heating test

5.3.3. Soil Temperature

The soil surrounding the foundation did not experience as large of an increase in temperature, as shown in Figure 5.6(a) and Figure 5.6(b) for the two boreholes closest to Foundation 4 (inside and outside of the building footprint). The shape of the rise in temperature curves also differs from that of the inlet/outlet fluids and the foundation, with a more convex shape during heating. Further, a lag of about 12 to 15 hours was observed after which the soil at 1.22 m from the foundation started to heat up. The slab must have provided a slight insulating effect, leading to greater temperature changes in the soil under the slab. The boreholes located at 2.44 m from the foundation showed negligible change in temperature during the testing period.

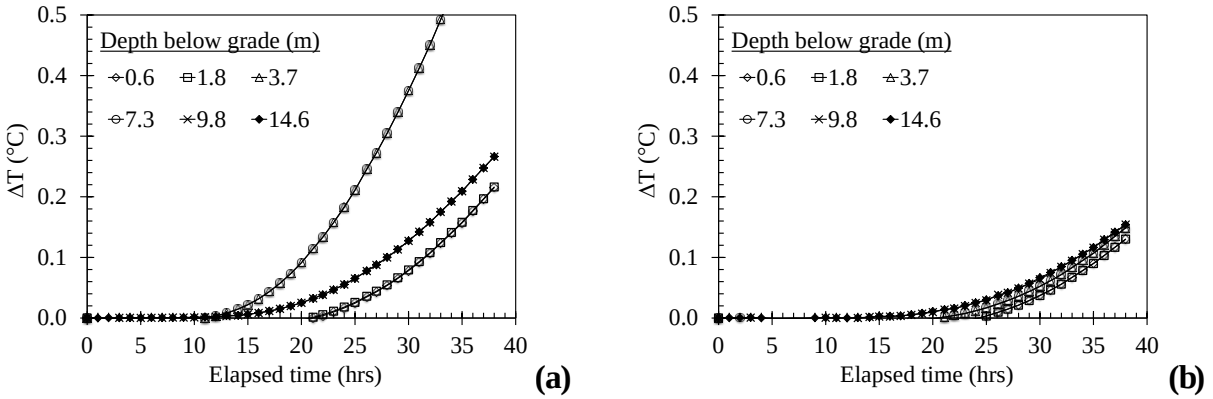

Figure 5.6: Temperatures during heating test: (a) Soil nearest foundation under slab; (b) Soil nearest foundation not under slab

5.4. Thermo-Mechanical Study: Phase 2

A heating test was performed on Foundations 1, 3, and 4 simultaneously for approximately 498 hours to evaluate the thermo-mechanical behavior of the foundations as they were heated together. Different from Phase 1, heating the foundations at the same time imposes a dissimilar upper boundary condition as adjacent foundations are expanding with one another.

5.4.1. Foundation Temperature

The temperatures of the three instrumented foundations at different depths are shown in Figure 5.7. The thermistor at the bottom of each of the foundations showed a substantially lower increase in temperature than in the rest of the foundation. This may be due to denser rock at the toe of the foundation, potential rises in the water table at the time of testing, or due to the geometry of how the heat exchangers were routed to the U-connector at the base of the foundation. After approximately 498 hours of heating, fluid circulation in Foundations 1-4 was stopped and the temperatures in the foundation were monitored during the cooling process. The deeper portions of the foundations cooled more rapidly, as they were not influenced by the warm ambient air temperature at the ground surface. The foundations returned to their original temperatures after approximately 700-1000 hours after the end of heating. Fluctuations in the

uppermost thermistors during cooling reflect the impact of the seasonal ground temperature fluctuations.

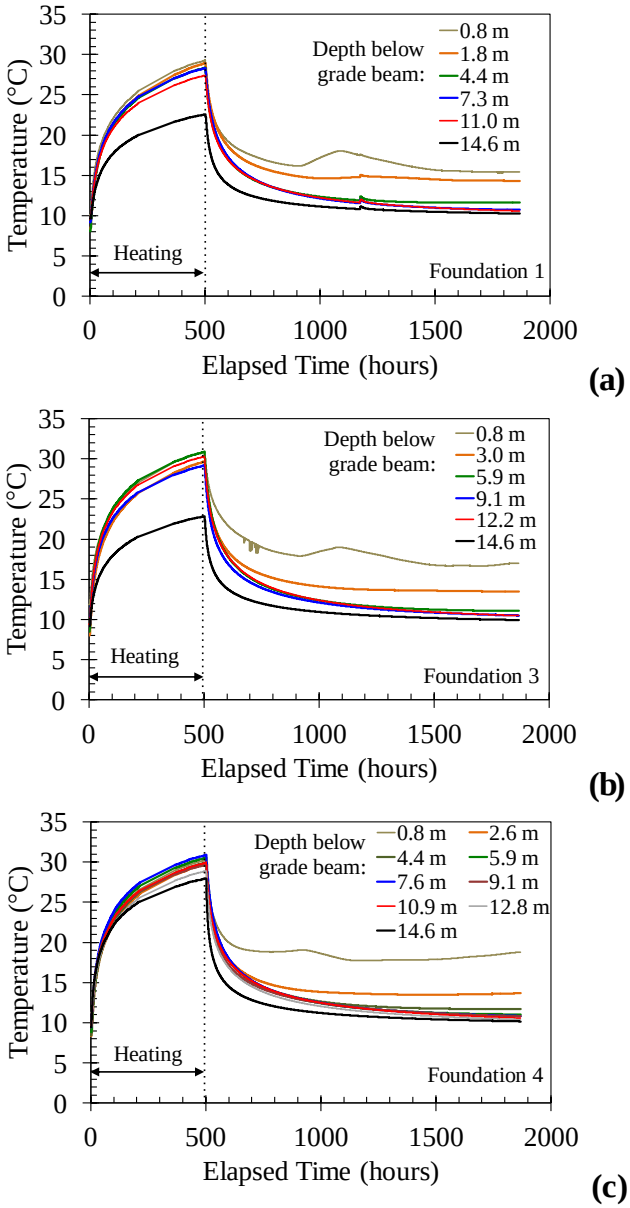

Figure 5.7: Foundation temperatures during thermal response testing. (a) Foundation 1; (b) Foundation 3; (c) Foundation 4.

5.4.2. Thermally Induced Axial Strains

The thermal axial strains calculated using Eq. 3.3 are shown in Figure 5.8. As the temperature increases in the foundations, the thermal axial strains become more negative indicating expansion. The fluctuations in thermal axial strain after heating was stopped correlate

well with the observed changes in foundation temperature due to the changes in surface temperature. The strain gauges near the top of each instrumented foundation display the greatest variation, as this is the depth range that is subjected to the greatest change in temperature.

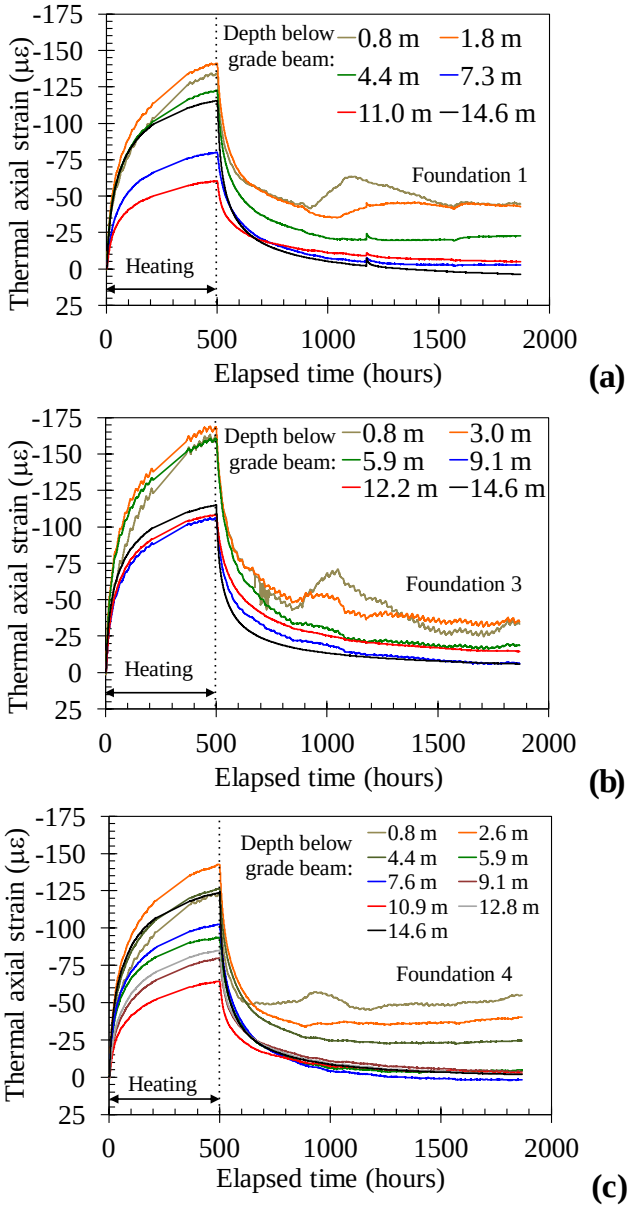

Figure 5.8: Time series of thermal axial strains during thermal response testing and subsequent cooling: (a) Foundation 1; (b) Foundation 3; (c) Foundation 4

5.4.3. Soil Temperature

Temperature profiles for Foundation 4 and Boreholes 5 and 6 are shown in Figure 5.9 for the first 200 hours of the heating test. Figure 5.9(a) shows the temperature in Foundation 4 for

with depth throughout heating and indicates that a relatively uniform temperature is present in the foundation. Temperature profiles for Boreholes 5 and 6 are shown in Figure 5.9(b) and (c), respectively. Temperature with depth is not uniform in the boreholes and remains about 3 °C warmer at 0.8 m depth throughout the duration of the test. The temperature in Borehole 5 begins to increase at 50 hours after Foundation undergoes heating, while Borehole 6 shows only minimal heating after 200 hours.

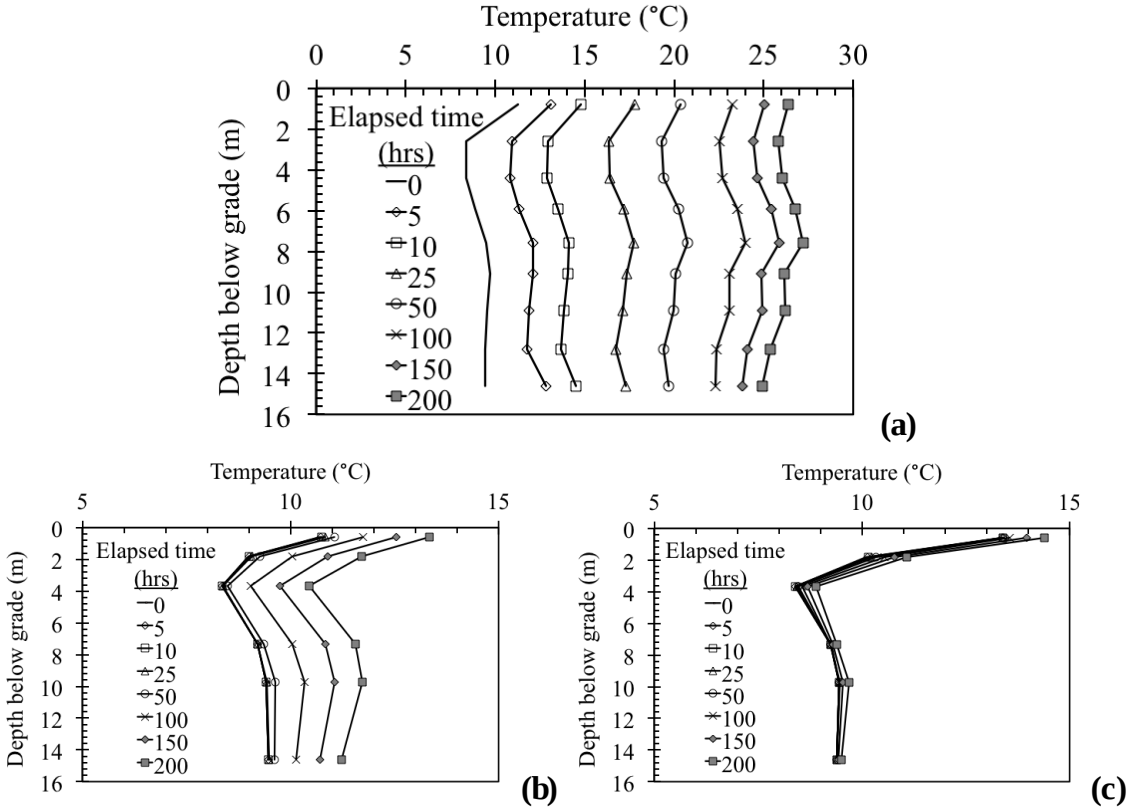

Figure 5.9: Temperature profiles during heating test: (a) Foundation 4; (b) Borehole 5; (c) Borehole 6

5.5. Results from Investigation on the Impact of Horizontal Runout Length on the Thermal Response of Energy Foundations

Figure 5.10 shows the fluid temperatures for each of the four foundations. The inlet and outlet temperatures are measured at the manifold as the heat exchange fluid enters and exits each geothermal loop. In all cases, a relatively rapid rise in temperature occurs in the first 25 hours

then becomes more gradual as steady state temperatures are approached. The difference in inlet and outlet temperature, ΔT, is plotted on the right vertical axis for each foundation. A constant value of ΔT indicates uniform heat input energy into the system. The variation of ΔT in Foundation 3 observed in Figure 5.10(c), was due to poor insulation surrounding the inlet ball valve during the first portion of the test. The insulation was reattached at an elapsed time of about 140 hours after which the change in temperature became steadier. At one instance during the test, the datalogger malfunctioned between 204 and 361 hours.

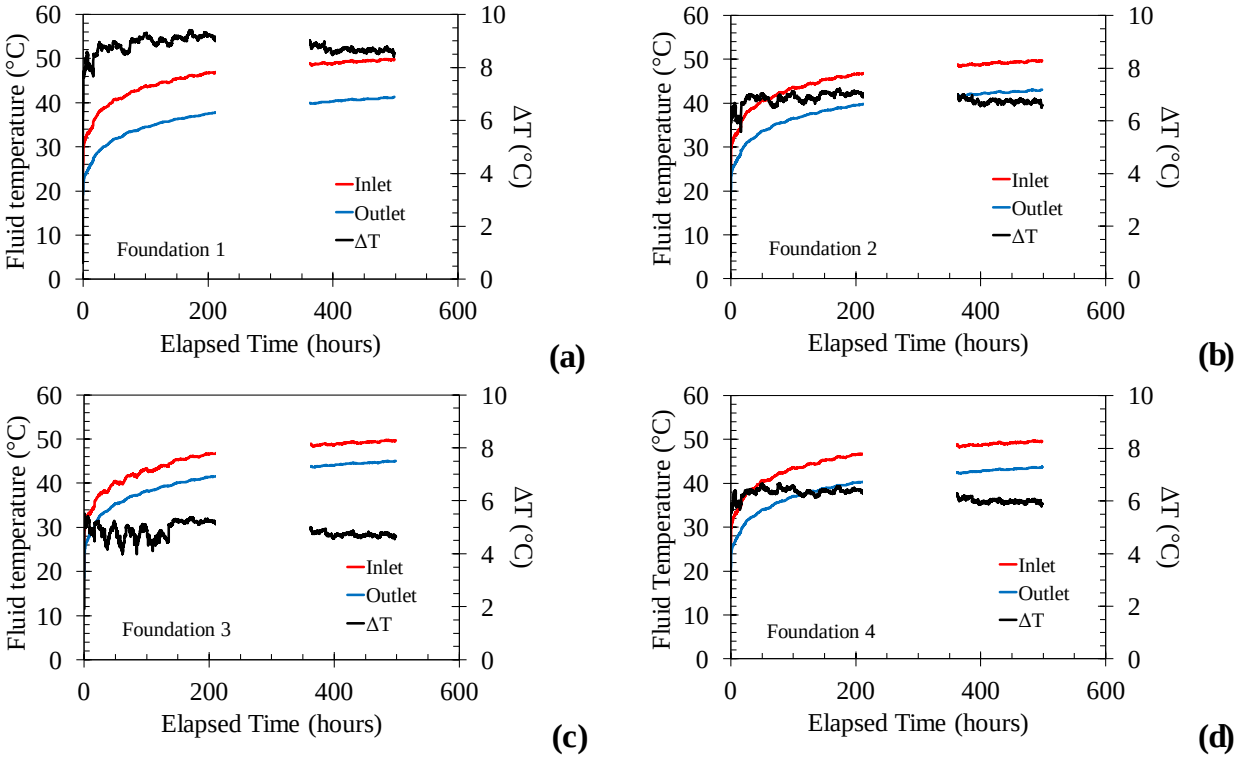

Figure 5.10: Fluid temperature rise curves and differential temperature during Stage 1 testing: (a) Foundation 1; (b) Foundation 2; (c) Foundation 3; (d) Foundation 4

5.6. Results from Tests Focused on the Influence of Loop Configuration on Thermal Output of Energy Foundations

Heat exchange fluid temperature rise curves for thermal response tests conducted on Foundations 5-8 are presented in Figure 5.11. As each foundation has a different heat exchanger loop configuration, it is expected that the heat exchange rate will differ between each foundation.

Each figure shows a relatively constant difference between inlet and outlet temperature, indicating a steady power input into the heat exchanger fluid.

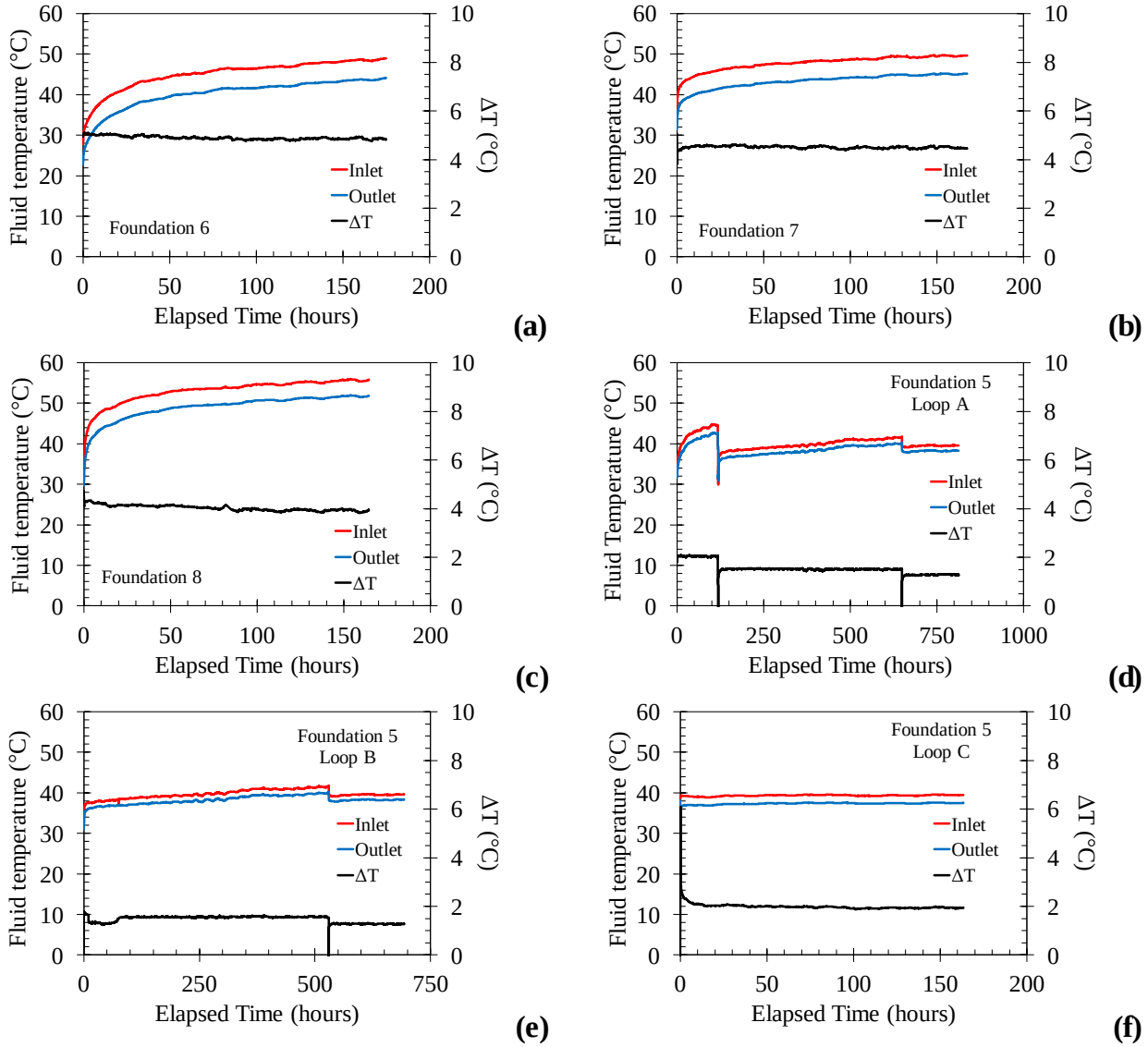

Figure 5.11: Temperature rise curve and differential temperature during testing: (a) Foundation 6 (3 continuous loops) Stage 2; (b) Foundation 7 (one loop) Stage 3; (c) Foundation 8 (one "retro-fit" loop) Stage 4; (d) Foundation 5 Loop A (3 individual loops) Stage 5, 6, 7; (e) Foundation 5 Loop B (3 individual loops) Stage 6, 7; (f) Foundation 5 Loop C (3 individual loops) Stage 7

5.7. Soil Temperatures during Thermal Response Testing

Foundation heating led to an increase in ground temperatures measured by the thermistor strings. The temperatures measured in Borehole 1, located at a distance of 4.6 meters outside of the building footprint, are shown in Figure 5.12(a). The temperature fluctuations occur only near the surface and appear to be due to hot weather. The temperatures measured in Borehole 2, located under the building slab in the center of Foundations 1-4, are shown in Figure 5.12(b). Although some changes in temperature near the top of the borehole appear to correspond with the increase in surface temperature during the summer, the temperature of the subsurface at the bottom of the borehole experienced an increase in temperature by about 2°C below a depth of 8m likely due to the heating of the subsurface due the operation of Foundations 1-4. After stage 1 ended, the borehole temperature decreased and remained constant from 8/15/13 to 9/4/13.

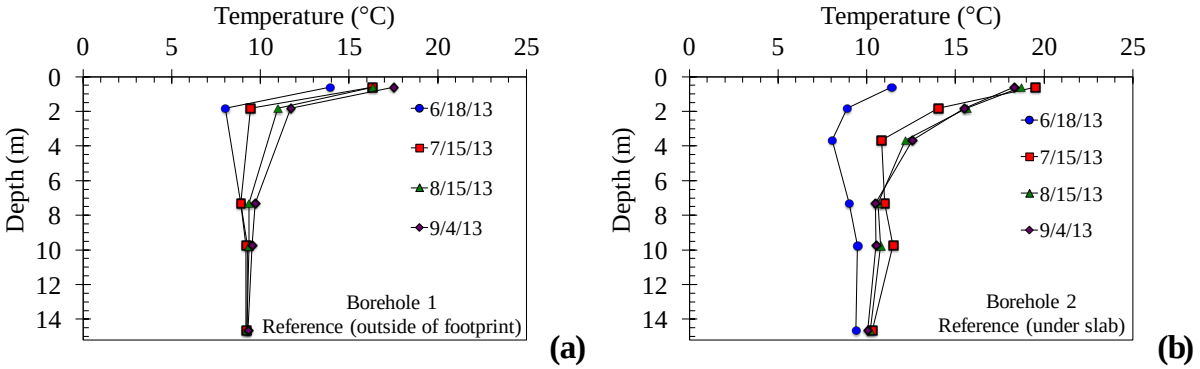

Figure 5.12: Temperatures of the subsurface during thermal response testing: (a) Reference Borehole 1; (b) Reference Borehole 2.

Boreholes 3, 4, 5, and 6 surround Foundation 4, with Boreholes 3 and 4 being located within the building footprint and Boreholes 5, and 6 outside of the building footprint. Boreholes 3 and 6 are located at 2.4 m from Foundation 4, while Boreholes 4 and 5 are located at 1.2 m from the foundation. A rise in temperature in Boreholes 4 and 5 occurs at approximately 50 hours after the test is started, as shown in Figure 5.13(a) and (b). Boreholes 3 and 6 indicate a

much slower rise in temperature than Boreholes 4 and 5. A relatively constant rate of temperature rise occurs throughout the later portion of the test, indicating a uniform heat flux.

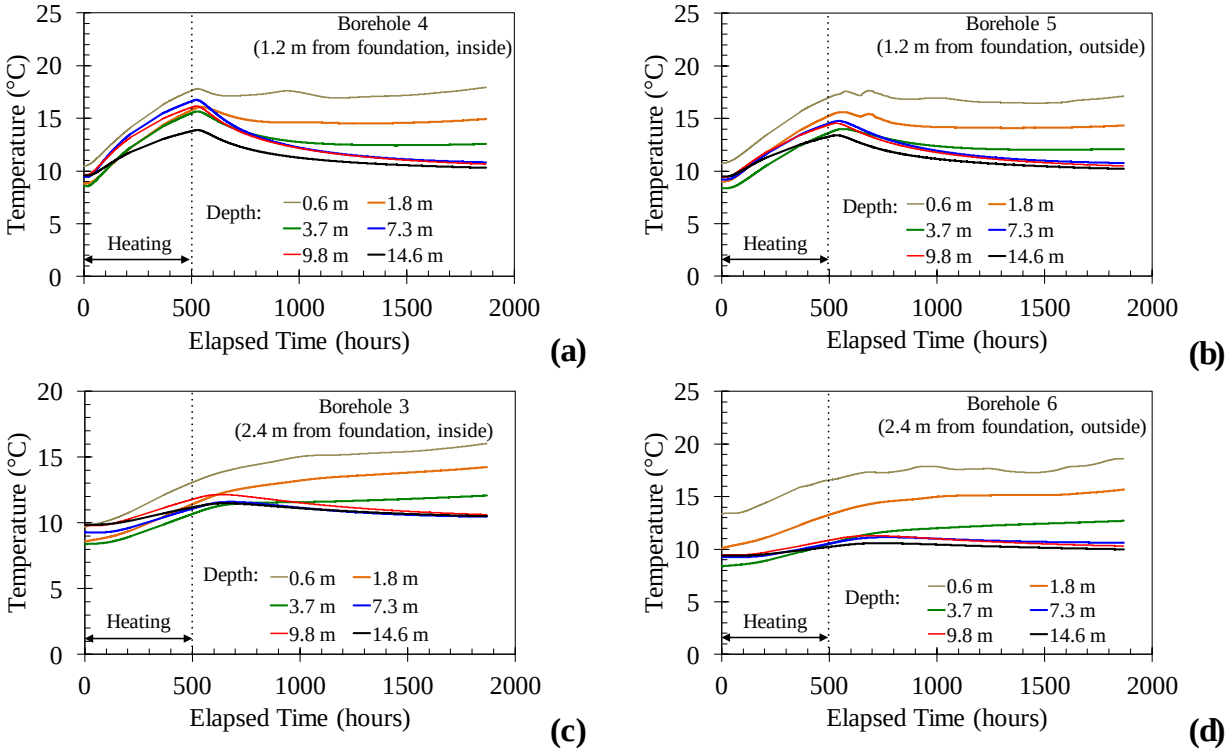

Figure 5.13: Temperature rise curves during heating tests in boreholes surrounding Foundation 4: (a) Borehole 4; (b) Borehole 5; (c) Borehole 3; (d) Borehole 6

6. ANALYSIS

6.1. Thermo-Mechanical Analysis

6.1.1. Denver Housing Authority: Thermo-Mechanical Behavior

Thermal axial stress and strain at a given time can be plotted with depth in order to give a sense of thermo-mechanical behavior in the foundation for the same average change in foundation temperature. Profiles can also be generated at specified instances in time to observe the progression in thermal axial stress and strain throughout the duration of a thermal response test. In order to define profiles of thermal axial strain representative of the energy foundation performance, instances in time at which the energy foundations had experienced average changes in temperature of 2°C increments were identified. The temperature profiles for these average temperature increments are shown in Figure 6.1(a) and Figure 6.1(b) for Foundations A and B, respectively.

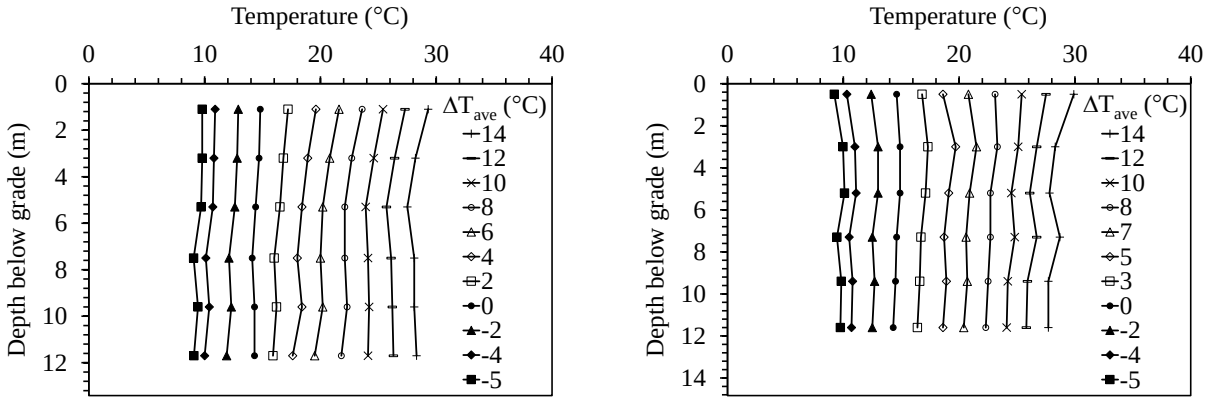

(a) **(b)**

Figure 6.1: Temperature profiles for different average changes in temperature during heat pump operation: (a) Foundation A, (b) Foundation B

For the period of data collected for this study, the maximum extents of temperature change corresponded to ΔT = -5°C during building heating and ΔT = +14°C during building cooling, with respect to the initial temperature of the foundation at startup of the heat pump. The slight differences in temperature at the top of Foundation B compared to the rest of the foundation are due to the influence of the outside air temperature.

The profiles of thermal axial strain corresponding to the average changes in temperature are shown in Figure 6.2(a) and Figure 6.2(b) for Foundations A and B, respectively. During cooling of the energy foundations (i.e., heating of the building), axial contraction occurs as reflected in the positive sign of the strain measurements. Conversely, during heating of the energy foundations (i.e., cooling of the building), axial expansion occurs as reflected in the negative sign of the strain measurements. The maximum thermal axial strain was -90 με in Foundation A during a temperature change of ΔT = +14°C, while the maximum thermal axial compressive strain is -102 με in Foundation B under a temperature change of ΔT = +14°C. The shapes of the thermal axial strain profiles in both energy foundations during cooling of the building are similar to those observed by Stewart and McCartney (2014) for end-bearing foundations characterized in a geotechnical centrifuge. Specifically, the smallest strain is observed at the bottom of the foundation, indicating that the foundations are expanding upwards from the relatively rigid bedrock.

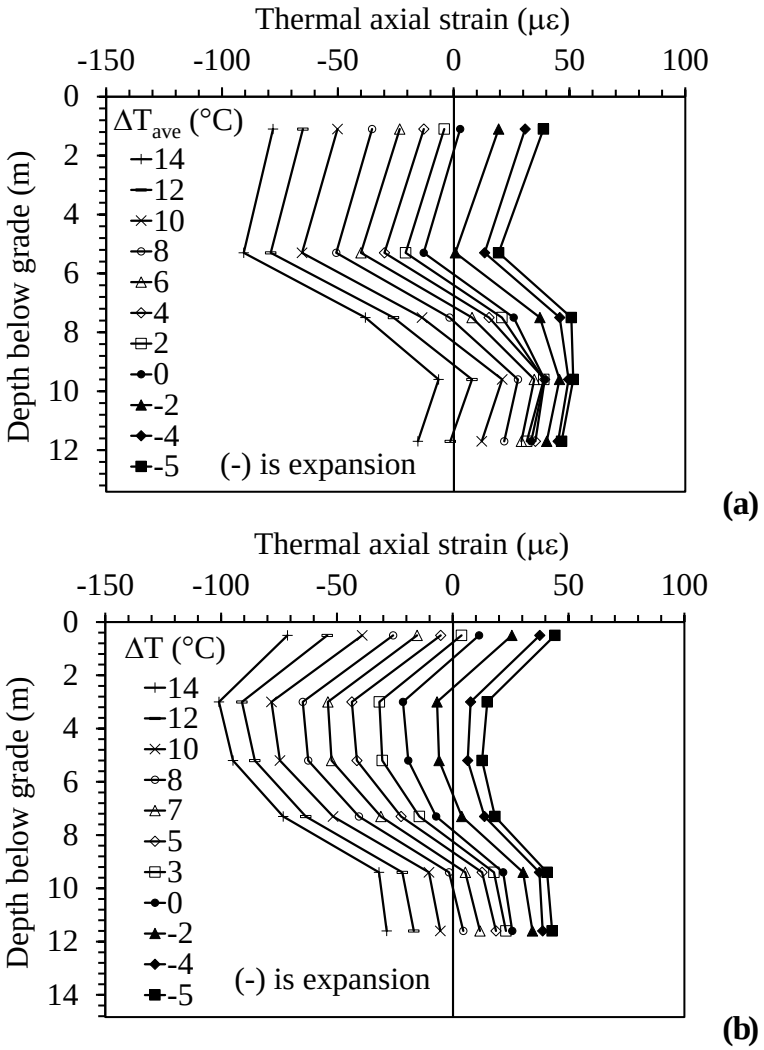

Figure 6.2: Thermal axial strain profiles during heat pump operation: (a) Foundation A, (b) Foundation B

The calculated thermal axial stress profiles are shown in Figure 6.3(a) and Figure 6.3(b) for Foundations A and B, respectively. These profiles were defined for a coefficient of thermal expansion of the reinforced concrete of -10 με/°C. The sign convention designates positive stress to be compression and negative stress to be tension. The locations of the smallest strain in the energy foundation correspond to locations of maximum thermal axial stress. Compressive (positive) thermal axial stresses occur during cooling of the building (heating of the foundation) when the axial expansion of the foundation is restrained by the overlying building, underlying bedrock, or the side shear resistance of the soil surrounding the foundation. With the exception

of the high thermal axial stresses noted at the top of Foundation B during heating, which are likely due to the higher ambient temperature at this time, the stress profiles indicate that the highest stresses are at the bottoms of both foundations. The decrease in compressive stress with height is due to resistance to thermal axial expansion from the mobilization of side shear stresses. It is possible that the smaller stresses noted in Foundation B between depths of 2 and 6 meters may have occurred due to residual stresses encountered during curing of the concrete in the foundation, which deserves further study.

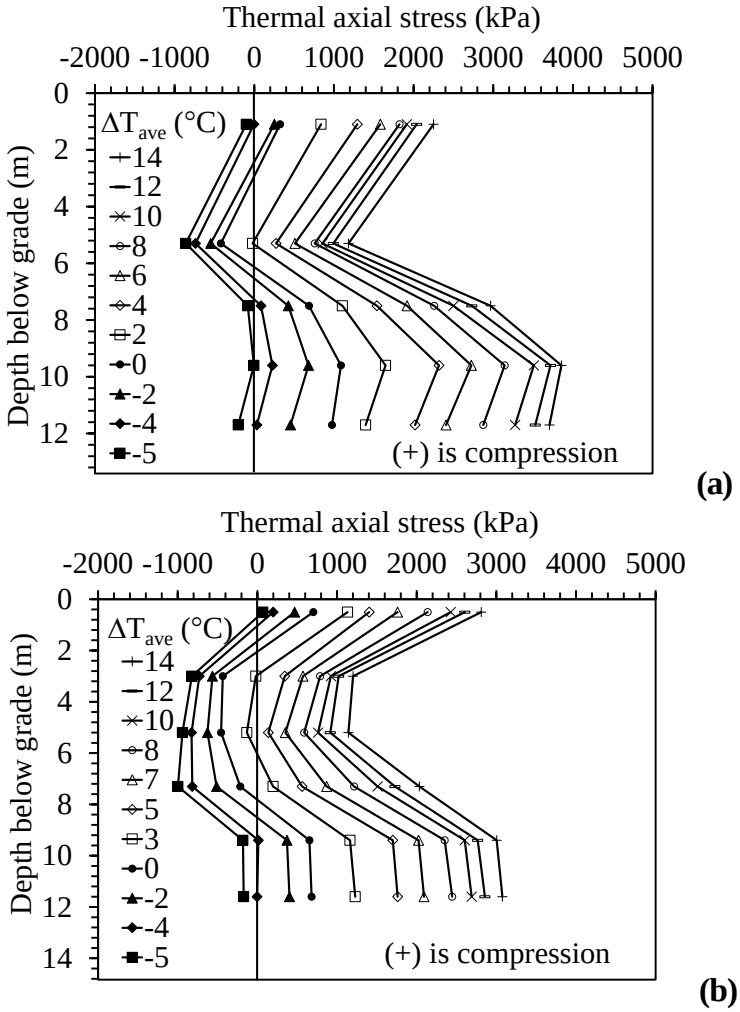

Figure 6.3: Thermally induced stress profiles during heat pump operation: (a) Foundation A, (b) Foundation B

The compressive and tensile profiles of thermal axial strain observed during heating and cooling of the building (cooling and heating of the energy foundation) were superimposed upon the strains due to mechanical loading to define the total thermo-mechanical axial strains, as shown in Figure 6.4(a) and Figure 6.4(b) for Foundations A and B, respectively. The mechanical strain profiles are difficult to interpret; it was expected that the greatest axial strain would be observed near the top of the foundation, and would either decrease with depth if there was side shear resistance or remain uniform with depth if there was negligible side shear resistance. However, both foundations show an inconsistent mechanical strain profile with depth. This is attributed partially to the impact of curing on the calculation of the mechanical strains in the foundations from the raw VWSG readings. Nonetheless, the magnitudes of the average mechanical strains are consistent with the design axial loads for the foundations, assuming a Young's modulus of 30 GPa. Regardless of the shapes of the mechanical strain profiles, it is clear that heating and cooling operations lead to a shift in the thermo-mechanical strain profiles to the left or right. However, the thermal axial strains are not as significant as those generated due to the self-weight of the building, and the magnitudes of the thermal axial stresses are well below those that may cause structural damage.

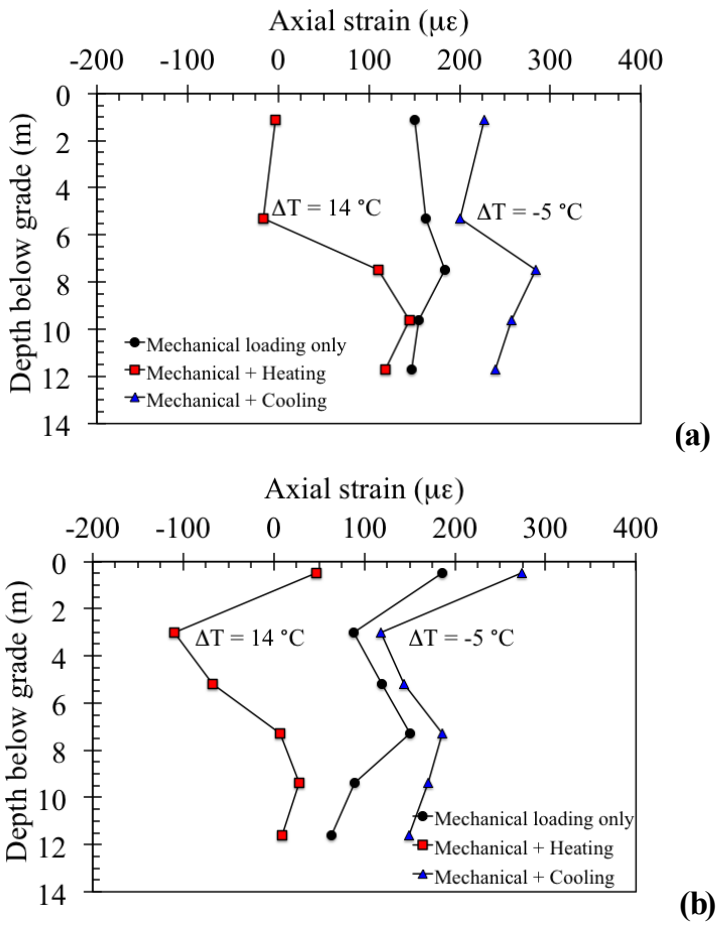

Figure 6.4: Axial strains induced by mechanical loading and those induced by thermo-mechanical loading during heating and cooling operations: (a) Foundation A, (b) Foundation B

Another way to evaluate the thermal soil-structure interaction is to evaluate the relationships between axial thermal strains and the change in temperature at the location of each gauge. The slopes of these lines reflect the mobilized coefficient of thermal expansion of the reinforced concrete. The maximum value of the mobilized coefficient of thermal expansion is that for free expansion conditions, which in this study is assumed to be -10 με/°C. The distribution in the mobilized coefficients of thermal expansion can be used to determine where in the foundation the lowest thermal axial strain occurs which corresponds to the location of highest

thermal axial stress. The thermal axial strains are shown as a function of temperature for Foundations A and B in Figure 6.5(a) and Figure 6.5(b), respectively.

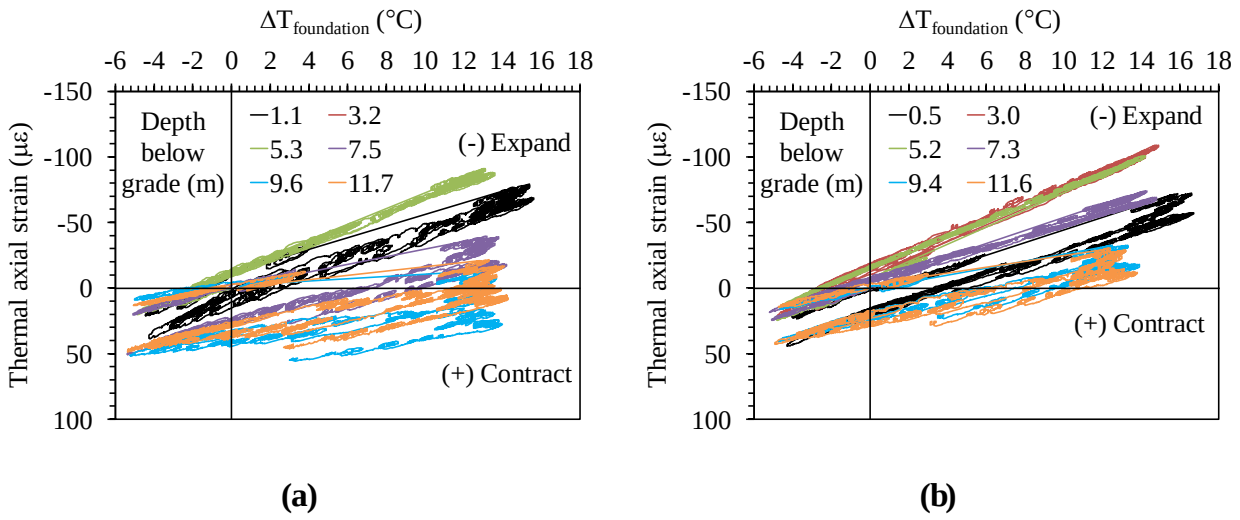

Figure 6.5: Change in temperature vs. change in strain during heating and cooling operations: (a) Foundation A, (b) Foundation B

Hysteresis is noted in the strain measurements during heating and cooling, which is likely due to an accumulation of residual strain as the heat pump cycles between heating and cooling modes. Nonetheless, the strain measurements follow a linear trend with temperature. The slopes of the thermal axial strain versus temperature plots were used to define the mobilized coefficient of thermal expansion for the reinforced concrete at the depth of each of the gauges, as shown in Figure 6.6. If the soil surrounding the foundation did not provide any resistance to movement, and if the building did not provide any constraint, then the mobilized coefficient of thermal expansion would equal that for free expansion (-10 με/°C). However, the results in this figure show that all of the gauges have an average mobilized coefficient of thermal expansion less than this value. The mobilized coefficients of thermal expansion are closest to that representing free expansion in the upper 6 meters of the foundation, indicating that the overlying building provides less constraint for thermal expansion than the underlying bedrock.

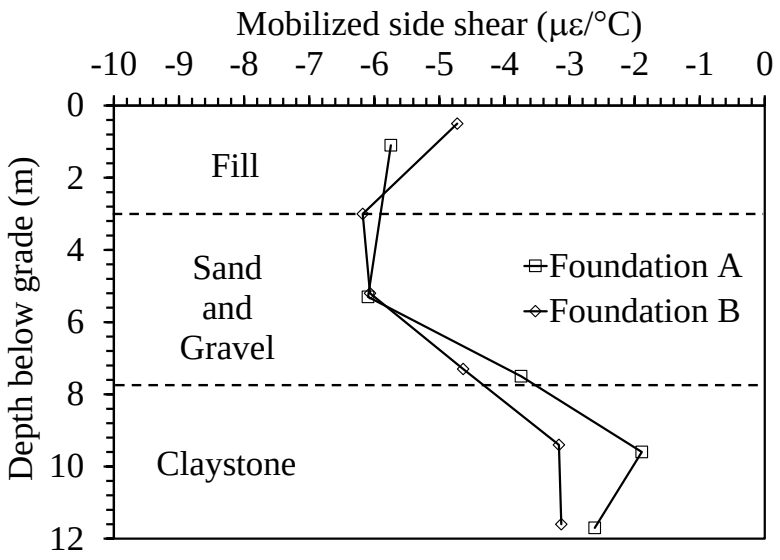

Figure 6.6: Mobilized thermal expansion coefficients vs. depth

The thermal axial displacement for each foundation for average changes in foundation temperature is shown in Figure 6.7 for Foundations A and B, assuming a fixed end condition for the toe of the foundation in the vertical direction. For the maximum change in temperature of 14°C observed in the data collected to date during cooling of the building (heating of the foundation), a maximum upward axial displacement of -0.6 mm is expected in Foundation A. Foundation B exhibited a slightly higher thermal axial displacement of -0.8 mm for the same increase in temperature, most likely due to the uppermost gauge in Foundation B being 0.6 m higher than the uppermost gauge in Foundation A. This analysis assumes that the bottom of the foundation is fixed from moving in the vertical direction. Since no actual displacement measurement was recorded in either case study, the assumption of a fixed base is the most practical approach to calculating foundation displacements. If the foundation were allowed to move downward, the displacement profiles would be less dramatic, since the foundation is allowed to move in both directions. The assumption of a fixed base gives the maximum upward

and downward displacements during foundation heating and cooling, respectively. The actual foundation displacements are likely to be less than the values reported in the following analysis.

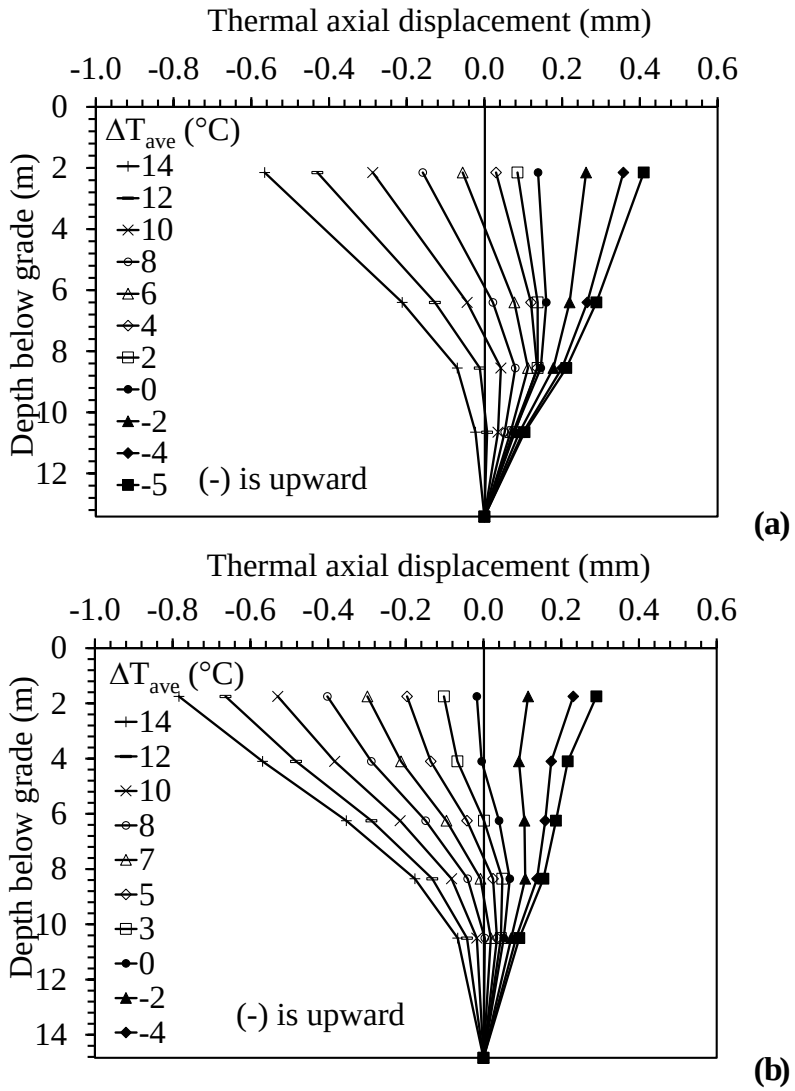

Figure 6.7: Thermally induced displacements during heating and cooling operations: (a) Foundation A, (b) Foundation B

6.1.2. U.S. Air Force Academy: Thermo-Mechanical Behavior: Phase 1

The axial thermal strain profiles observed during the heating process are shown in Figure 6.8. The strain was found to be the greatest at the top and bottom of the foundation. The bottom of the foundation experienced slightly greater strains due to the higher temperatures at the base of the foundation shown in Figure 5.6(a). The distribution in strain in this figure reflects the fact that soil-structure interaction due to mobilization of side shear resistance leads to a nonlinear distribution in thermal strain with depth, with a behavior similar to that noted by Laloui et al. (2006) and Bourne-Webb et al. (2009).

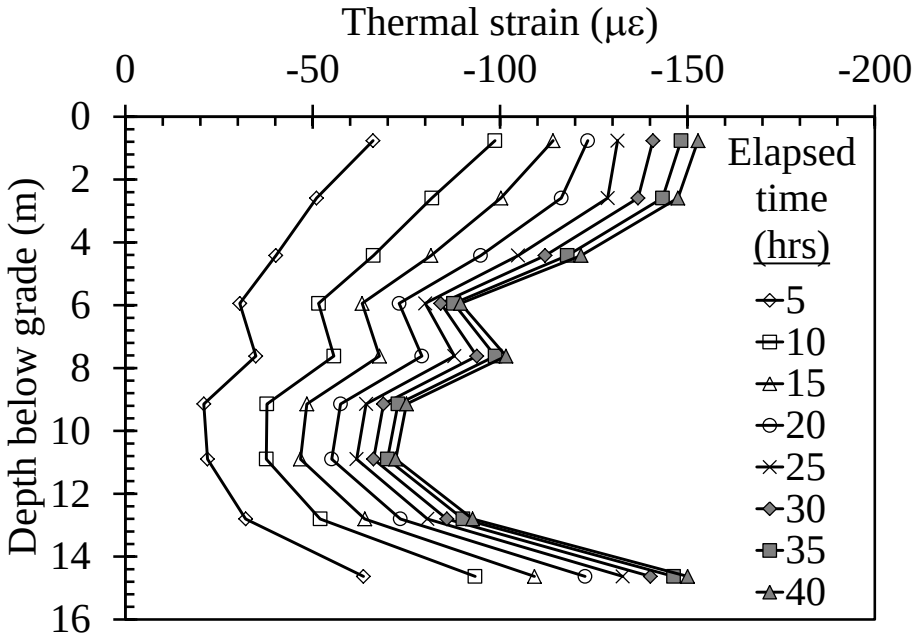

Figure 6.8: Profiles of axial thermal strains induced during heating test

Profiles of temperatures in the foundation are shown in Figure 6.9 for different times after the start of heating. It is clear that the temperature of the foundation is relatively uniform. The reason for the slightly higher temperature at the toe of the foundation is due to the proximity of the sensor to the U-bend of the pipe at the base, which may have heated this portion more than the rest of the foundation.

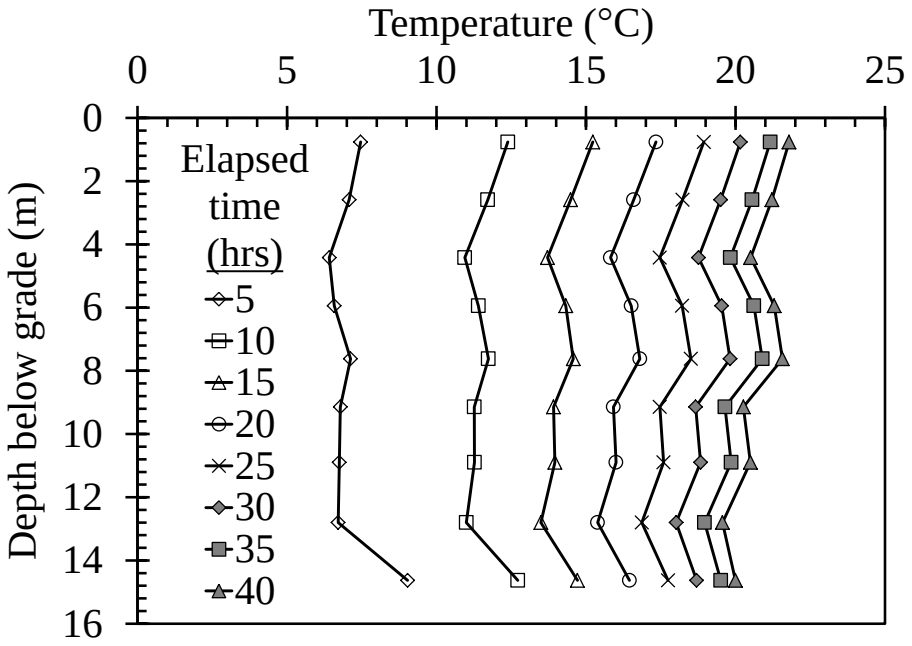

Figure 6.9: Foundation temperature profiles during heating test

The axial thermal stresses shown in Figure 6.10 indicate that the greatest values occur in the bottom half of the foundation, and that the thermal stresses are compressive. This is expected as the foundation has the potential to expand during heating, and when this expansion is resisted, compressive stresses are developed. The formulation of the thermal stress calculated using Equation (2) indicates that the greatest stresses will occur at the locations of the lowest strain. Accordingly, the point at which the greatest stress occurs is usually referred to as the null point (Knellwolf et al. 2011). The greater thermal stress at a depth of 6 m could have been due to a transition in the soil stratigraphy. McCartney et al. (2013) summarized the results from field-scale and centrifuge-scale end-bearing foundations, and observed that the greatest axial thermal stress generally occurs near the toe for this type of foundation. The fact that the thermal stresses in this case decrease at the toe of the energy foundation indicates that the bottom of the drilled shaft may not have been properly cleaned out during construction, leading to a softer response during heating.

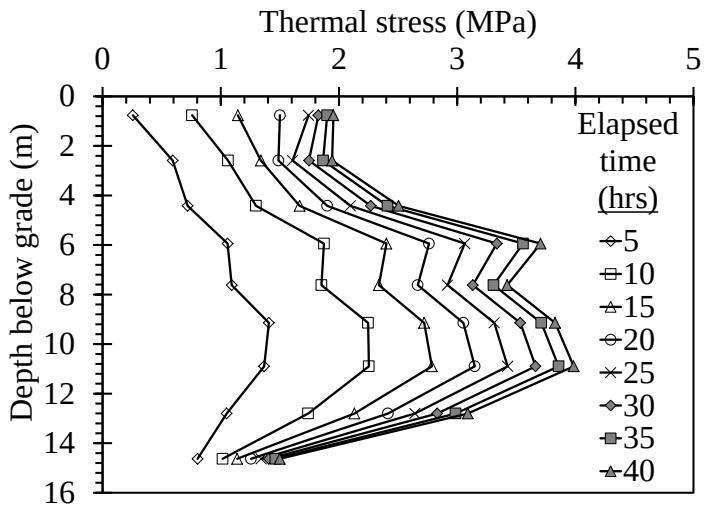

Figure 6.10: Thermally induced stresses in Foundation 4 during heating test

The change in thermal axial strain vs. change in temperature is shown in Figure 6.11. As temperature increases, the foundation expands, and as a result, the thermal axial strain decreases linearly. The slope of each line was calculated to obtain the mobilized coefficient of thermal expansion, presented in Figure 6.12. The location of minimum strain is located at a depth of 10.9 meters and corresponds to the null point during heating.

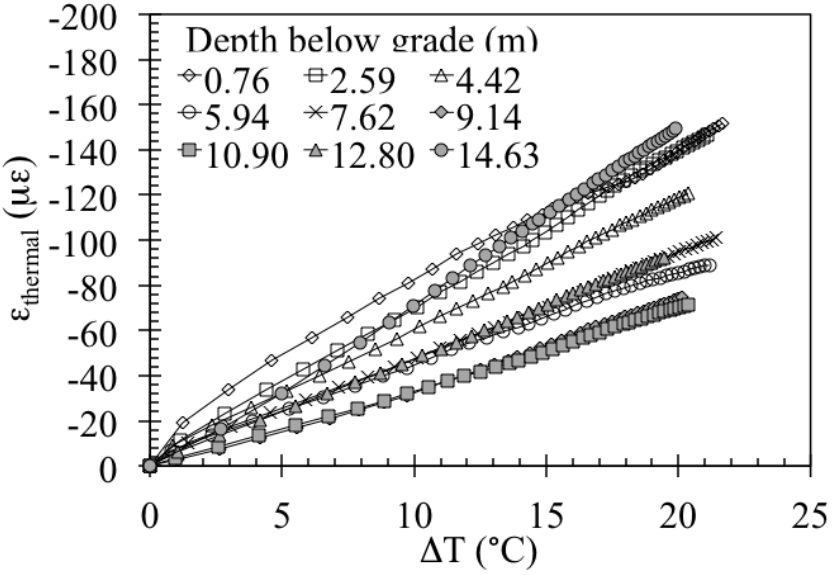

Figure 6.11: Thermally induced strain vs. change in temperature for Foundation 4

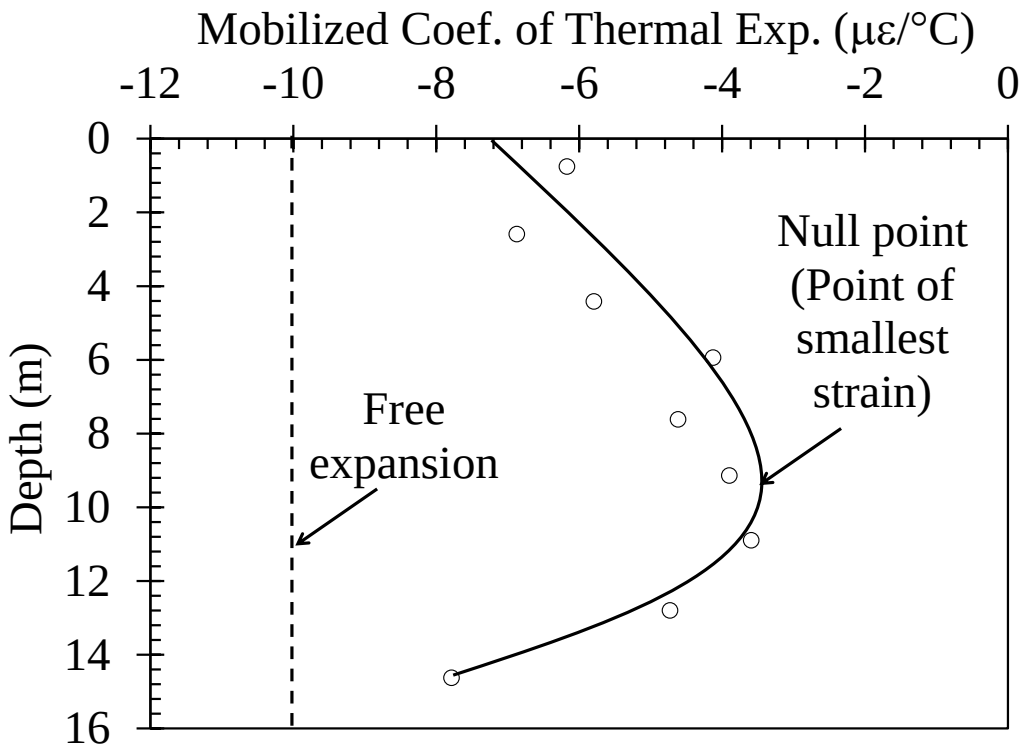

Figure 6.12: Mobilized coefficient of thermal expansion vs. depth for Foundation 4

Thermal axial displacements were calculated using equation 6.3. For a maximum increase in temperature of 21.7 °C, displacement was determined to be approximately 1.6 mm. This assumes that the toe of the foundation is completely fixed from moving in the vertical direction. Since the foundation does exhibit some strain near the toe, it is expected that the foundation would move downward slightly, thus reducing the displacement trends shown in Figure 6.13.

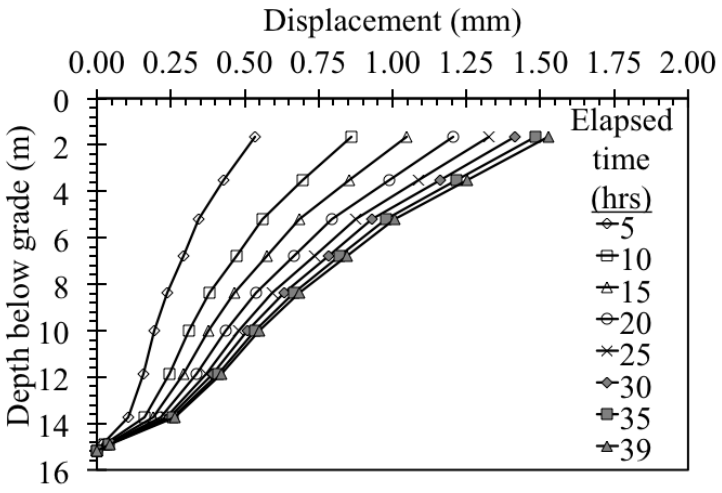

Figure 6.13: Upward displacement profiles during heating test on Foundation 4

6.1.3. U.S. Air Force Academy: Thermo-Mechanical Behavior: Phase 2

Instances in time corresponding to average changes in foundation temperature of 6 °C during heating and cooling were selected to generate thermo-mechanical profiles for each foundation. The profiles of foundation temperature in Figure 6.14 show that the temperature is relatively constant in the foundation, except for the base of the foundations, and slight variations in the shape of the temperature profile with time are observed in the top of the foundation due to surface temperature effects. The corresponding changes in thermal axial strain are shown in Figure 6.15. The shapes of the thermal axial strain profiles are relatively consistent for each foundation. A large thermal axial strain at the toe of each foundation was observed even through the change in temperature was not significant. Although this could be due to issues with the temperature measured by the thermistors at these depths, it could also reflect the possibility that the toe of the foundations may be relatively soft. This would be the case if the loose sandstone cuttings were not thoroughly removed from the bottom of the holes during construction. The distributions in thermal axial strain in Figure 6.15reflects that soil-structure interaction due to mobilization of side shear resistance leads to a nonlinear distribution in thermal strain with

depth, similar to the observations of Laloui et al. (2006) and Bourne-Webb et al. (2009) during the heating portions of their tests.

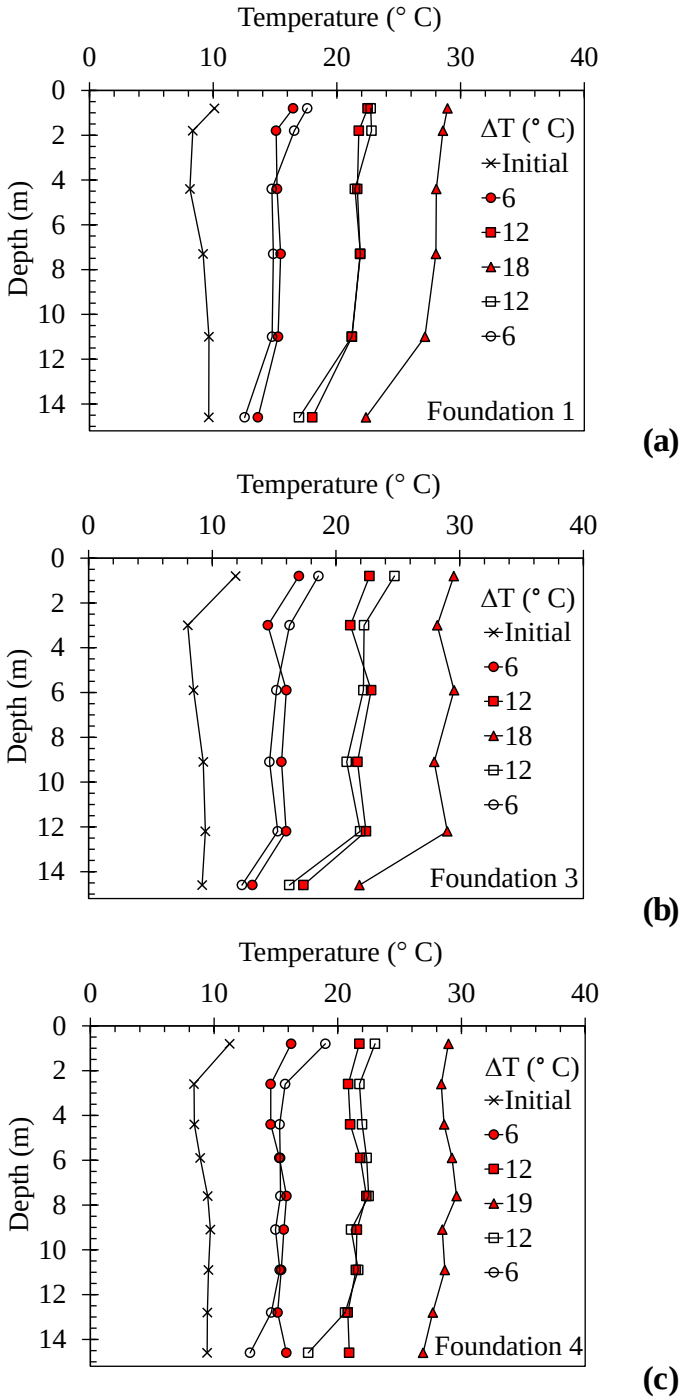

Figure 6.14: Profiles of temperature for different average changes in foundation temperature during heating (red) and cooling (open): (a) Foundation 1; (b) Foundation 3; (c) Foundation 4

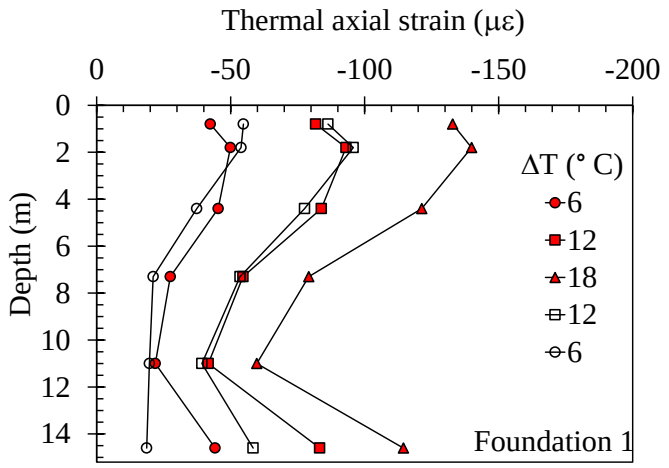

(a)

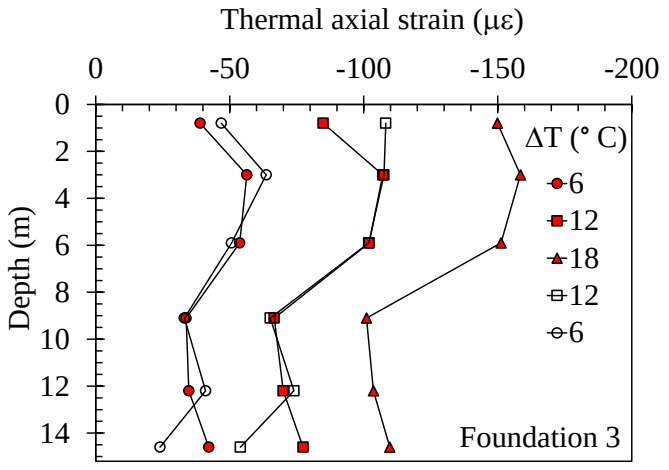

(b)

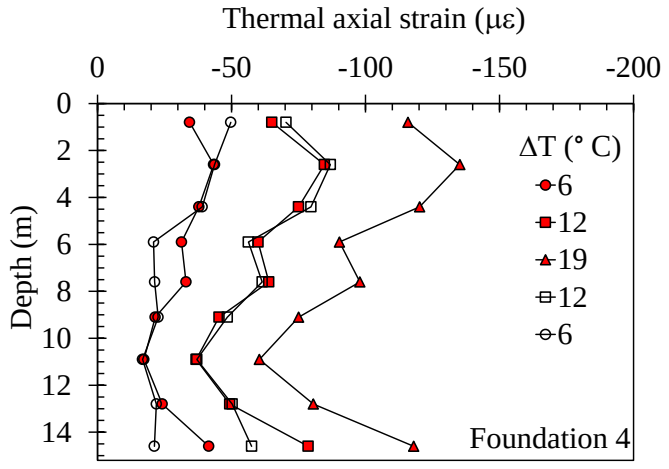

(c)

Figure 6.15: Profiles of thermal axial strain for different average changes in foundation temperature during heating (red) and cooling (open): (a) Foundation 1; (b) Foundation 3; (c) Foundation 4

Profiles of thermal axial stress were calculated using Eq. (6.2) with a Young's modulus of 30 GPa (Figure 6.16). If the foundations were completely restrained, the maximum thermal axial stress that could be generated for an increase in temperature of 18 °C is 6.48 MPa. As the strain gage measurements indicate that some strain occurs in the foundations during heating, the thermal axial stresses in the foundations are all lower than this value. The thermal axial stress generally increases with depth for each of the foundations, although the stress appears to decrease below a depth of 11 to 12 m in each of the foundations. As the point of maximum thermal axial stress typically coincides with the point of zero axial displacements, it is possible that the null point in the foundations occurs at a depth of 11 to 12 m below the grade beam. The thermal axial stresses in Foundation 3 were observed to be nearly 1 MPa lower than in the other two foundations. This could be attributed to the lower amount of restraint provided by the corner of the building compared to the center of the grade beam. Further, Foundations 5 and 8 were not heated, so they may provide greater constraint to Foundations 1 and 4 than to Foundation 3. The thermal axial stresses observed in these three foundations are below 33% of the compressive strength of reinforced concrete (f'_c). Even if the foundations were fully restrained (i.e., the case where the measured thermal axial strain is close to zero), the maximum thermal axial stress of 6.48 MPa would be less than this limit.

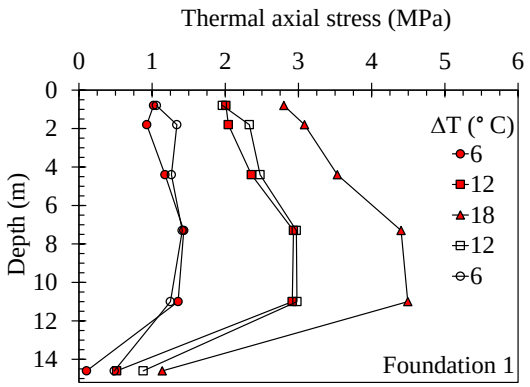

(a)

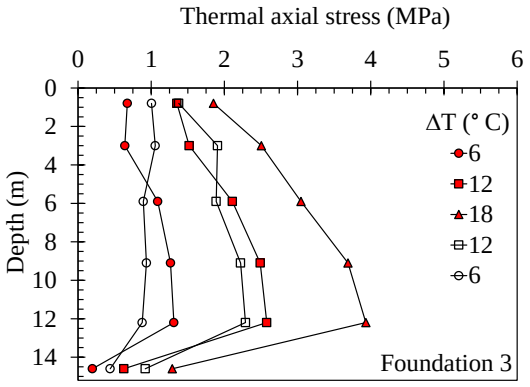

(b)

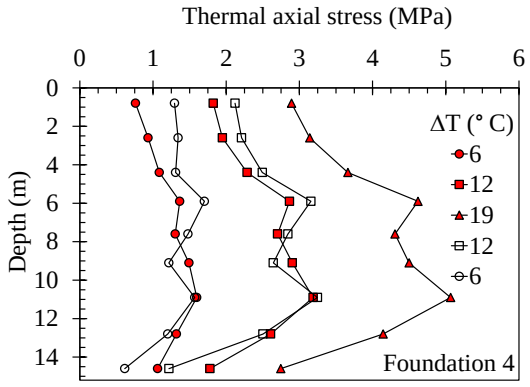

(c)

Figure 6.16: Profiles of thermal axial stress for different average changes in foundation temperature during heating (red) and cooling (open): (a) Foundation 1; (b) Foundation 3; (c) Foundation 4

The foundations experienced linear changes in thermal axial strain with changes in temperature (Figure 6.17). During the cooling phase, the strain for each foundation was observed to nearly return to the values that were experienced during the heating portion of the test, further indicating linear elastic behavior of the reinforced concrete. Relatively little hysteresis was

observed, indicating that the mobilized side shear resistance during the heating test did not lead to locked-in plastic strains at the interface.

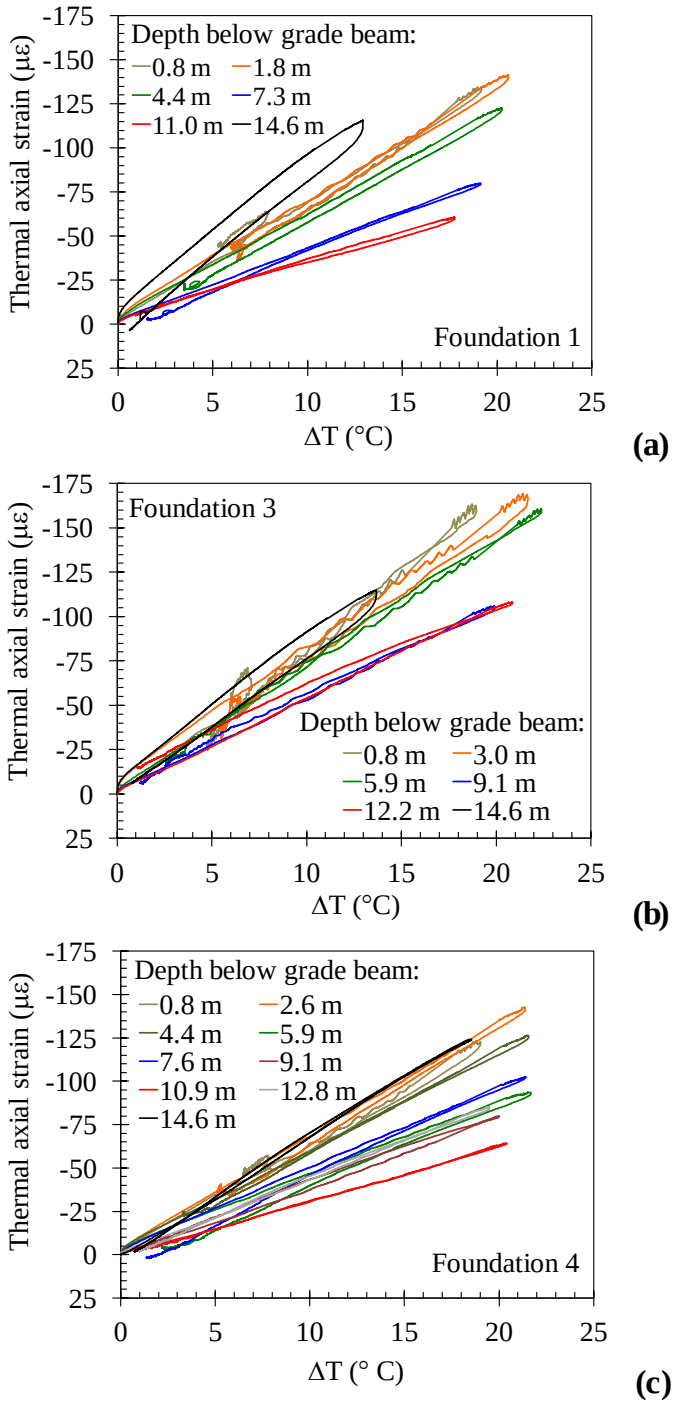

Figure 6.17: Thermal axial strain with change in foundation temperature at each depth: (a) Foundation 1; (b) Foundation 3; (c) Foundation 4

The slope of each trend was defined as the mobilized coefficient of thermal expansion, and the profiles of this coefficient with depth are plotted in Figure 6.18. For each foundation, the mobilized coefficient of thermal expansion was less than that of free expansion ($\alpha_c = -12$ με/°C), indicating that side shear resistance and the end restraint boundary conditions prevented the foundation from expanding as much as it possibly could in free-expansion conditions. The lowest value of the mobilized coefficient of thermal expansion in each of the foundations was observed at a depth of 11 to 12 m, consistent with the location of the maximum thermal axial stress. Foundation 3 exhibited slightly greater mobilized coefficients of thermal expansion likely due to the lower amount of restraint provided by the corner of the building.

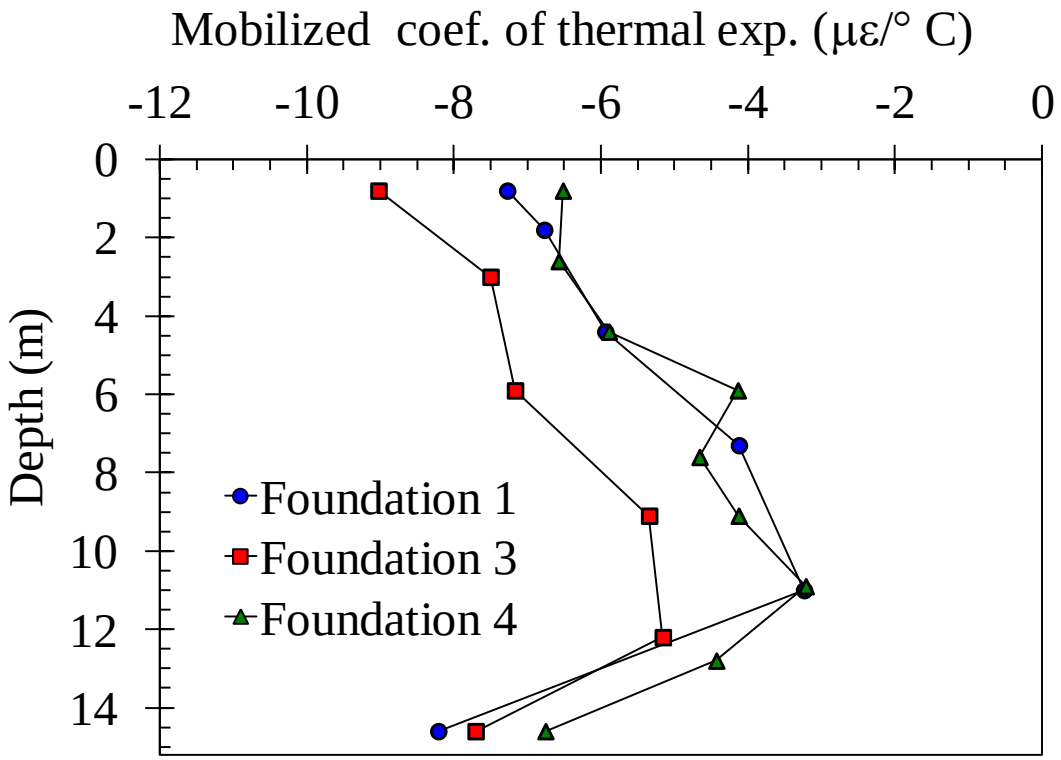

Figure 6.18: Mobilized coefficient of thermal expansion with depth for the three instrumented energy foundations.

The profiles of thermal axial displacement for the three foundations suggest that Foundation 3 experienced a greater displacement at the head of the foundation than the other two foundations (Figure 6.19), likely for similar reasons contributing to the lower thermal axial stress in it. Although the relative displacement at the toe is assumed to be zero for the purposes of calculating the thermal axial displacements, this does not assume that the null point is at the toe. For a rigid, end-bearing foundation, it is expected that the null point should be close to the toe as by definition it should not be able to move downward. If this were the case, then the maximum upward movement of the head would range from -1.3 to -1.7 mm during a change in temperature of about 18 to 19 °C. On the other hand, if loose cuttings are present at the toe, it is possible that the null point would move upward. If the null point is assumed to be at a depth of 11 to 12 m, then the point of zero axial displacement can also be assumed to occur at this depth, shifting the profiles of displacement to the left. In this case, the upward displacement at the foundation head would range from -1.0 to -1.4 mm and the downward displacement at the foundation toe would range from 0.2 to 0.3 mm. If the toe does not move, the maximum upward displacements will lead to an angular distortion δ/L_s, where δ is the difference in displacements of two adjacent energy foundations and L_s is the horizontal spacing between the foundations, of less than 1/5000. This value is lower than the limit expected to cause architectural damage in the building (Skempton and MacDonald 1956, Bjerrum 1963).

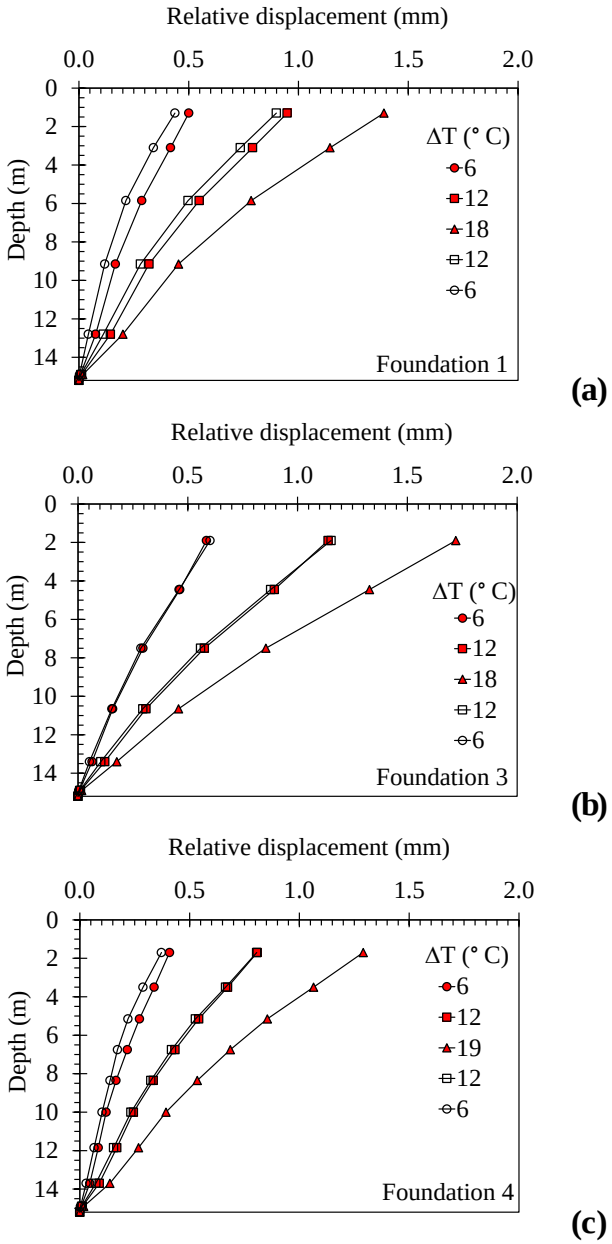

Figure 6.19: Profiles of thermal axial displacement for different average changes in foundation temperature during heating (red) and cooling (open): (a) Foundation 1; (b) Foundation 3; (c) Foundation 4

The mobilized side shear stress profiles calculated for the greatest change in temperature of 18 °C for all three foundations are shown in Figure 6.20. The results indicate that a negative (downward) side shear stress was observed in the upper portion of the foundation, and a positive (upward) side shear stress was observed in the lower portion of the foundation. The point at which the signs of the mobilized side shear stress changes is in the region of the maximum

thermal axial stress and corresponds to the position of the null point. The mobilized side shear stress increases with depth as expected, and the absolute value is less than 200 kPa, which is reasonable for a weakly cemented sandstone.

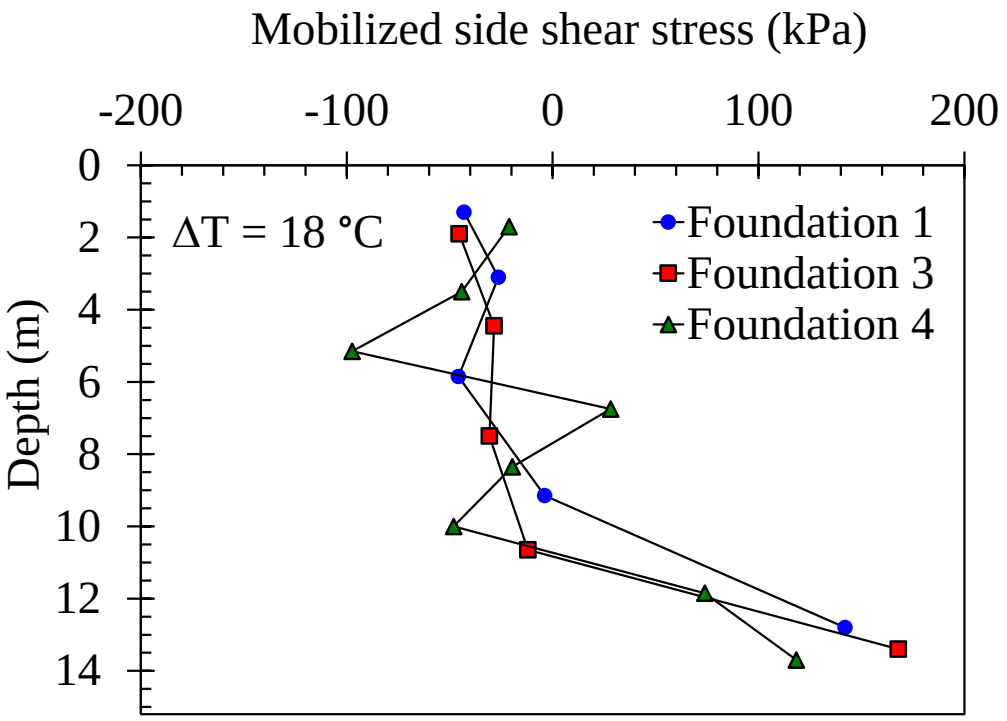

Figure 6.20: Profiles of mobilized side shear for a change in temperature of 18 °C for Foundations 1, 3, and 4

6.1.4. Comparison of Thermo-Mechanical Behavior to Cases from Literature

Thermo-mechanical behavior from the DHA and USAFA cases were compared to previously published case histories. Table 6.1 provides a summary of relevant results between each study. The change in thermal axial stress during heating for Foundations 1, 3, and 4 heating test at USAFA is shown along with published data from the literature. Three different depths within the foundation were considered to show the maximum and minimum rates of axial stress during heating. Due to the hysteretic behavior of the results at DHA and the residual strains that were observed during cyclic heating and cooling, the conditions for this comparison did not

apply. The stress at the depths presented corresponds to the null point and shows the greatest thermal axial stress. Rates of σ_t = 210ΔT to 260ΔT were determined from the results in this study, which are slightly higher than values from Laloui et al. (2006) and Bourne-Webb et al. (2009), but are consistent with those calculated from the results of McCartney and Murphy (2012). This may be due to the greater coefficient of thermal expansion of the reinforced concrete used in this study (-12 με/°C), which is slightly higher than the value of -9.5 με/°C used in the studies of Laloui et al. (2006) and Bourne-Webb et al. (2009).

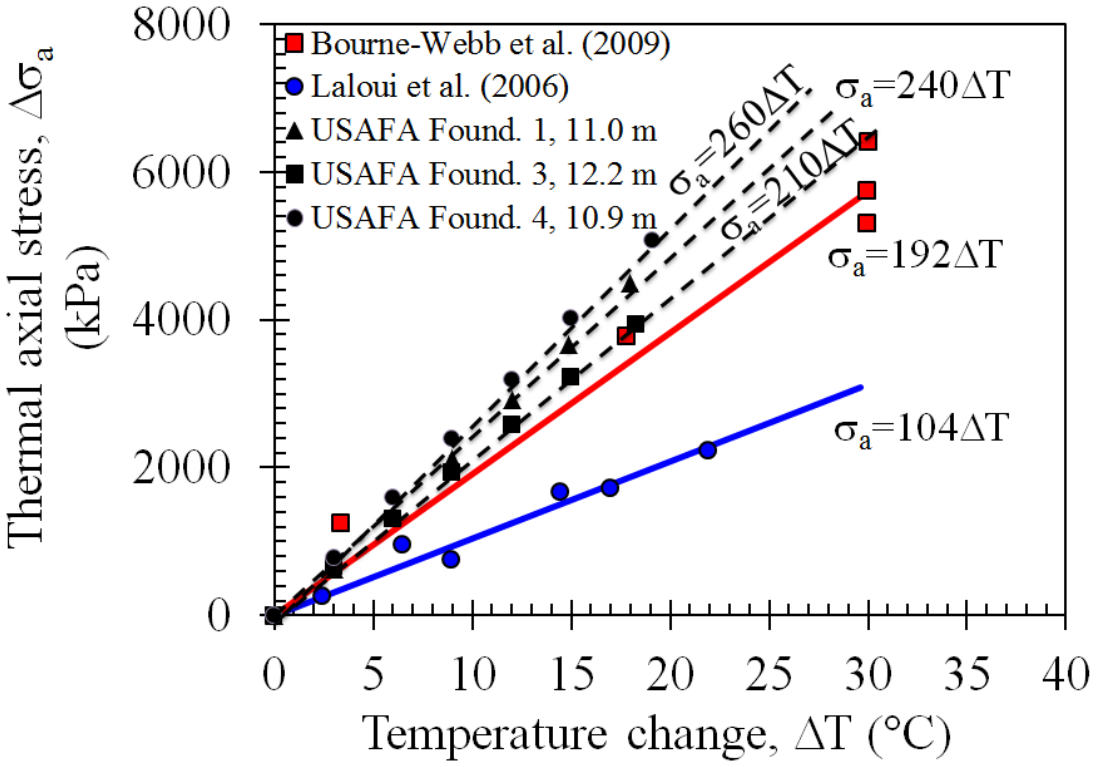

Figure 6.21: Thermally induced axial stress during heating of Foundation 4 at USAFA compared to energy foundations reported in the literature (after Amatya et al. 2012)

Table 6.1: Comparison of results from thermo-mechanical tests at DHA and USAFA to previous studies in the literature

Case	EPFL, Switzerland (Laloui et al. 2006)	Lambeth College, UK (Boume-Webb et al. 2009)	Denver Housing Authority	USAFA Foundation 4
Site stratigraphy	Alluvial soil, sand and gravel, founded in soft sandstone, groundwater table near surface	Granular fill and sand and gravel, founded in stiff fissured silty clay, groundwater table at 3 m.b.g.l.	Urban fill, sand and gravel, founded in Denver Blue Shale, perched groundwater	Sandy fill, dense sands, silty sandstone, groundwater table not encountered
Foundation type	Piled raft	Single foundation	Piled raft	Perimeter grade beam
Foundation length (m)	25.8	23	14.8 (A), 13.4 (B)	15.2
Foundation diameter (m)	0.88	0.56	0.91	0.61
Load mechanism at foundation head	Building dead load	Load frame	Building dead load	Building dead load
Max. mech. load during heating test (kN)	0 (T-1), 1300 (T-7)	1200	3840 (A), 3640 (B)	Negligible
Max. ΔT (°C)	+20.9 (T-1), +13.4 (T-7)	-19, +29.4	+14	+21.7
Location of min. thermally induced strain after heating (m)	21	17	11.6	10.9, 11.0, 12.2
Max. rate of increase of axial stress (kPa/°C)	104	192	275	210, 240, 260

6.2. Thermal Analysis

6.2.1. Overview

Fluid temperatures and mass flow rate recorded throughout a thermal response test can be analyzed to determine apparent system thermal conductivity. The heat input flux into an energy foundation can be calculated using the following equation:

$$Q = \Delta T \dot{V} \rho_{fluid} C_{fluid} \tag{6.4}$$

where ΔT is the difference between the supply fluid temperature (T_{supply}) and return fluid temperature (T_{return}) in Kelvin, $\dot{V}$ is the fluid flow rate in ml/s, ρ_{fluid} is the mass density of the fluid kg/ml, and C_{fluid} is the specific heat capacity of the fluid in J/(kgK). The simplified infinite line source method can then be used to determine system thermal conductivity as previously discussed in Section 2.3.1, as follows:

$$\lambda_{app} = \frac{Q}{4\pi L}\left[\frac{dT}{d(\ln t)}\right]^{-1} \tag{6.5}$$

where λ_{app} is the apparent thermal conductivity of each foundation, L is the effective length of each foundation system which represents the distance from the manifold to the tip of the foundation, and the term in brackets represents the slope of the change in mean fluid temperature versus logarithmic time. It is important to permit a certain amount of time to ensure that steady-state conditions have been established, as the differential form of the line source equation does not consider the impact of heat storage (i.e., the heat capacity) of the line source heat exchanger (i.e., the energy foundation) on the transient heating response, as shown in Figure 6.22.

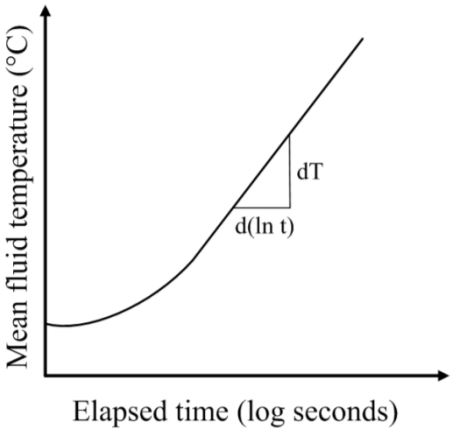

Figure 6.22: Hypothetical representation of mean fluid temperature vs. log time for a heat exchange element embedded in a continuous half-space

6.2.2. *Analysis of Heating Test at USAFA to Investigate Impact of Horizontal Runout Length on Thermal Response of Energy Foundation System*

The mean fluid temperature vs. logarithmic time for Foundations 1-4 is plotted in Figure 6.23. The results in this figure indicate that it took about 20 hours for the foundations to start increasing in temperature at a log-linear rate. The time period is attributed to the time needed to reach the thermal storage capacity of the foundations. All four of the foundations have similar cross-sectional areas and the same heat exchanger configuration. Although the temperature rise curves are similar, each foundation has a different runout length.

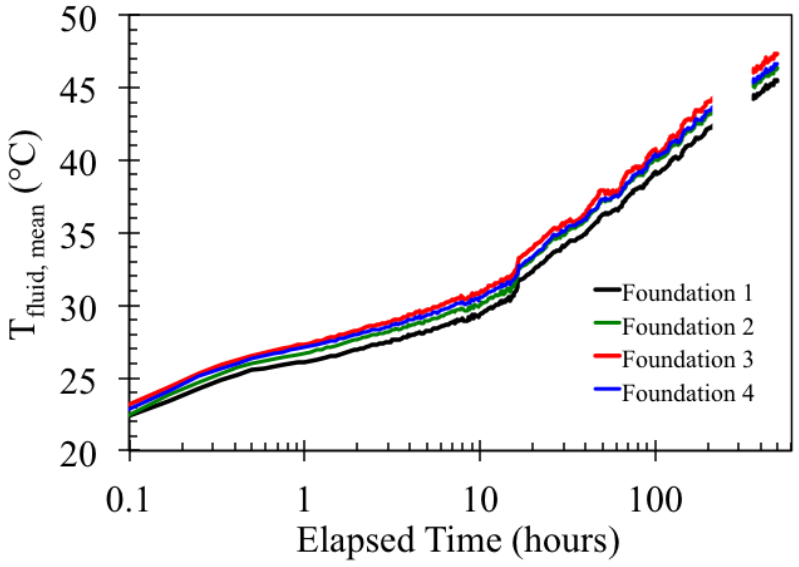

Figure 6.23: Mean fluid temperature rise vs. logarithm of elapsed time for Foundations 1-4

As the horizontal run-out length is increased, the heat exchange rate is observed to decrease as some heat loss or gain occurs in the grade beam. The effect of the horizontal run-out length can be assessed by evaluating the Q/L results from Foundations 1 through 4, as shown in Figure 6.24. The effective length, L, is defined as the distance from the manifold to the tip of the foundation. The effective length includes the horizontal run-out length of tubing cast in the grade beam in addition to the 15.2 m length of each foundation. These foundations have different

horizontal run-out lengths, but have the same heat exchanger configuration and were tested together in the same stage. A linear relationship was used to estimate the corrected value of Q/L representing the response of a foundation without the effect of horizontal run-out length, as follows:

$$(Q/L)_{corrected} = Q/L - m_{HR} \times H_{RO} \quad (6.6)$$

where m_{HR} is the run-out length correction factor in (W/m)/m, and H_{RO} is the horizontal run-out length in meters. A value of m_{HR} of -1.16 (W/m)/m was obtained from the slope of the line in Figure 6.24. The corrected values of Q/L are reported in Table 6.2. After the correction is applied, values of Q/L for Foundations 1 through 4 ranged from 97.9 to 109.4 W/m. The small differences after correction may be due to the differences in flow rates through each foundation.

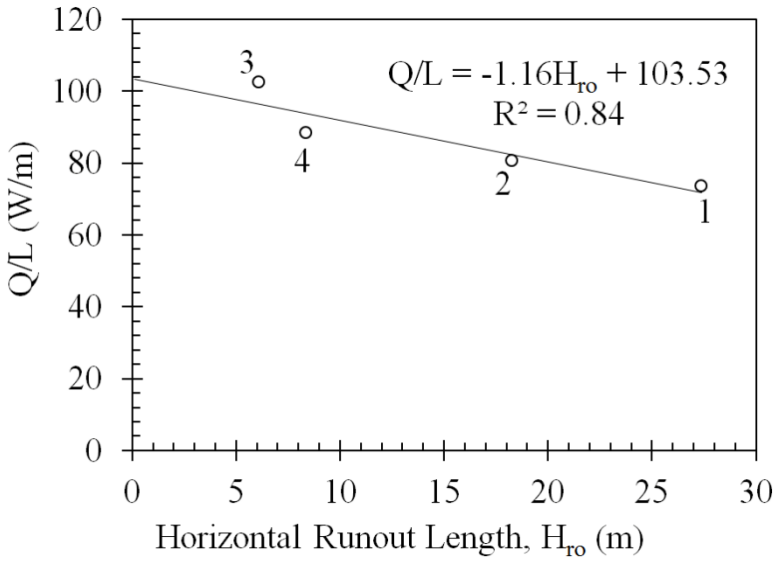

Figure 6.24: Trends in heat flux per unit length

Foundation 1 has the longest horizontal run-out length, and therefore the longest effective length, since each of the four foundations contains the same amount of heat exchanger tubing. Foundation 1 has the highest heat input energy consumption, Q, and has the highest average value of ΔT. However, the heat transfer per unit length, Q/L, in Foundation 1 is the lowest of the

four foundations tested. Foundation 3 has the shortest run-out length as well as the lowest heat energy consumption of all the foundations but the heat transfer per unit effective length is actually the highest, indicating higher energy efficiency of the geothermal loop. The apparent heat transfer versus the effective length for each of the four foundations is shown in Figure 6.24. For greater effective lengths, the heat input energy per unit length decreases. The response is similar to the decrease in heat transfer for increasing length to diameter ratios observed by Boume-Webb (2013). This indicates that in the design phase of an energy foundation system, consideration for energy loss through the horizontal portion of the geothermal loop needs to be considered. In practice, energy foundations may be connected in series to reduce this effect. The system described in this study was plumbed in parallel in order to characterize and operate each energy foundation individually.

6.2.3. Influence of Loop Configuration on Thermal Output of Energy Foundations

The details of each heating stage and results from the thermal response tests are summarized in Table 6.2. The measured heat input for each heat exchanger configuration was normalized over the effective length of the energy foundation system element to define the heat flux per unit meter of heat exchanger Q/L. The heat exchange rate is used in this study to assess the relative heat exchange behavior of each foundation because of the geometry of the horizontal connection between the energy foundations and the manifold, which does not satisfy the assumptions of the available analytical methods. The values of Q/L range from 24.4 to 108.5 W/m, which are within the range reported by Boume-Webb (2013). The value of Q/L was found to be highly dependent on the effective length and nominal heat input, with a decrease in Q/L with increasing effective length. The response is similar to the decrease in heat flux for increasing length to diameter ratios observed by Boume-Webb (2013).

Table 6.2: Summary of results from thermal response testing for each stage (Note: all foundations have a length of 15.2 m).

Test stage	Foundation	Heat exchanger configuration	Effective length, L (m)	Flow rate (ml/s)	Avg. ΔT_{fluid} (°C)	Measured heat flux, Q (W)	Q/L (W/m)	Corrected Q/L (W/m)
1	1	2 loops	42.6	108	8.8	3133	73.5	105.2
	2		33.5	119	6.9	2696	80.5	101.6
	3		21.3	137	4.8	2180	102.3	109.4
	4		23.6	106	6.0	2081	88.2	97.9
2	6	3 loops	41.8	144	4.8	4534	108.5	139.2
3	7	1 loop	54.0	108	4.5	4431	82.1	126.9
4	8	1 loop in center	63.1	126	3.9	4075	64.6	120.0
5	5A	1 loop	32.7	347	2.0	2285	69.9	90.1
6	5A	1 loop	32.7	226	1.6	1164	35.6	55.8
	5B			226	1.6	1150	35.2	55.4
7	5A	1 loop	32.7	189	1.3	797	24.4	44.6
	5B			189	1.3	803	24.6	44.8
	5C			189	1.9	1201	36.7	56.9

The correction approach was applied to the other foundations at the site to eliminate the impact of horizontal run-out length to evaluate the thermal properties of the foundation-soil system alone. The results in Table 6.2 indicate that Foundation 6 had the highest value of Q/L of 139.2 W/m; and it had the longest continuous length of heat exchanger within the foundation. However, Foundations 7 and 8 both have similar high values of Q/L of 120 and 126.9 W/m even though they only have one continuous heat exchanger. It is possible that these tests were not performed for a long-enough duration so that the effect of the heat capacity of the concrete could be overcome (Loveridge and Powrie 2012). The Q/L for Foundation 5 when only loop 5A was included was lower, but this could have been due to the much higher flow rate used in this test. The flow rate decreased when the valves for loops 5B and 5C were opened as flow was distributed amongst the three loops.

6.2.4. Determination of Soil Thermal Conductivity from Borehole Temperature Readings

The thermal conductivity of the subsurface surrounding the foundations could be assessed using the temperatures of the subsurface measured using the thermistor strings in the boreholes. The temperatures of Foundation 4 and the surrounding subsurface were plotted at different instances in time, as shown in Figure 6.25. The vertical line in this figure denotes the outside limit of the building slab, and the distances are measured from the center of the foundation. As expected, as Foundation 4 heats up, the temperature of the soil also increases. The thermal conductivity as a function of time at a depth of 7.3 m was calculated using the temperatures from Boreholes 4 and 5 using Eq. 2.3, as shown in Figure 6.26. For greater times, the temperature gradient, dT/dr, between the foundation and adjacent boreholes became steadier, which produced thermal conductivity values that were constant between 400 and 500 hours. Thermal conductivity of the soil near the end of heating in stage 1 was calculated to be 2.0 and 2.3 W/mK for heat flow through the subsurface in the directions of Boreholes 4 and 5, respectively. These values of thermal conductivity are consistent with the corrected system thermal conductivity values using the line source method to analyze the heating response data reported for Stage 1, even though the details of the foundation system do not satisfy the assumptions of this analysis.

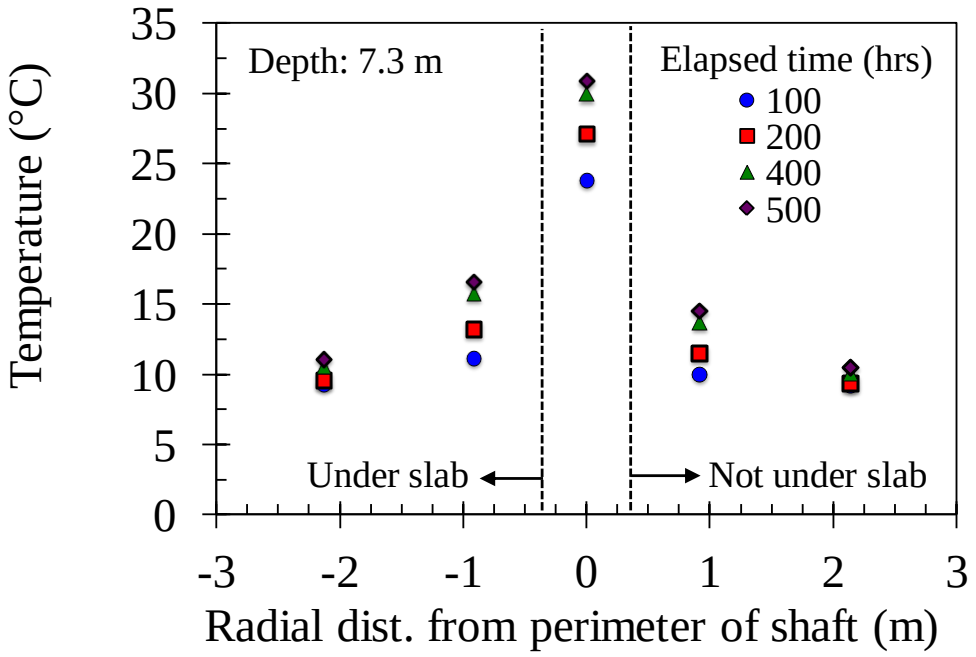

Figure 6.25: Temperatures of Foundation 4 and surrounding soil

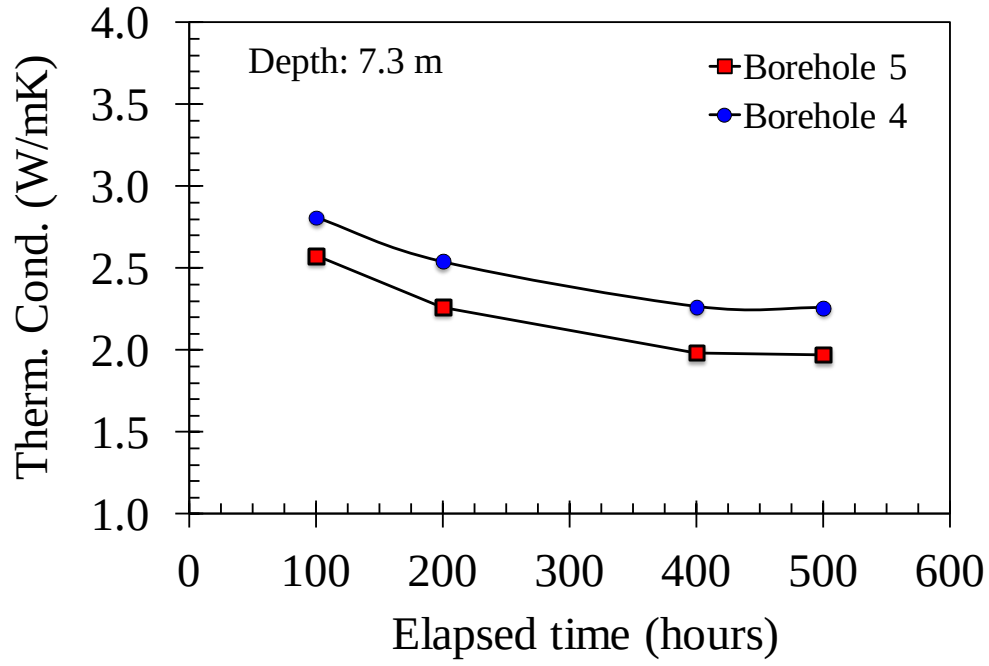

Figure 6.26: Thermal conductivity over the duration of heating from the thermal gradient between the foundation and Boreholes 4 and 5.

6.2.5. Comparison of Thermal Behavior to Cases from Literature

The thermal behavior from the USAFA thermal response test was compared to previously published results in the literature, as shown in Table 6.3. The heat exchange rate during heating from USAFA ranged from 44.6 to 139.2 W/m after a correction for runout length, which is consistent with other TRT studies having similar energy foundation geometry and heat exchanger loop configurations. The system thermal conductivity from USAFA varied from 1.7 to 2.3 W/mK, increasing with decreasing tubing runout length. The values of thermal conductivity obtained in this study are reasonable for sandstone and fall within the range of previously reported data. The line source method gave appropriate results for system thermal conductivity, as the test duration was long enough to avoid transient effects.

Table 6.3: Comparison of Thermal Behavior from Literature to USAFA Case

Case	Hamada et al.(2007)	Ooka et al. (2007)	Gao et al. (2008)	Lennon et al. (2009)	Brettmann and Amis (2011)	USAFA
Foundation type	26×D.P.	2×D.S.	1×D.S.	4×D.P.	3×A.C.I.P.	8×D.S.
Foundation length (m)	9	20	25	12-17	18.3	15.2
Foundation diameter (mm)	300	1500	600	244-270	300-450	610
# Heat Exchanger Loops	1,2, Indirect/ Direct Pipe	8	1-3	1	2	1-3
TRT Analysis Method	N/A	N/A	Num. Method	Line Source	Line Source	Line Source
Thermal Conductivity (W/mK)	N/A	N/A	5.8-6.0	2.4-2.6	2.5-2.6	1.7-2.3 (Found. 1-4)
Heat Exchange Rate (W/m)	54-69 (ext.)	100-120 (rej.) 44-52 (ext.)	57-108 (rej.)	N/A	73-80 (rej.)	74-103 (rej.) (Found. 1-4)

***DS: Drilled shaft, A.C.I.P.: Auger cast in place pile, D.P.: Driven Pile**
**** Rej.: Heat rejection into foundation, Ext.: Heat extraction from pile**

7. CONCLUSIONS

This study presented the results from two case histories involving full-scale energy foundation systems installed under buildings located in Colorado. The energy foundations in both cases were drilled shafts with embedded heat exchanger loops, and the measurements from the studies permits evaluation of variables including energy foundation geometry, heat exchanger configuration, and subsurface stratigraphy. Instrumentation incorporated into the energy foundations to measure temperatures and axial strains during heat exchange operations. Sensors were also installed to measure the subsurface temperature around the energy foundations, along with the temperature and flow rate of the heat exchanger fluid circulating through the energy foundations. The measurements from the different sets of instrumentation permitted evaluation of both the thermal response of the energy foundation-subsurface system, as well as the thermo-mechanical soil-structure interaction behavior selected energy foundations. The specific conclusions that can be drawn from the study of thermo-mechanical behavior of the energy foundations are as follows:

Denver Housing Authority

- Heating and cooling of energy foundations at the DHA led to uniform changes in temperature of the foundations ranging from 9 to 32 °C. These changes in temperature led to thermal axial strains ranging from -102 to 51 με. These thermal axial strains correspond to changes in thermal axial stress of -1.0 to 3.1 MPa, which are within acceptable limits for reinforced concrete. The maximum axial stress was observed at the toe of both energy foundations at the site, confirming the behavior expected from end-bearing foundations. The thermal axial strains were also integrated to define thermal axial displacements, which ranged from -0.8 mm upward during foundation heating to 0.4 mm upward during foundation cooling. These

displacements are within acceptable limits for the thermal changes experienced in other types of reinforced concrete structures like bridges.

Thermo-mechanical Behavior at USAFA: Phase 1

- Heating of an energy foundation at USAFA led to a uniform change in temperature of 21 °C. This change in temperature led to thermal axial strains ranging from -70 με at a depth of 10.9 m to 150 με near the top and bottom of the foundation.
- These thermal axial strains correspond to changes in thermal axial stress of 1.6 to 4 MPa, which are within acceptable limits for reinforced concrete.
- The maximum axial stress was observed at a depth of 10.9 m, indicating that the foundation was allowed to move upward and downward during thermal expansion due to heating.
- The thermal axial strains were also integrated to define a thermal axial displacement of 1.55 mm upward during foundation heating, assuming zero displacement at the toe of the foundation. This displacement is sufficient to not cause any adverse structural effects to the building.

Thermo-Mechanical Behavior at USAFA: Phase 2

- During heating over a change in temperature of 18 °C, Foundations 1, 3, and 4 experienced a relatively uniform change in temperature with depth.
- The increase in temperature led to expansive thermal axial strains in each foundation that were smaller than the estimated free expansion strain. The maximum strains in each foundation occurred near the top and bottom.
- The location of the maximum compressive thermal axial stress, which ranged from 4.0 to 5.1 MPa, was located between a depth of 11 and 12 m (at a normalized depth of 0.72 to

0.78). The thermal axial strains were used to calculate the thermal axial stresses induced in each foundation during heating.

- The relative displacement between the head and toe of each instrumented foundation was found to increase nonlinearly upwards. If the toe of the foundation was assumed not to move, the upward displacement of the head of the foundation was estimated to range from -1.3 to -1.7 mm for the maximum increase in temperature. However, if the toe of the foundation was assumed to move downward (which would be the case if the hole was not adequately cleaned) and the null point was co-located with the depth of the maximum thermal axial stress, the upward displacement of the head of the foundation was estimated to range from -1.0 to -1.4 mm. In either case, the thermal axial movements are not sufficient to induce structural or aesthetic damage to the building.
- The end restraint boundary conditions were found to play an important role in the thermal axial stress and displacement profiles in the energy foundations. Foundation 3 was located at the corner of the building and had the lowest end restraint at the top compared to Foundations 1 and 4 which are located beneath the middle of the grade beam, especially considering the fact that Foundations 1 and 4 were also expanding during the same test. The lower head stiffness was found to lead to a lower thermal axial stress in Foundation 3, along with a slightly greater displacement.
- The thermal axial strains, stresses, and displacements during cooling were similar to those during heating, indicating linear thermo-elastic behavior. Little hysteresis was observed, which indicates that permanent thermo-plastic deformations did not occur at the foundation-subsurface interface.

- A common observation from both case histories is that the end-restraint boundary conditions at the top and bottom of an energy foundation play a significant role in stress distribution during heating, as does the side shear stress distribution.

Evaluation of Thermal Behavior at Both Sites

The thermal behavior of the energy foundations at both sites was interpreted using a series of thermistors that measure heat exchange fluid temperature, foundation temperature, and soil temperature in boreholes. The specific conclusions that can be drawn from the evaluation of the thermal response tests on the energy foundations are as follows:

- The thermal conductivity of the foundation-subsurface system at the USAFA project calculated using the line source equation were found to range from 1.7 to 2.3 W/mK, which is within the range for values reported in the literature for other energy foundations.
- The length of heat exchanger tubing required to connect energy foundations to a heat pump plays a significant role in the heat transfer rate calculated for each foundation. The results from the USAFA project indicate that greater run-out lengths leads to a lower heat exchange rate. This observation is consistent with trends published by Bourne-Webb (2013), which indicate a decreasing trend between the heat transfer rate and the aspect ratio of the foundation. Consideration for the run-out length can play an important role in the design of the configuration of heat exchanger tubing in energy foundation systems.
- The heat flux ranged from 64.5 to 108.5 W/m for the foundations considering the role of the horizontal run-out length of tubing connecting the foundations to the manifold, although lower values of 34.5 W/m were measured when performing staged heating tests on Foundation 5.

- The foundations with a single heat exchanger loop had relatively high values of heat flux per meter, nearly as high as that of a foundation with 3 continuous heat exchangers. This may be due to the large thermal mass that the single heat exchanger must overcome, leading to a higher Q/L than expected in a long-term test.
- The building slab was observed to lead to an insulating effect that led to more stable temperatures in the subsurface. This issue may become more significant when the temperature of the building is maintained at a constant temperature.
- The temperatures of the subsurface measured using thermistor strings in boreholes surrounding Foundation 4 were used to calculate thermal conductivity of the subsurface. The thermal conductivity at a depth of 7.3 m was observed to range from 2.0 to 2.3 W/mK, which is consistent with the thermal conductivity values obtained from a line source analysis of the thermal response tests results.

8. REFERENCES

Adam, D. and Markiewicz, R. (2009). "Energy from earth-coupled structures, foundations, tunnels and sewers." Géotechnique. 59(3), 229–236.

Amatya, B.L., Soga, K., Bourne-Webb, P.J., Amis, T. and Laloui, L. (2012). "Thermo-mechanical behaviour of energy piles." Géotechnique. 62(6), 503–519.

Bourne-Webb, P.J., Amatya, B., Soga, K., Amis, T., Davidson, C. and Payne, P. (2009). "Energy pile test at Lambeth College, London: Geotechnical and thermodynamic aspects of pile response to heat cycles." Géotechnique. 59(3), 237–248.

Bourne-Webb, P. (2013). "An overview of observed thermal and thermo-mechanical response of piled energy foundations." European Geothermal Congress. 8 pg.

Brandl, H. (2006). "Energy foundations and other thermo-active ground structures." Géotechnique. 56(2), 81-122.

Brettmann, T. and Amis, T. (2011). "Thermal conductivity evaluation of a pile group using geothermal energy piles." GeoFrontiers 2012. Dallas, TX. 10 pg.

Burlon, S., Habert, J., Szymkievicz, F., Suryatriyastuti, M., and Mroueh, H. (2013). "Towards a design approach of bearing capacity of thermo-active piles." European Geothermal Congress 2013. Pisa, Italy. 6 pg.

Campbell, G.S., Callissendorff, G.S., and Williams, J.H. (1991). "Probe for measuring soil specific heat using a heat pulse method." Soil Sci. Soc. Am. J. 55, 291-393.

Energy Information Agency (EIA). (2008). Annual Energy Review. Report No. DOE/EIA-0384(2008).

Ennigkeit, A. and Katzenbach, R. (2001). "The double use of piles as foundation and heat exchanging elements." Proc. 15th International Conference on Soil Mechanics and Geotechnical Engineering. Istanbul, Turkey. p. 893-896.

Farouki, O.T., 1981. Thermal Properties of Soils. Cold Regions Science and Engineering, CRREL Monograpg 81-1, 136.

Gao, J., Zhang, X., Liu, J., Li, K. and Yang, J. (2008). "Numerical and experimental assessment of thermal performance of vertical energy piles: an application." Applied Energy. 85(10): 901-910.

GSHPA (2012). Thermal Pile Design, Installation, and Materials Standards Issue 1.0. Ground Source Heat Pump Association. Milton Keynes, U.K.

Hamada, Y., Saitoh, H., Nakamura, M., Kubota, H. & Ochifuji, K. (2007). "Field performance of an energy pile system for space heating." Energy and Buildings 39, No. 5, 517–524.

Hueckel, T. and Borsetto, M. (1990). "Thermoplasticity of saturated soils and shales: Constitutive equations." ASCE Journal of Geotechnical Engineering. 116, 1765-1777.

Laloui, L. (2011). "In-situ testing of heat exchanger pile." Geo-Frontiers: Advances in Geotechnical Engineering. Proc. of the Geo-Frontiers 2011 Conference. Dallas, TX. 10 pg.

Laloui, L., Nuth, M., and Vulliet, L. (2006). "Experimental and numerical investigations of the behaviour of a heat exchanger pile." International Journal for Numerical and Analytical Methods in Geomechanics 30, 763–781.

Laloui, N. and Nuth, M. (2006). "Numerical modeling of some features of heat exchanger pile." Foundation Analysis and Design: Innovative Methods (GSP 153). ASCE. Reston, VA. pp. 189-195.

Lennon, D.J., Watt, E., and Suckling, T.P. (2009). "Energy piles in Scotland." Proceedings of the 5th International Conference on Deep Foundations on Bored and Auger Piles, Frankfurt (Van Impe, W.F. and Van Impe, P.O., eds). Taylor and Francis, London, UK.

Loveridge, F. and Powrie, W. (2013). "Pile heat exchangers: Thermal behaviour and

interactions." *Proc. ICE – Geotechnical Engineering*. 166(GE2), 178-196.

McCartney, J.S. and Murphy, K.D. (2012). "Strain distributions in full-scale energy foundations." DFI Journal. 6(2): 28-36.

McCartney, J.S., Murphy, K.D., and Stewart, M.A. (2013). "Thermo-mechanical strain distributions in full-scale energy foundations." Proc. *18th International Conference on Soil Mechanics and Foundation Engineering*. Paris, France. September 1-5, 2013. 4 pg.

McCartney, J.S. and Rosenberg, J.E. (2011). "Impact of heat exchange on the axial capacity of thermo-active foundations." GeoFrontiers 2011. Dallas, TX. 10 pg.

Mimouni T. and Laloui L. (2013). "Towards a secure basis for the design of geothermal piles." Acta Geotechnica. DOI 10.1007/s11440-013-0245-4. 12 pg.

Murphy, K.D., McCartney, J.S., and Henry, K.S. (2014). "Impact of horizontal run-out length on the thermal response of full-scale energy foundations." GeoCongress 2014. 10 pg. In press.

Murphy, K.D., McCartney, J.S., and Henry, K.S. (2014). "Characterization of a full-scale energy foundation." ASCE GSP Honoring Roy Olson. 12 pg. In press.

Murphy, K.D., McCartney, J.S., and Henry, K.S. (2014). "Evaluation of thermo-mechanical and thermal behavior of full-scale energy foundations." Acta Geotechnica Special Issue. Thermoactive Geotechnical Systems for Near-Surface Geothermal Energy. In press.

Ooka, R., Sekine, K., Mutsumi, Y., Yoshiro, S., and SuckHo, H. (2007). "Development of a ground source heat pump system with ground heat exchanger utilizing the cast-in place concrete pile foundations of a building." EcoStock 2007. 8 pp.

Ozudogru, T., Brettmann, T., Olgun, G., Martin, J., and Senol, A. (2012). "Thermal conductivity testing of energy piles: Field testing and numerical modeling." *ASCE GeoCongress 2012*. Oakland, CA. March 25-29th, 2012. 10 pg. CD ROM.

Regueiro, R., Wang, W., Stewart, M.A., and McCartney, J.S. (2012). "Coupled thermo-poro-mechanical finite element analysis of a heated single pile centrifuge experiment in saturated silt." ASCE GeoCongress 2012. Oakland, CA. March 25-29th, 2012.

Rosenberg, J.E. (2010). Centrifuge Modeling of Soil Structure Interaction in Thermo-Active Foundation. M.S. Thesis. University of Colorado Boulder.

Sanner, B. (2001). "Shallow geothermal energy." *GHC Bulletin*. June, 19-25.

Sanner, B., Hellstrom, G., Spitler, J., and Gehlin, S.E.A. (2005). "Thermal response test – current status and world-wide application." *World Geothermal Cong*ress. Antalya, Turkey.

Shonder, J. A. and Beck, J. V. (1997). A New Method to Determine the Thermal Properties of Soil Formations from In-Situ Field Tests. ORNL/TM-2000/97. 40 p.

Stewart, M.A. and McCartney, J.S. (2014). "Centrifuge modeling of soil-structure interaction in energy foundations." ASCE Journal of Geotechnical and Geoenvironmental Engineering. In press.

Suver, P. (2012). "Heating and cooling structures with steel pile foundations."Deep Foundations Institute. September, 2012. Houston, TX. Pg. 387-394

Wood, C.J., Liu, H. and Riffat, S.B. (2009). "Use of energy piles in a residential building, and effects on ground temperature." Géotechnique. 59(3): 287-290.